

For Reference

NOT TO BE TAKEN FROM THIS ROOM

Ex LIBRIS
UNIVERSITATIS
ALBERTAENSIS





Digitized by the Internet Archive
in 2019 with funding from
University of Alberta Libraries

<https://archive.org/details/Hallam1980>

THE UNIVERSITY OF ALBERTA

RELEASE FORM

NAME OF AUTHOR Richard John HALLAM
TITLE OF THESIS THE FLOW OF OIL-IN-WATER EMULSIONS
 THROUGH A POROUS MEDIUM
DEGREE FOR WHICH THESIS WAS PRESENTED MASTER OF SCIENCE
YEAR THIS DEGREE GRANTED FALL 1980

Permission is hereby granted to THE UNIVERSITY OF ALBERTA LIBRARY to reproduce single copies of this thesis and to lend or sell such copies for private, scholarly or scientific research purposes only.

The author reserves other publication rights, and neither the thesis nor extensive extracts from it may be printed or otherwise reproduced without the author's written permission.

THE UNIVERSITY OF ALBERTA

THE FLOW OF OIL-IN-WATER EMULSIONS THROUGH A POROUS MEDIUM

by



Richard J. HALLAM

A THESIS

SUBMITTED TO THE FACULTY OF GRADUATE STUDIES AND RESEARCH

IN PARTIAL FULFILMENT OF THE REQUIREMENTS FOR THE DEGREE

OF MASTER OF SCIENCE

IN

PETROLEUM ENGINEERING

DEPARTMENT OF MINERAL ENGINEERING

EDMONTON, ALBERTA

FALL, 1980

801

THE UNIVERSITY OF ALBERTA
FACULTY OF GRADUATE STUDIES AND RESEARCH

The undersigned certify that they have read, and recommend to the Faculty of Graduate Studies and Research, for acceptance, a thesis entitled THE FLOW OF OIL-IN-WATER EMULSIONS THROUGH A POROUS MEDIUM submitted by Richard John HALLAM in partial fulfilment of the requirements for the degree of MASTER OF SCIENCE in PETROLEUM ENGINEERING.

To my parents
Barbara and Eric

ABSTRACT

The flow characteristics of emulsions, in a porous medium, were examined by studying the flow of two low concentration ($\Gamma = 0.15$ and 0.30) oil-in-water emulsions, through one consolidated core and cores made from three different unconsolidated sands.

The results showed that an emulsion effectively reduces the permeability of a core, when the emulsion droplets are larger than the pore throats in the porous medium. When emulsions plug a porous medium, the relationship between flow rate and pressure drop is not linear and therefore emulsion flow in a porous medium is a non-Darcy flow process. The shape of the fractional permeability versus flow rate or pressure drop curve is a function of the pore throat size distribution in the porous medium. There is no simple relationship between the permeability reduction and the porosity and permeability of the core.

The shape of the produced emulsion concentration profile was examined for the 0.15 concentration emulsion. The droplet size distribution of the produced emulsion was examined in one experiment. The results showed that the degree of retention was higher for the larger oil droplets.

A model based upon the assumption that the droplets can plug the porous medium and this rate of plugging can be modelled by a rate equation is proposed. The model has to be

compared with the experimental data to evaluate the various unknown parameters. Three models were proposed in this study and one model effectively fitted the experimental data.

Acknowledgements

The author would like to thank Dr. D.L.Flock for his guidance in preparing this manuscript.

Thanks are also due to Robert Symonds for his helpful suggestions concerning the use of the computer program COMPLX.

Especial thanks go to my parents, for their financial and emotional support given to me throughout my academic career.

Special thanks are due to the Provincial Government of Alberta for granting the Premier's Scholarship. The author gratefully acknowledges the partial financial support provided by the Alberta Oil Sands Technology and Research Authority.

TABLE OF CONTENTS

CHAPTER		PAGE
1.	INTRODUCTION	
1.1	Background	1
1.2	Purpose of the Study	3
2.	THEORY AND LITERATURE REVIEW	
2.1	Emulsion Rheology	5
2.2	A Concept of Emulsion Flow	13
2.3	Review of Emulsion Flow Characteristics	17
2.4	Emulsion Flow Models	21
3.	EMULSION FLOW MODELS	
3.1	Introduction	28
3.2	Material Balance Equation	29
3.3	Plugging Mechanisms - The Kinetic Equation	30
3.4	Integration of the Differential Equations	37
3.4.1	Plugging Process at the Inlet End of the Porous Medium	39
3.4.2	Solution of the Retained Oil Saturation Equation	41
3.4.3	Solution in Terms of the Flowing Emulsion Concentration	44
3.4.4	Comparisons of the Flow Models	44
3.4.5	N-Fractional Size Emulsion	46
3.5	The Emulsion Flow Model	47
4.	EXPERIMENTAL EQUIPMENT AND PROCEDURE	
4.1	Porous Media	49
4.2	Emulsion and Emulsifier System	50

4.3	Fluid Injection, Core Holder and Pressure	
	Recording Systems	51
4.4	Emulsion Preparation	54
4.5	Properties of the Emulsion	54
	4.5.1 Density	54
	4.5.2 Droplet Size Distribution	55
	4.5.3 Emulsion Stability	55
	4.5.4 Viscosity	56
4.6	Typical Runs	57
	4.6.1 Core Preparation	57
	4.6.2 The Emulsion Flood	57
5.	RESULTS AND DISCUSSION	
5.1	Sand, Core and Emulsion Properties	61
5.2	Steady State Flow Characteristics of Emulsions in a Porous Medium	69
	5.2.1 Reduction of the Core Permeability by Emulsion Flow	72
	5.2.2 Degree of Core Permeability Reduction by Emulsion Flow	72
	5.2.3 Non-Darcy Flow Nature of Emulsions in a Porous Medium	77
5.3	Prediction Techniques for the Degree of Core Plugging	80
5.4	Emulsion Viscosity Correlation	96
5.5	Unsteady State Flow Characteristics of Emulsions in a Porous Medium	98
	5.5.1 Produced Emulsion Concentration Profile	101

5.5.2 Oil Retention in the Porous Medium . . .	106
5.5.3 Pressure Profile	111
5.5.4 Effect of Interrupting the Flow on the Equilibrium of the Flow System	111
5.6 Emulsion Flow Model	112
5.6.1 Emulsion Flow Model	112
5.6.2 N-Fractional Size Emulsion	120
5.6.3 Emulsion Saturation and Concentration Profiles	123
5.6.4 Pressure Profile Predicted Using Model .	127
5.6.5 Applicability, Capability and Deficiencies of the Model	130
6. CONCLUSIONS	134
Recommendations	136
References	137
Appendix A Parameter Evaluation	141
Appendix B Sensitivity Analysis on the Critical Capillary Number	145
Appendix C Experimental Data	148
Appendix D Emulsion Droplet Size Distribution Run 120	170
Appendix E Evaluation of the Constants in the Model	186

LIST OF TABLES

TABLE		PAGE
4.1	Properties of Bon Accord Oil	50
5.1	Core Sand Properties	62
5.2	Core and Emulsion Properties	63
5.3	Droplet Size Distribution - 15 Percent Emulsion Concentration	64
5.4	Droplet Size Distribution - 30 Percent Emulsion Concentration	65
5.5	Permeability of the Core to Emulsion	70
5.6	Fractional Permeability of the Core to Emulsion	71
5.7	Critical d_g/d_p Ratios	81
5.8	Parameter d_g/d_e	85
5.9	Critical Capillary Number	89
5.10	Critical Blockage Parameters	94
5.11	Constants for the Viscosity Correlation	98
5.12	Summary of Pertinent Experimental Data - Unsteady State Flow Characteristic Run	99
5.13	Summary of Experimental Data for Run 129	100
5.14	Best Fit Coefficients for Model 3	118
5.15	Best Fit Coefficients for the N=4 Fractional Sized Emulsion	121
B1	Sensitivity Analysis on the Critical Number	147
C1	Experimental Data - Run 119	152
C2	Produced Emulsion Concentration Profile Run 119	153

C3	Summary of Experimental Data and Coefficients for Model - Run 119	154
C4	Experimental Data - Run 120	157
C5	Produced Emulsion Concentration Profile Run 120	158
C6	Summary of Experimental Data and Coefficients for Model - Run 120	159
C7	Experimental Data - Run 128	162
C8	Produced Emulsion Concentration Profile Run 128	163
C9	Summary of Experimental Data and Coefficients for Model - Run 128	164
C10	Experimental Data - Run 129	167
C11	Produced Emulsion Concentration Profile Run 129	168
C12	Summary of Experimental Data and Coefficients for Model - Run 129	169
D1	Produced Emulsion Droplet Size Distribution - Percentage Each Channel	171
D2	Produced Emulsion Droplet Size Distribution - Percentage of the Inlet Concentration	172
D3	Production History - 4 Fractional Size Emulsion	173
D4	Inlet Emulsion Properties	174
D5	Retained Oil Saturation, Each Channel - Used in the Mathematical Model : Smoothed Data	175
D6	Summary of Experimental Parameters - Each Channel	180

D7	Summary of the Mathematical Model Parameters . .	180
D8	Produced Emulsion Concentration Profile	181
D9	Produced Emulsion Concentration Profile	
	Four Channel Model	185
E1	Pore Model	189

LIST OF FIGURES

FIGURE	PAGE
2.1 Schematic Diagram of an Emulsion Oil Droplet Trapped by Capillarity and a Pore Constriction .	14
2.2 Definition of the Flow Parameters for Linear Flow Geometry Model of Devereux	24
2.3 Possible Mechanisms Leading to a Capillary Factor	26
3.1 Retention Sites	32
3.2 Illustration of the Forms of the Three Kinetic Equations	38
3.3 The Plugging Process at the Inlet End of the Porous Medium	40
4.1 Schematic Diagram of the Experimental Equipment	52
4.2 Schematic Diagram of the Consolidated Sand Core Holder	53
5.1 Droplet Size Distribtuion for the 30% Quality Emulsion	66
5.2 Droplet Size Distribution for the 15% Quality Emulsion	67
5.3 Emulsion Droplet Size Distribtuion	68
5.4 Effective Permeability Versus Flow Rate	75
5.5 Fractional Permeability Versus Flow Rate	76
5.6 Examination of Darcy's Law	79
5.7 Size of Emulsion Droplet Related to Triangular Constriction Sites	83

5.8	Schematic Diagram of the Deformed Emulsion	
	Droplet	87
5.9	Critical Capillary Number for Permeability	
	Reduction	93
5.10	Emulsion Viscosity Correlation - Run 119	97
5.11	Produced Emulsion Concentration - Run 119	102
5.12	Produced Emulsion Concentration - Run 120	103
5.13	Produced Emulsion Concentration - Run 128	104
5.14	Produced Emulsion Concentration - Run 129	105
5.15	Droplet Size Distribution of Produced Emulsion	108
5.16	Pressure Drop Profiles for Runs 119, 120, 128 and 129	113
5.17	Examination of Model 3 - Run 119	114
5.18	Examination of Model 3 - Run 120	115
5.19	Examination of Model 3 - Run 128	116
5.20	Examination of Model 3 - Run 129	117
5.21	Examination of Model 3 for Each Size Range - Run 129	122
5.22	Retained Oil Concentration Profile	124
5.23	Flowing Emulsion Concentration Profile	125
5.24	Pressure Drop Model for Run 129	128
5.25	Illustration of the Form of the New Kinetic Equation	133
C1	Outlet End Concentration : Run 119	151
C2	Outlet End Concentration : Run 120	156
C3	Outlet End Concentration : Run 128	161
C4	Outlet End Concentration : Run 129	166

E1	Relationship Between Plugged Porosity and	
	Permeability	189

NOMENCLATURE

Parameter		Dimensions
A	Cross-sectional area	L^2
b	Blockage Coefficient	-
C_1	Constant in emulsion viscosity equations	-
C_2	Constant in emulsion viscosity equations	-
C_3	Constant in emulsion viscosity equations	-
C_4	Constant of integration in Equation 3.26	-
C_5	Constant of integration in Equation 3.31	-
d_d	Droplet diameter	L
d_e	Deformed diameter of the oil droplet	L
d_g	Grain Diameter	L
d_p	Pore throat diameter	L
$\frac{dP}{dL}$	Pressure gradient	$F L^{-1}$
d_s	Maximum suspension size	L
f_r	Fractional retention	-
f_{rl}	Fractional retention per unit length	L^{-1}
f_{rt}	Fractional retention per unit time	T^{-1}
$f(x)$	Function dependent on the parameters that affect the viscosity	-
$f(\sigma)$	Function of the retained oil saturation	-
G	Function defined in Equation 3.24	-
h	Volume Factor of Sibree (23)	-
H	Plugging coefficient	T^{-1}
H_o	Plugging rate constant	T^{-1}

H_r	Rate at which droplets break away from their capture sites	T^{-1}
j	Counter in Equation 3.40	-
k	Constant in Equations 2.6 and 2.7	-
K	Permeability of the porous medium	L^2
K_f	Fractional permeability	-
K_r	Relative permeability	-
l_d	Dimensionless length	-
L	Length of the porous medium	L
L_d	Droplet length	L
m	Number of C_2H_4O groups in Triton X-100	-
M	Absolute mobility (permeability/viscosity) of the porous media to the external phase with no internal phase in the porous medium	L^2/FT
M_e	Mobility of the external phase during the emulsion flood	L^2/FT
M_i	Mobility of the internal phase during the emulsion flood	L^2/FT
n	Number of size ranges in the emulsion	-
N_c	Capillary Number	-
P	Pressure differential	$F L^{-1}$
q	Flow rate	$L^3 T^{-1}$
Q	Cumulative injected emulsion	L^3
r_d	Radius of particles	L
r_e	Deformed emulsion droplet radius	L
r_m	Maximum emulsion droplet radius	L
r_o	Emulsion droplet radius	L

r_p	Pore throat size	L
r_1	Pore throat size	L
r_2	Upstream oil droplet radius	L
S_o	Oil saturation	-
t	Time	T
t_d	Dimensionless time	-
t_{bt}	Breakthrough time	T
v	Superficial velocity	L T ⁻¹
v_f	Frontal velocity	L T ⁻¹
α	Plugging coefficient ($H_o A \phi / q$)	L ⁻¹
β	Constant in the kinetic Equations 3.13 and 3.14	-
γ	Interfacial tension	F L ⁻¹
γ'	Capillary constant	F L ⁻¹
Γ	Emulsion concentration	-
Γ_i	Emulsion inlet concentration	-
ΔP	Differential Pressure	F
$\frac{\Delta P}{\Delta L}$	Pressure Gradient	F L ⁻¹
ΔL	Length	L
ϵ	ϕ_e / ϕ	-
ϵ_p	Ratio of the plugged porosity to the total porosity	-
ϵ'	Dielectric constant of the dispersion medium	-
$\bar{\epsilon}$	Average value for ϵ in the emulsion front	-

ζ	Electrokinetic potential of the charged particles in the emulsion	-
θ	Contact angle	-
θ_1	Contact angle at the leading edge of the droplet	-
θ_2	Contact angle at the trailing edge of the droplet	-
μ	Viscosity	FT
μ_e	Emulsion viscosity	FT
μ_{ex}	Viscosity of the external phase	FT
μ_i	Viscosity of the internal phase	FT
μ_w	Water viscosity	FT
ν_e	Emulsion kinematic viscosity	$L^2 T^{-1}$
ν_w	Water kinematic viscosity	$L^2 T^{-1}$
κ	Electrical conductivity	-
λ	Constant in Equation 5.11	-
σ	Retained (plugged) oil saturation	-
σ_m	Maximum retained oil saturation	-
τ	Retention age ($t - L/v_f$)	T
ϕ	Porosity	-
ϕ_e	Porosity through which the emulsion is flowing	-
Ψ	Length on Figure 5.8	L

CHAPTER 1

INTRODUCTION

1.1 BACKGROUND

In the oil industry, it has been known for many years, from as early as the 1942 patent of Subkow (1), that emulsion formation within the reservoir can improve oil recoveries. Since that time, a number of researchers (2) - (6) have reported a significant increase in oil displacement efficiency as a result of in situ emulsification during water and caustic floods.

Besides the possibility of naturally forming an emulsion within the formation matrix, a number of processes directed towards increasing oil recovery efficiencies by injecting externally produced emulsions, have been patented (7) - (9). McAuliffe (10) has reported the results of the only emulsion flood field test conducted. The wells in this test showed improved oil recoveries and lower water-oil ratios, than the wells in the surrounding conventional waterflooding patterns.

Initially, interest in emulsions was primarily related to obtaining a clearer understanding of caustic flooding. This process was recently reviewed by Johnson (11). He discussed the four principal mechanisms for caustic flooding:

- 1) Emulsification and Entrapment
- 2) Emulsification and Entrainment
- 3) Wettability Reversal (water-wet to oil-wet)

4) Wettability Reversal (oil-wet to water-wet)
of which three involve the formation and flow of emulsions.

More recently, comparisons and investigations on caustic, acid, water and emulsion floods of viscous oil formations has received some attention (12) - (14). The work of Farouq Ali et al (14) showed that emulsion slugs were more effective in recovering oil than caustic or acid slugs, or continuous water injection. D'Elia and Ferrer (13) and McAuliffe (12) both reported improved recoveries of emulsion floods over waterfloods.

Emulsion and caustic flooding methods have proven to be more effective than conventional non-thermal methods of recovery for moderately viscous oils, because they can in part overcome the three main factors responsible for low recoveries, which are:

- 1) the unfavourable mobility ratio,
- 2) the adverse surface and interfacial forces between the oil, water and formation matrix and
- 3) the poor sweep efficiency obtained during flooding.

Principally emulsion flooding, as an oil recovery process, has an application in only certain types of heavy oil reservoirs. The prime candidates are thin, relatively deep, high permeability formations, containing moderately viscous oils. In such situations, thermal recovery may not be feasible in view of depth and small thicknesses. Another candidate is one where the oil formation is underlain by a water bearing sand (14).

Although extensive work has been carried out on the oil recovery efficiency of caustic and emulsion floods, relatively little has been published on specific aspects of emulsion flow in a porous medium. Thus if the processes of emulsion and caustic flooding are to be carried out economically, the properties of the emulsion and the porous medium, and more importantly, the effects of these properties on the flow of emulsions through a porous medium must be clearly defined.

With a better understanding of emulsion flow, justifiable engineering decisions could be made to improve oil production. A mathematical model for emulsion flow could also be incorporated into reservoir simulators to obtain more reliable estimates of such processes as caustic and steam flooding. The end result of the improved knowledge should be to improve the oil recovery efficiency.

1.2 PURPOSE OF THE STUDY

The study of the flow of macroemulsions through a porous medium was the broad objective. Specifically the objectives were:

- 1) to demonstrate that emulsion flow in a porous medium is a non-Darcy flow process, because the degree of pore plugging and thus the permeability of the medium is dependent on the pressure gradient;

- 2) to examine the flow behaviour of an emulsion through various porous media;

3) to examine the change in the droplet size distribution of the produced emulsion as compared to the injected emulsion during emulsion flow;

4) to develop a mathematical model that describes emulsion flow in a porous medium, previously saturated with the external phase of the emulsion. This model assumes that emulsion droplets partially plug off the porous medium and the rate of plugging can be modelled by a rate equation. The coupling of this kinetic equation of plugging with a material balance equation yields a model which predicts the emulsion oil saturation within the porous medium. This type of approach has been successfully used for the flow of suspensions through porous media, a good review of which is given by Herzig, Leclerc and LeGoff (15).

CHAPTER 2

THEORY AND LITERATURE REVIEW

2.1 EMULSION RHEOLOGY

In this study, an emulsion viscosity correlation was used to evaluate the produced emulsion oil concentration,

$$\nu_e = \nu_w (1 + C_1 \Gamma + C_2 \Gamma^2) \quad (2.1)$$

where

ν_e = emulsion viscosity ($\text{mm}^2 \text{ s}^{-1}$)

ν_w = water (external phase) viscosity ($\text{mm}^2 \text{ s}^{-1}$)

Γ = oil (internal phase) concentration (-)

C_1, C_2 = constants (-).

The factors which affect emulsion viscosity are reviewed briefly and the incorporation of these factors in the correlation is described. The review was based on the books of Becher (16) and Sherman (17) and therefore these books should be consulted for the reference to the original papers.

Sherman (18) listed six factors which may affect the rheological properties of an emulsion:

- 1) Viscosity of the external phase (μ_{ex}),
- 2) Volume concentration of the disperse phase (Γ),
- 3) Viscosity of the internal phase (μ_i),
- 4) Nature of the emulsifying agent and the
interfacial film formed at the interface,
- 5) Electroviscous effects and

6) Particle size distribution.

Each of these variables are reviewed individually below.

1) Viscosity of the External Phase

Virtually all emulsion viscosity equations indicate a direct proportionality between the external phase viscosity and the emulsion viscosity. The general form of the relationship is:

$$\mu_e = \mu_{ex} \cdot f(x) \quad (2.2)$$

where

μ_e = emulsion viscosity (Pa.s)

μ_{ex} = viscosity of the external phase (Pa.s)

$f(x)$ = function dependent on other properties which
affect the viscosity (-)

2) Volume Concentration of the Internal Phase

The principle attention of researchers in the field of emulsion viscosity has been directed towards the effect of the volume concentration of the internal phase.

The classic equation relating the viscosity of a suspension with that of the suspending liquid and the volume fraction is that of Einstein (19)

$$\mu_e = \mu_w (1 + 2.5\Gamma) \quad (2.3)$$

This equation is probably only valid for values of Γ less than 0.02. Subsequent workers have attempted to modify Equation 2.3 by introducing a power series in the volume concentration. These take the general form:

$$\mu_e = \mu_w (1 + C_1\Gamma + C_2\Gamma^2 + C_3\Gamma^3 + \dots) \quad (2.4)$$

where

$C_1, C_2, C_3 = \text{constants}$

and C_1 is usually taken to be 2.5, as in Equation 2.3.

Guth, Gold and Simha (20) calculated the value of C_2 on theoretical grounds and arrived at the equation

$$\mu_e = \mu_w (1 + 2.5\Gamma + 14.1\Gamma^2) \quad (2.5)$$

which increases the validity of the equation to a value of Γ of about 0.06.

Oliver and Ward (21), analysing data on model emulsions consisting of suspensions of rigid spheres of varying size distributions, discovered that a straight line relationship existed if $1 - \mu_w/\mu_e$ was plotted versus Γ for values of the volume concentration up to 20 per cent (or slightly higher). Algebraically expressed, this yields

$$\mu_e = \mu_w / (1 - k\Gamma) \quad (2.6)$$

which for low concentrations can be written as:

$$\mu_e = \mu_w (1 + k\Gamma + k^2\Gamma^2 + k^3\Gamma^3 + \dots) \quad (2.7)$$

where $k = \text{constant}$.

Equation 2.7 is a form of Equation 2.4, except that a functional relationship is supposed to exist between the constants.

For emulsions containing more than 50 per cent of the disperse phase, it is generally considered they will show a non-Newtonian behaviour. For such systems, Hatschek (22) derived the equation

$$\mu_e = \mu_w / (1 - \Gamma^{1/3}) \quad (2.8)$$

Sibree (23) in a series of investigations on paraffin-in-water emulsions, found it necessary to modify Hatschek's equation

$$\mu_e = \mu_w / \left\{ 1 - (h\Gamma)^{1/3} \right\} \quad (2.9)$$

where the constant h was termed the volume factor by Sibree. Sibree found that h was nearly 1.3 for a number of oil-in-water emulsions of a variety of particle sizes. From these data it was concluded that the droplets behaved as though they were 30 percent greater in volume than would be expected from the volume concentration.

The majority of the equations found in the literature, some of which are listed above, relating emulsion viscosity and the internal phase concentration, under certain conditions, can be reduced to the power series shown as Equation 2.4.

3) Viscosity of the Internal Phase

The effect of the viscosity of the internal phase was introduced to correct for currents set up within the dispersed droplets under the shearing flow force, under the supposition that the droplet behaves like a fluid rather than a solid particle. This effect was reported by Taylor (24), who extended the hydrodynamic considerations of the classical Einstein relation, Equation 2.2, by assuming that any interfacial film which existed merely transmitted tangential stress from one phase to the other, and arrived at the relation

$$\mu_e = \mu_{ex} \left\{ 1 + 2.5 \Gamma \frac{\mu_i + 2/5 \mu_{ex}}{\mu_i + \mu_{ex}} \right\} \quad (2.10)$$

which can be rewritten as

$$\mu_e = \mu_{ex} \left\{ 1 + \Gamma \frac{5/2 \frac{\mu_i}{\mu_{ex}} + 1}{\frac{\mu_i}{\mu_{ex}} + 1} \right\} \quad (2.11)$$

where μ_i = viscosity of the internal phase.

Therefore according to Taylor's equation, the coefficient in Einstein's equation varies from 1.0 to 2.5 as μ_i / μ_{ex} varies from zero to infinity. The effect of increasing the internal phase viscosity is to increase the viscosity of the emulsion.

Taylor's hydrodynamic theory, that the internal phase viscosity significantly affects the emulsion viscosity, is valid when the droplets behave as liquids. If however, the droplets behave as rigid spheres, then the chemical nature of the disperse phase has a greater effect.

4) Interfacial Film and Emulsifying Agent

The interfacial film may affect the emulsion viscosity by reason of its effect on the internal circulation and/or movement of the droplet.

Toms (25) made an intensive investigation on a series of oil-in-water emulsions to evaluate the effect of changing the emulsifier and emulsifier concentration on the emulsion viscosity. The data were used to calculate the volume factor h of Equation 2.9 and the average value was close to the value of 1.3. Individual variations were

considerable and appeared to be attributable to both a variation in the type of emulsifying agent and the internal phase. Variations in the emulsifier concentration appeared to have a lesser effect.

5) Electroviscous Effect

Smoluchowski (26) reported that particles bearing an electric charge showed a viscosity exceeding that of a similar system of uncharged particles. The contribution of the charge was to increase the viscosity of the emulsion, regardless of the sign of the charge. Taking this effect into account, Smoluchowski extended Einstein's equation to

$$\mu_e = \mu_{ex} \left[1 + 2.5 \Gamma \left\{ 1 + \frac{1}{r_d^2 \kappa \mu_{ex}} \left(\frac{\epsilon' \zeta}{2\pi} \right)^2 \right\} \right] \quad (2.12)$$

where

κ = the specific conductivity of the suspension
(mhos cm^{-1})

ϵ' = the dielectric constant of the dispersion
medium (coulomb volt $^{-1}$ cm^{-1})

ζ = the electrokinetic potential of the charged
particles (volts)

r_d = the radius of the particles (cm)

6) Particle Size Distribution

Richardson (27) concluded from his studies that the apparent viscosity of emulsions, having the same concentration and the same size distribution about a mean

droplet diameter, was inversely proportional to the mean droplet diameter. The observed viscosity variations, of a concentrated emulsion, with concentration and rate of shear can be explained in terms of the work done in distorting the droplets and sliding them past each other.

Roscoe (28) obtained two modified forms of the Einstein equation, one of which applies to systems in which the particle size distribution is broad

$$\mu_e = \mu_w (1 - \Gamma)^{-2.5} \quad (2.13)$$

and one for sharply-distributed emulsions

$$\mu_e = \mu_w (1 - 3.5\Gamma)^{-2.5} \quad (2.14)$$

Equation 2.13 is applicable over all concentration ranges.

Equation 2.14 is appropriate at high concentrations, but for concentrations of Γ below 0.05 the Einstein equation applies to such sharply-distributed systems.

The work of Sherman (29) showed, that for water-in-oil emulsions and high concentration oil-in-water emulsions, that the emulsion viscosity decreased with an increase in the mean droplet size. However, for lower concentration oil-in-water emulsions, the emulsion viscosity was independent of the droplet size.

In summary, the factors of:

- 1) the viscosity of the external phase and
- 2) the volume concentration of the internal phase can be accounted for with an equation of the type

$$\mu_e = \mu_w (1 + C_1\Gamma + C_2\Gamma^2) \quad (2.15)$$

The factors of

- 3) the viscosity of the internal phase,
- 4) the interfacial film and emulsifying agent,
- 5) the electroviscous effect and
- 6) the particle size distribution

have been shown to affect the constants in the Einstein and power series models. Therefore on defining the oil and emulsifier for the system, the effects of the above four factors can be incorporated into the constants of the model.

During an emulsion flood the emulsion parameters

- 1) emulsifier concentration,
- 2) particle size distribution and
- 3) emulsion internal phase concentration

will vary with position and time. The first two parameters are expected to have only a small effect on the emulsion viscosity for a low concentration ($\Gamma = 0.15$) oil-in-water emulsion. Therefore a correlation of the type

$$\mu_e = \mu_{ex} (1 + C_1 \Gamma + C_2 \Gamma^2 + C_3 \Gamma^3) \quad (2.7)$$

can be used to evaluate the produced emulsion concentration from its viscosity, because the variable which has the most significant effect on the emulsion viscosity during a flood, is the concentration of the disperse phase.

In this study, the correlation was defined in terms of the kinematic rather than the dynamic viscosity because this was the parameter measured. This also removed the necessity of measuring the density of the produced emulsion. The general model

$$\nu_e = \nu_w (1 + C_1 \Gamma + C_2 \Gamma^2 + C_3 \Gamma^3) \quad (2.16)$$

was compared with the experimental data and it was found that Equation 2.1 could provide a good correlation.

2.2 A CONCEPT OF EMULSION FLOW

A concept required in dealing with emulsion flow in a porous medium may be examined by considering a single droplet of oil in the emulsion entering a pore constriction of smaller diameter, schematically illustrated in Figure 2.1. The leading edge has a smaller radius than that portion of the droplet still in the pore, thus the capillary pressure is greater at the front than at the back of the droplet. A pressure differential is required to force the droplet through the constriction. The pressure differential is given by the equation

$$\Delta P = 2 \gamma \cos \theta \left\{ \frac{1}{r_1} - \frac{1}{r_2} \right\} \quad (2.17)$$

where

ΔP = pressure differential (Pa)

γ = interfacial tension between the oil and water
(N/m)

θ = contact angle (-)

r_1 = pore throat radius (m)

r_2 = upstream oil droplet radius (m)

Thus if the pressure differential across the droplet is greater than ΔP , then the oil droplet will deform and pass through the constriction. If however, the pressure

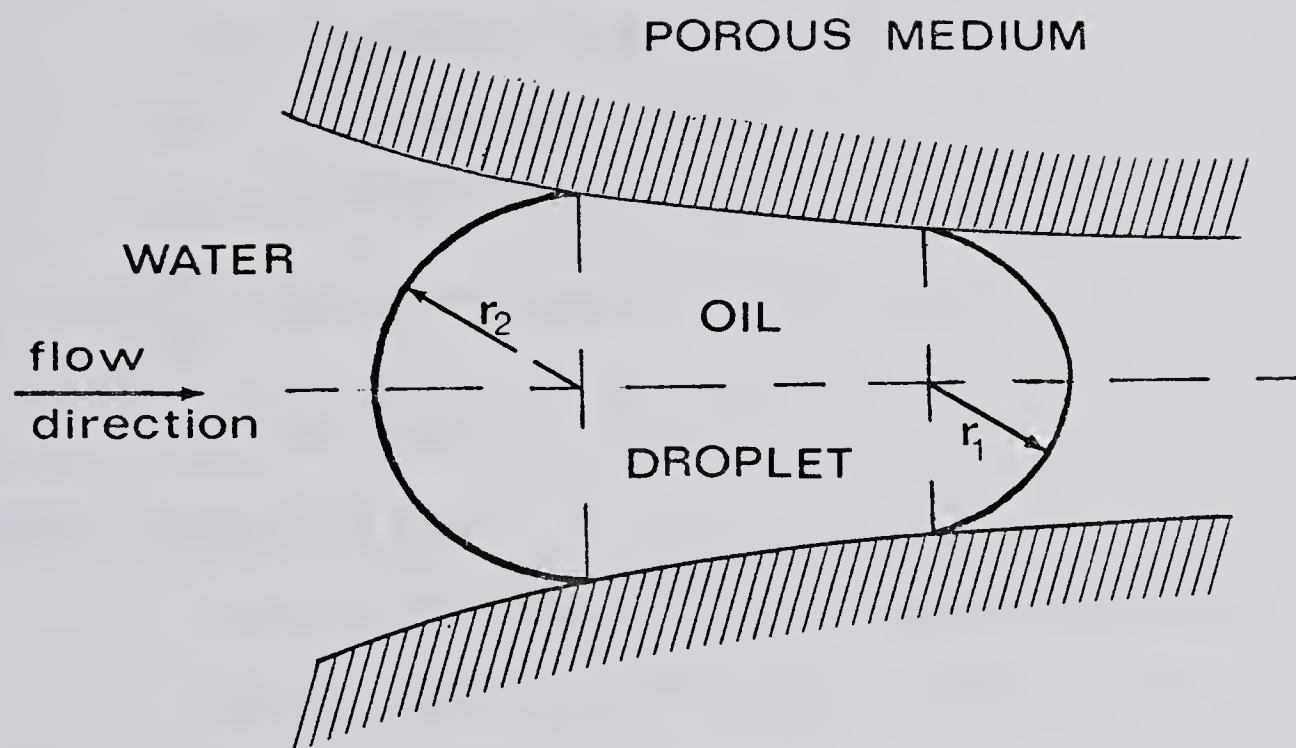


FIGURE 2.1 SCHEMATIC DIAGRAM OF AN EMULSION OIL DROPLET TRAPPED BY CAPILLARITY AND A PORE CONSTRICTION

differential is less than ΔP , then the oil droplet will plug the pore constriction. This describes the basis for permeability reduction of the porous medium by emulsions.

Conditions conducive to pore plugging and permeability reduction can be implied from Equation 2.17 and Darcy's Law

$$q = \frac{K A}{\mu} \frac{dP}{dL} \quad (2.18)$$

where

q = volumetric flowrate (cm^3 / s)

K = permeability (cm^2)

A = cross-sectional area (cm^2)

$\frac{dP}{dL}$ = pressure gradient (Pa / cm)

μ = viscosity (Pa.s).

These conditions are:

- 1) the oil droplets within the emulsion should be larger than the pore throat constrictions in the porous medium,
- 2) a higher interfacial tension between the water and oil will favour the blockage of the pore constrictions,
- 3) the flow rate has to be less than some critical value in order that the pressure differential acting across the droplet is less than ΔP , thus allowing plugging and
- 4) for emulsions with the same maximum droplet sizes

and interfacial properties and flowing at the same rate, the emulsion with the lower viscosity will favour plugging because the pressure gradient will be lower for such systems.

The 'non-Darcy' flow concept of emulsion flow, described by McAuliffe (12) as 'pseudo non-Newtonian', may be explained by examining Equation 2.17. At lower pressure gradients, the average pore size which can be plugged will be larger and the pore volume plugged or isolated within the core will also increase. Due to the increase in the pore volume unavailable for fluid flow, the permeability of the core will be reduced; thus the core permeability is a function of the pressure gradient. The dependence of the permeability on the pressure gradient makes emulsion flow a 'non-Darcy' flow process.

A topic allied to emulsion flow is the mobilisation of ganglia and its influence on the oil recovery process. Both processes involve understanding oil droplets and their flow behaviour through constrictions. Two of the critical properties are the maximum oil droplet size and the minimum pore constriction size. These dimensions determine the maximum pressure gradient necessary to mobilise an oil ganglia and the maximum pressure gradient below which plugging will occur in emulsion flow. More work has been carried out on the mobilisation of ganglia (30) - (35) than on emulsion flow. A useful concept relating the capillary number necessary to mobilise oil

droplets, has been developed (30) - (34). The application of this type of concept for describing emulsion flow is discussed in Section 5.3 of this study.

2.3 REVIEW OF EMULSION FLOW CHARACTERISTICS

McAuliffe's laboratory work (12) showed that oil-in-water emulsions could effectively reduce the water permeability of sandstone cores when the initial water permeability was less than two darcies. The permeability reduction was retained even when the flowing emulsion was followed by many pore volumes of water.

McAuliffe further showed that the degree of permeability reduction increased with an increase in oil droplet size and decreased with an increase in the pressure differential. He described the flow of oil-in-water emulsions through a porous medium as 'pseudo non-Newtonian', regardless of the emulsion concentration.

Results on the flow of an oil-in-water emulsion through three cores of different permeabilities (1460, 595 and 395 md) mounted in parallel, showed that the core permeabilities were reduced by factors of 35, 21 and 12 times, respectively. The results of this experiment also showed that initially a large amount of emulsion entered the more permeable core. As this occurred, the flow became more restricted and the emulsion began to flow into the less permeable cores. Eventually the same number of pore volumes passed through each core, resulting in an

improvement of the displacement or pore volume sweep efficiency. A further observation of this experiment was that, apparently, emulsified oil is much more efficient at reducing the permeability of the core than is oil left after waterflooding.

McAuliffe's results also showed that oil-in-water emulsions displaced oil from sandstone core material more efficiently than did water alone. McAuliffe believed this was due to a correction of heterogeneity of the porous medium.

McAuliffe (10) reported the results of an emulsion flood field test which was conducted to see if oil-in-water emulsions would reduce channeling from injection to producing wells. A conclusion of the field test was that the emulsified oil decreased fingering and increased volumetric sweep efficiency. These results were based on the following observations:

- 1) increased oil production and lower WOR's from the wells surrounding the emulsion treated injectors, compared with little or no increase in oil production and increasing WOR's in the surrounding conventional waterflooding patterns,
- 2) production of a greater proportion of saline formation water from several wells after emulsion injection, indicating a decrease in the injection-water channeling and
- 3) a favourable change in the flood pattern after

emulsion injection, as suggested by radioactive tracer analysis.

The work of Uzoigwe and Marsden (36) showed that no flow restriction occurred when an oil-in-water emulsion was flowed through glass bead packs. This was probably because the pore throats in the unconsolidated glass bead pack were larger than the maximum size of the oil droplets.

Alvarado (37) reported that for the conditions of his study, oil-in-water emulsions would reduce the core permeability. Over the flow rates investigated, 312 - 1116 ft/day, the reduction was independent of flow rate and pressure gradients and thus the flow of emulsions was classified as a Darcy flow process. At these rates, the pressure drops varied from 26 - 150 psi/ft. Both the flow rates and the pressure drops were much higher than those at normal field conditions, which are of the order of 1 ft/day and 1 - 5 psi/ft.

Alvarado further reported that permeability reduction increased with emulsion concentration, which conflicts with the results described in Section 2.2. Permeability reduction should increase with a decrease in the emulsion viscosity and thus a decrease in the concentration. However, Alvarado's observation was based on studies where the core permeability was different for each experiment. The core permeability was higher for higher emulsion concentrations. As McAuliffe has already shown that permeability reduction is a function of the core permeability, it is believed that

Alvarado's observation is invalid as two parameters were varied simultaneously.

Cartmill (38) carried out experiments on the flow of oil-in-water emulsions to establish if oil migrates through the reservoir sands in the form of an emulsion. He found retention of the oil at the interface between the coarse and fine media in the core packs, and as a consequence, the permeability of the porous medium was reduced. Since the size difference between the $1\frac{1}{2}$ micron oil droplets and the porous media of 37 - 88 microns was substantial, he reasoned that electrostatic, rather than capillary forces, were the cause of the oil accumulation.

Devereux (39) showed that the amount of oil retained in a porous medium during emulsion flooding decreased as the pressure differential increased. Also over the range of emulsion concentrations (0.001 - 0.05) and pressure differentials (8 - 100 psi/ft) studied, the retained oil concentration increased with an increase in the inlet emulsion concentration for the pressure range from 8 - 40 psi/ft. For the pressure range from 60 - 100 psi/ft, the retained oil concentration passed through a maximum at an emulsion concentration of 0.01.

The results of Devereux also showed that for, low oil concentration emulsions, the oil saturation front moved through the core at a slower velocity than the injection velocity, because the oil saturation within the invaded region was much higher than the injected emulsion

concentration.

The general flow characteristics of emulsion flow are reviewed above, the consequences of which are listed below:

- 1) emulsions are more efficient at displacing oil than either water, caustic or acid displacing agents,
- 2) emulsion flooding improves the volumetric sweep efficiency and decreases fingering (10) and
- 3) the 'non-Darcy' flow nature is an advantage when an emulsion is injected into an oil reservoir, where the largest change in pressure for a unit distance occurs near the wellbore. As the pressure drop per unit distance decreases logarithmically with distance from the injection well, emulsions can be injected into the formation easily and will be most effective in reducing the permeability at some distance away from the wellbore (10).

2.4 EMULSION FLOW MODELS

Two models for emulsion flow in a porous medium were found in the literature. The model of Spielman and Goren (40) is related to the coalescence and flow of an emulsion in a porous bed, and is specifically related to oil-water separators. As such it will not be discussed further in this thesis.

The model of Devereux (41) is related to the flow of an oil-in-water emulsion in a porous medium previously

saturated with water. Devereux derived an equation for the one-dimensional flow of an emulsion in a porous medium and the relationship found is as follows:

$$\frac{t}{L \phi S} = \left\{ \frac{M - M_i - M_e}{M_i (M - M_e) \gamma'} \right\} \frac{Q \Gamma}{L \phi S_o} - \left\{ \frac{M M_i \gamma' + (M - M_i - M_e) MP/L}{M_i (M - M_e)^2 \gamma'^2} \right\} \times \ln \left\{ \frac{1 - \frac{(M - M_e) \gamma'}{MP/L - M_e \gamma'}}{\frac{Q \Gamma}{L \phi S_o}} \right\} \quad (2.19)$$

where

t = time (seconds)

L = length of solid (cm)

ϕ = porosity (-)

S_o = oil saturation in the invaded region (-)

M = absolute mobility (permeability / viscosity)
of the porous media to the external phase with
no internal phase in the porous media ($\text{cm}^2 / \text{poise}$)

M_i = mobility of the internal phase during the
emulsion flood ($\text{cm}^2 / \text{poise}$)

M_e = mobility of the external phase during the
emulsion flood ($\text{cm}^2 / \text{poise}$)

γ' = capillary constant (dyn / cm)

Γ = emulsion concentration, volume of internal
phase to volume of emulsion (-)

Q = cumulative injected emulsion per unit cross-
sectional area ($\text{cm}^3 / \text{cm}^2$)

P = pressure differential (dyn / cm)

The pertinent parameters of this model are shown in Figure 2.2. Within the invaded region, the internal phase flows at a rate q_i , with mobility M_i and the external phase flows at a rate q_e , with mobility M_e . Beyond this region, the external phase flows at a rate q . The saturation is presumed to have a uniform value of S_o in the invaded region, changing discontinuously to zero in the uninvaded region. The model assumes incompressibility and absence of gravitational effects but capillary effects were not neglected.

The driving force for flow of the internal phase was assumed to consist of the pressure gradient in the external phase minus a retarding force due to capillary effects. The retarding force was attributed to three phase (internal phase, external phase and solid) contact and this may represent:

- a) contact angle hysteresis for an emulsion droplet moving through an essentially cylindrical capillary,
- b) variation in the length of advancing versus receding contact line for a droplet moving through a pore of varying cross section with whose walls it forms a well-defined contact angle, or
- c) increase in surface area due to deformation of a drop moving through a pore of varying cross section with which it forms no contact.

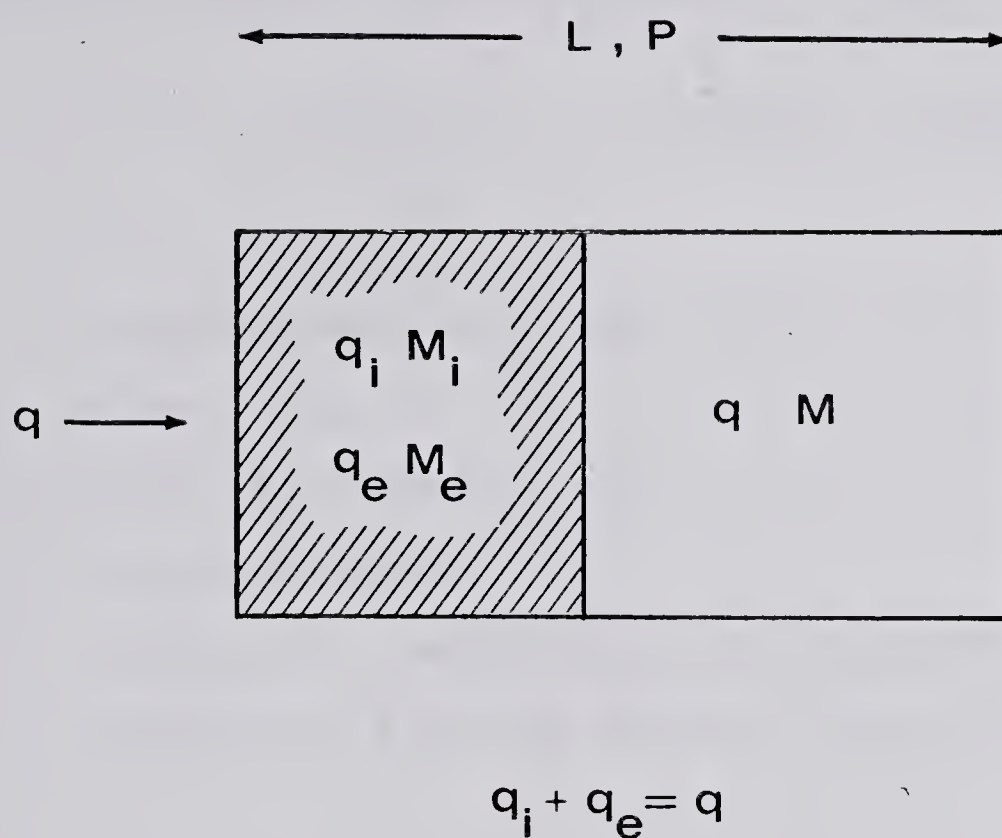


FIGURE 2.2 DEFINITION OF THE FLOW
PARAMETERS FOR LINEAR
FLOW GEOMETRY MODEL
OF DEVEREUX

These three effects are shown schematically in Figure 2.3. The capillary factor is thus a summation of several effects which cannot be expressly calculated. Simple expressions can be used to calculate the typical contributions of the suggested models to the capillary factor. The capillary force due to contact angle hysteresis is given by

$$\gamma' = \frac{6 S_o d' \gamma}{d_d} (\cos \theta_1 - \cos \theta_2) \quad (2.20)$$

where

γ = surface tension (dyn / cm)

d' = pore diameter (cm)

d_d = droplet diameter (cm)

θ = contact angle (-)

1 = refers to leading edge of the droplet

2 = refers to trailing edge of the droplet

The assumptions made in the derivation of the model were:

- 1) the emulsion does not coalesce, or adhere to the solid surface,
- 2) M_i , M_e and γ' are functions only of saturation S_o ,
- 3) the saturation is invariant in time and
- 4) the pressure differential across the system was invariant in time.

The consequences of the assumptions described above are:

- 1) that plugging of the medium is not incorporated in the model, as all of the oil phase is assumed to be mobile,

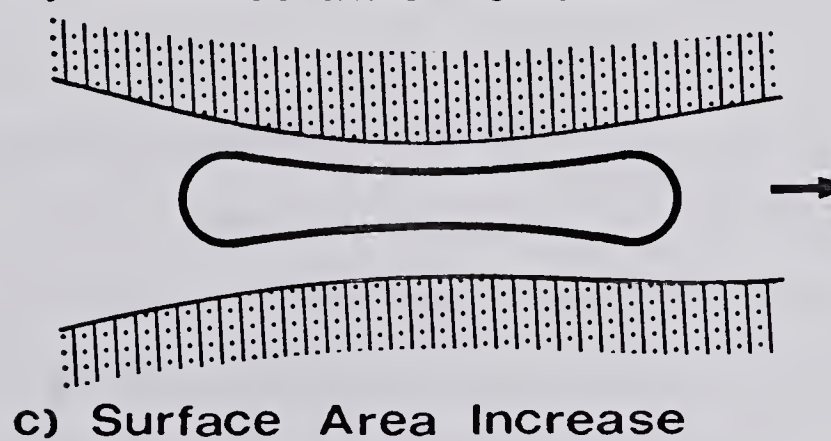
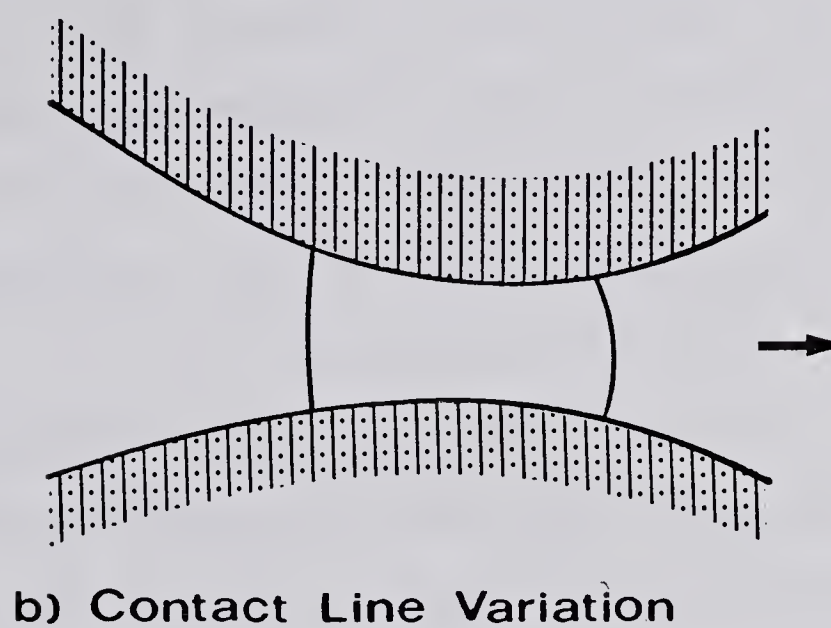
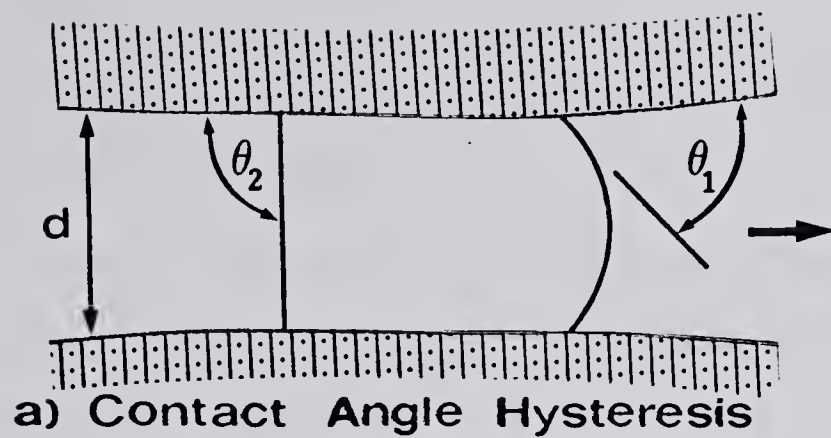


FIGURE 2.3 POSSIBLE MECHANISMS
LEADING TO A CAPILLARY
FACTOR

- 2) the oil saturation front is treated as a moving boundary, rather than as a front with a saturation distribution.

With all the physical data known or recorded, the three constants M_i , M_e and γ' were then fitted to the experimental data using a least squares method. The flow model was a good exhibit of the results for high pressure, low emulsion concentration systems. The model did not fit the behaviour for a high emulsion concentration, low pressure system. An explanation for the poor description of the high concentration, low pressure systems was the violation of assumptions 1 and 3 above. Both McAuliffe (12) and Jennings et al (3) have reported that droplets become lodged in pore constrictions, which conflicts with assumption 1. While Devereux reported that the saturation is time dependent and therefore conflicts with assumption 3.

Further, Devereux assumed that all the oil in the invaded region is mobile and contributes to the flow constant. It is more likely that the majority of this oil is lodged within a pore constriction and only a small proportion of the oil is flowing within the core.

Thus the conditions under which Devereux's model provides a good correlation, are the conditions most unlikely to be found in an actual reservoir. Therefore, another concept for emulsion flow needs to be formulated.

CHAPTER 3

EMULSION FLOW MODEL

3.1 INTRODUCTION

At present, immiscible displacement theory is based upon Darcy's Law for multiphase flow, an equation defining capillary pressure and the conservation of mass in the porous medium. This formulation was originally derived for the non-capillary, two phase flow model of waterflooding by Buckley and Leverett (42) and has since been extended to predict other flooding processes such as miscible flooding (43).

Inherent in the Buckley-Leverett solution and subsequent numerical solutions of the immiscible displacement equation, is that one or both of the effective permeability - saturation and the capillary pressure - saturation relationships must be known. This formulation requires experimentally determined properties and/or mathematical models for the above relationships. Due to these inherent uncertainties and the problem of defining the fractional flow equation for emulsion flow, it was felt that a further extension of their theory to predict emulsion flow was not feasible and a new concept for emulsion flow would need to be formulated.

For this new theory it was assumed that the plugging of the porous medium by oil droplets could occur and that the rate of plugging could be modelled by a rate equation. The combination of this rate equation and a material balance

equation, was analytically solved and resulted in a one-dimensional saturation profile for emulsion flow in a porous medium, previously saturated with the external phase of the emulsion.

3.2 MATERIAL BALANCE EQUATION

It is assumed that both the water and oil phases are incompressible and therefore a volume balance, rather than a mass balance, could be carried out over the core.

Having assumed that oil droplets can plug off pore constrictions, then two types of oil might be assumed to exist in the core:

- 1) stationary oil, plugged within pore constrictions and
- 2) moving oil, within the flowing emulsion.

Considering a porous medium of length ΔL , area A and porosity ϕ , the expression

$A \Delta L \phi \sigma$ represents the volume of retained or plugged oil and

$A \Delta L \phi_e \Gamma$ represents the volume of flowing oil within the emulsion,

where

σ = volume of retained (plugged) oil per unit pore volume (-)

Γ = emulsion concentration (-)

ϕ_e = porosity through which the emulsion is flowing (-)

Associated with the retained, immobile oil droplets, is a volume of immobile water given by

$$\phi A \Delta L (b - 1) \sigma$$

where b = a blockage coefficient defined as

$$\frac{\text{volume immobile oil} + \text{volume immobile water}}{\text{volume of immobile oil}}$$

such that

$$\phi = \phi_e + b\sigma \quad (3.1)$$

The general volume material balance is given by

$$\frac{\partial}{\partial t} \left[A (\phi \sigma + \phi_e \Gamma) \right] + \frac{\partial}{\partial L} [q \Gamma] = 0 \quad (3.2)$$

where q = volumetric emulsion flow rate (cc/hr).

For a constant flow rate experiment, Equation 3.2 simplifies to

$$\frac{\partial [\sigma + \epsilon \Gamma]}{\partial t} + \frac{q}{A \phi} \frac{\partial \Gamma}{\partial L} = 0 \quad (3.3)$$

which can be written

$$\frac{\partial S_o}{\partial t} + \frac{q}{A \phi} \frac{\partial \Gamma}{\partial L} = 0 \quad (3.4)$$

where $\epsilon = \phi_e / \phi$

S_o = oil saturation, total volume of oil per unit pore volume (-)

3.3 PLUGGING MECHANISMS - THE KINETIC EQUATION

Unlike the material balance equation, the form of the rate equation is unknown and has to be derived from actual

experimental data. Before discussing the possible forms of the rate equation, the various oil retention sites and capture mechanisms will be considered.

The most likely retention site for larger particles, described in Section 2.2, is the constriction site, where the droplet is captured by capillarity when the pressure differential is not sufficient to squeeze the droplet through the pore constriction. Another likely retention site, is a dead end cavern site behind a plugged constriction site.

The results of Cartmill (38) showed that small particles tend to collect on the solid surface and to each other, whenever the pore diameter of the porous medium was abruptly reduced. The suggested reason for the oil accumulation was electrostatic forces rather than capillary forces. These long chains and clusters of droplets, formed by agglomeration and flocculation, were found on the surface and crevice sites. A schematic diagram showing each of these retention sites is given in Figure 3.1.

In emulsion flooding, as in waterflooding, the flood can be divided into three zones:

zone 1 : behind the front, where the retained oil saturation has reached its maximum value σ_m , and the emulsion is flowing with the inlet concentration Γ_i . In this zone the pressure gradient is constant in a linear flow system and the highest in the emulsion flow system.

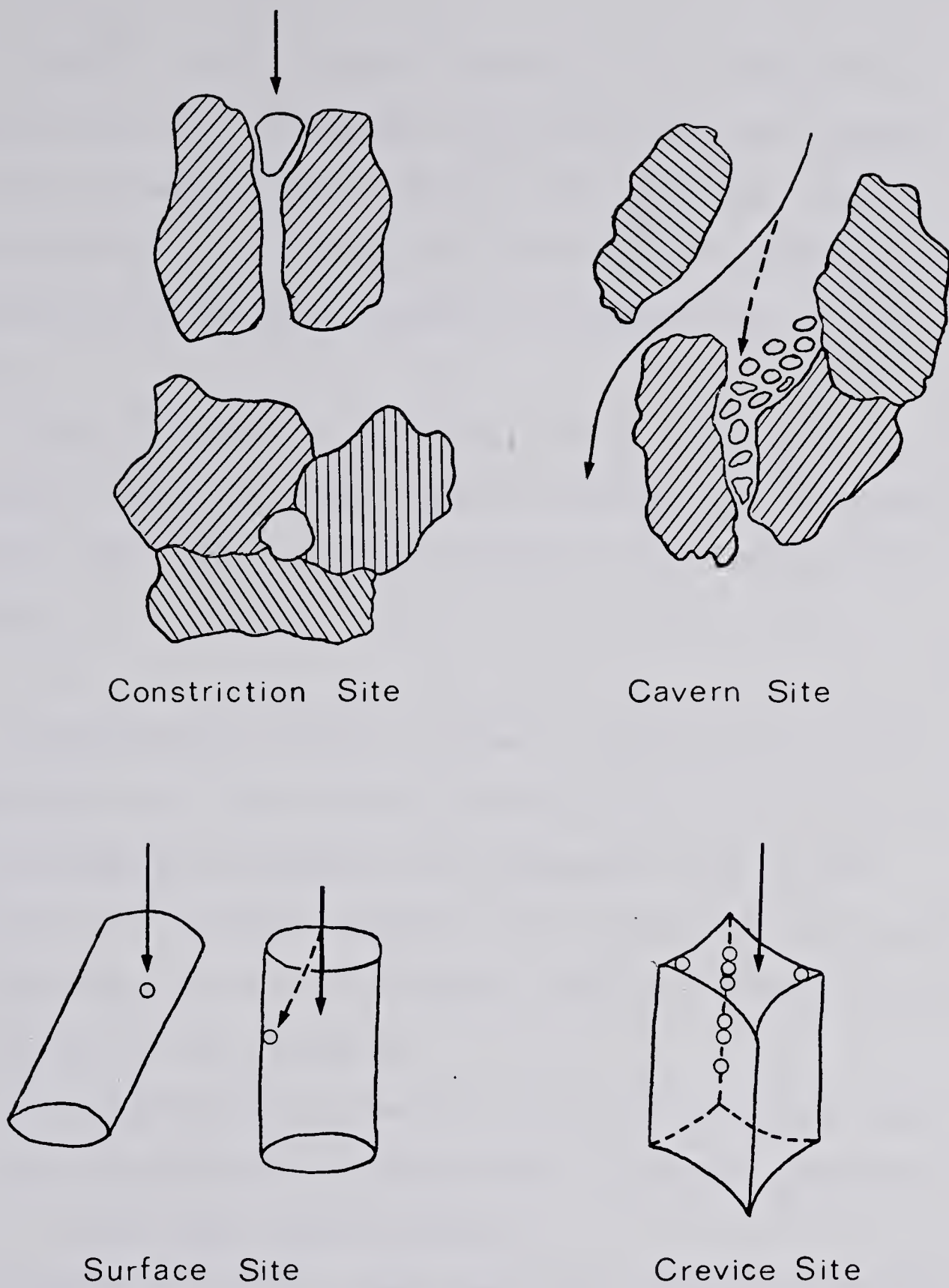


FIGURE 3.1 RETENTION SITES

zone 2 : in the front, where the oil retained is between zero and its maximum saturation and the flowing emulsion concentration is between zero and the inlet concentration Γ_i . In this zone the pressure gradient increases with distance behind the leading edge of the front.

zone 3 : ahead of the front, where only water is flowing. In this zone the pressure gradient is constant in a linear flow system and the lowest in the emulsion flow system.

Considering a point in time, a droplet may become constricted in a pore throat, then as zone 2 continues to pass through this position, the pressure gradient may increase sufficiently to deform the oil droplet and cause the breaking away of the droplet. Therefore within zone 2, there will be two processes:

- 1) plugging of the medium by the oil droplets and
- 2) the possible breaking away of the oil droplets from their capture sites.

The droplets that break away then flow through the medium, where they may find another pore constriction small enough for capture. Thus within the system there are two types of capture:

- 1) permanent capture : where the droplet becomes constricted and stays there while the system flow rate remains unchanged and

2) semi-permanent capture : where while the pressure gradient is less than the critical, the droplet remains constricted. However when the pressure gradient reaches a critical level, the oil droplet breaks away from the capture site.

Gruesbeck and Collins' data (44) on the entrainment and deposition of fine materials in a porous media substantiated that the above phenomenon does occur.

Modelling the system of permanent and semi-permanent capture would be extremely difficult. Therefore the rate equation proposed in the mathematical model, describes the rate at which droplets find permanent capture sites, with the breaking away of the droplets not being considered. This is the approach taken by Gruesbeck and Collins, although they reported that they could modify their theory to include this stochastic effect.

Although a number of different retention sites and mechanisms for capture may occur within the medium, it is assumed that the fractional retention can be defined by the equation

$$f_r = A \phi \Delta L \frac{\partial \sigma}{\partial t} \frac{1}{q \Gamma} \quad (3.5)$$

and the fractional retention per unit length as

$$f_{rl} = \frac{A \phi}{q \Gamma} \frac{\partial \sigma}{\partial t} \quad (3.6)$$

where the fractional retention is defined as the volume of

oil which becomes plugged in pore constrictions as a fraction of the total oil which entered an element of the porous medium.

The above equation can be defined in terms of unit time rather than length, by introducing the time interval for passage through the unit length, which is $q / A \phi_e$.

Thus

$$f_{rt} = f_{rl} \frac{q}{A \phi_e} \quad (3.7)$$

which after substituting into Equation 3.6 yields:

$$f_{rl} = \frac{1}{\epsilon \Gamma} \frac{\partial \sigma}{\partial t} \quad (3.8)$$

Equations 3.6 and 3.8 can be rearranged to yield

$$\frac{\partial \sigma}{\partial t} = f_{rt} \epsilon \Gamma \quad (3.8)$$

$$\frac{\partial \sigma}{\partial t} = f_{rl} \frac{q \Gamma}{A \phi} \quad (3.6)$$

where f_{rt} and f_{rl} depend on the parameters which characterise the emulsion flow system and particularly on the retention parameter σ . Differential Equations 3.6 and 3.8 are analogous to the classical equations of chemical kinetics and for this reason they can be called the kinetic equations of plugging. In fact, they form one kinetic equation only:

$$\frac{\partial \sigma}{\partial t} = H \Gamma \quad (3.9)$$

where H is called the plugging rate constant and has the

dimensions of time⁻¹ and is a function of the retained oil saturation. The plugging rate constant is related to f_{rt} and f_{rl} by the equation

$$H = f_{rt} \epsilon = f_{rl} \frac{q}{A \phi} \quad (3.10)$$

The parameters which have an effect on the clogging kinetics are:

- 1) the emulsion which is characterised by its viscosity μ_e , flow rate q , the droplet size d_d , and the concentration Γ , and
- 2) the porous medium which is characterised by its permeability K , porosity ϕ , and the grain size d_g . As the bed clogs, the parameters K , ϕ , and H vary with the oil retention σ .

Therefore in general, the rate constant H can be written

$$H = \text{function} (\mu_e, \sigma, \phi, K, q, d_g, d_d, \phi_e)$$

and more specifically

$$H = H_0 f(\sigma) \quad (3.11)$$

where

$$H_0 = \text{function} (\mu_e, \phi, K, q, d_g, d_d)$$

and the parameters of σ and ϕ_e are incorporated into the function $f(\sigma)$.

The form of $f(\sigma)$ is unknown and must be assumed and the resultant emulsion flow model compared with the experimental data. The three forms of $f(\sigma)$ investigated in this study are

$$\text{case 1 : } f(\sigma) = (\sigma_m - \sigma) \quad (3.12)$$

$$\text{case 2 : } f(\sigma) = (\sigma_m - \sigma)(\beta - \sigma) \quad (3.13)$$

$$\text{case 3 : } f(\sigma) = (\sigma_m - \sigma)(\beta + \sigma) \quad (3.14)$$

where β is a constant for the kinetic equation.

An illustration of the forms of the three rate Equations 3.12 - 3.14 are shown in Figure 3.2. For the kinetic Equations 3.12, 3.13 and 3.14 when $\sigma_m < \beta$, the plugging rate is highest at time $t = 0$, when, as yet, no plugging has occurred. With the growth of the plugged constrictions, the rate decreases, reaching a zero value after some time t ; at this point plugging is complete.

The kinetic Equation 3.14, when $\sigma_m > \beta$, assumes that the surface activity of the medium for droplet capture is greater when some plugging has occurred. An explanation for this form of kinetic equation is that cavern sites and dead zones, as well as constriction sites, have been created, thus increasing the number of capture sites. However, the increase is not permanent, with eventually the rate decreasing due to the number of sites available, with the rate reaching zero after some time t .

3.4 INTEGRATION OF THE DIFFERENTIAL EQUATIONS

Although the three kinetic Equations 3.12 - 3.14 are compared in this study, the integration of the differential equations will only be illustrated using Equation 3.14. Only the solutions and assumptions made in solving Equations 3.12 and 3.13 are reported.

The equations to be solved for the unknowns $\Gamma(L, t)$

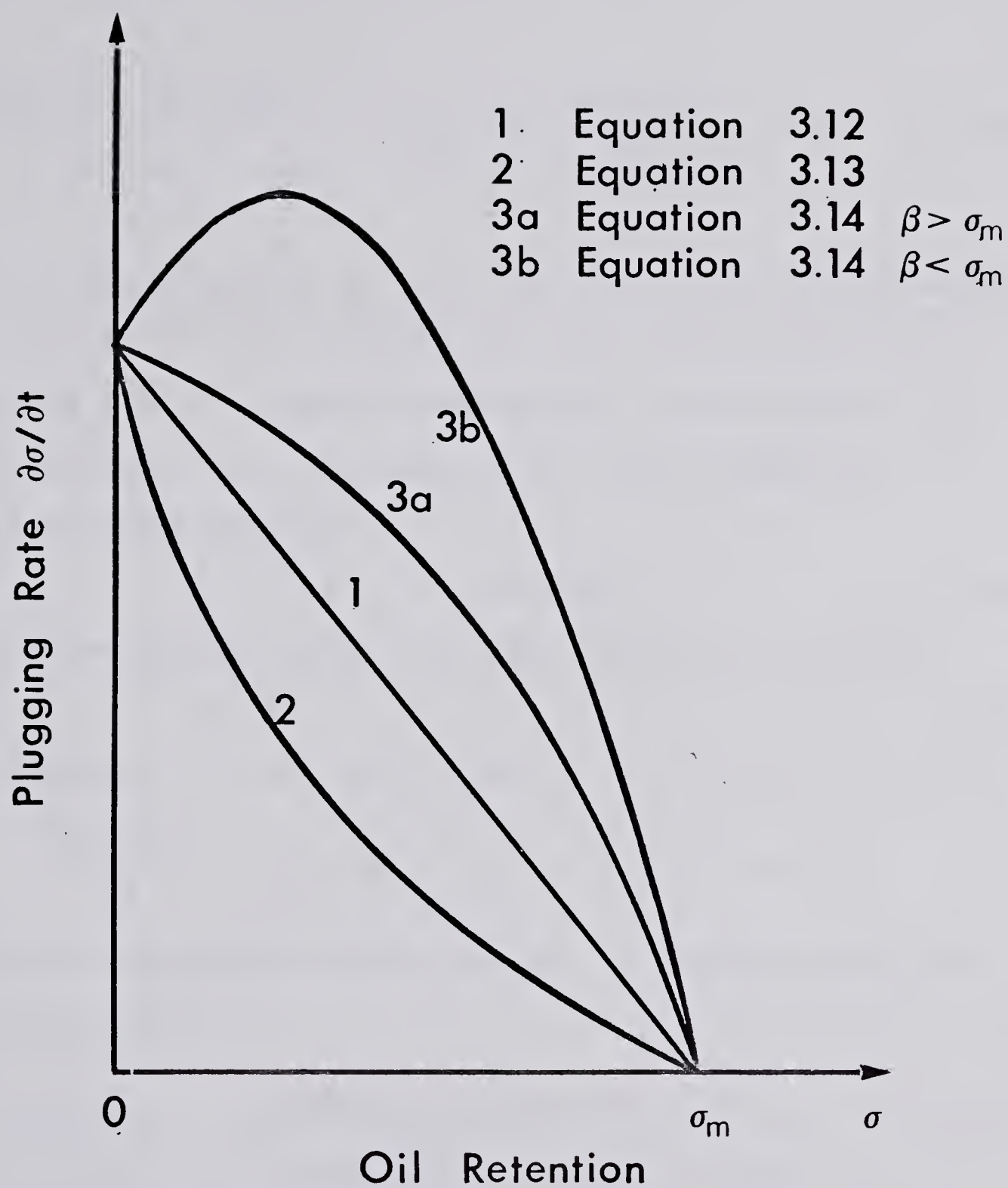


FIGURE 3.2 ILLUSTRATION OF THE FORMS OF THE THREE KINETIC EQUATIONS

and $\sigma(L, t)$ are

$$\frac{\partial \sigma(L, t)}{\partial t} = H_o (\sigma_m - \sigma(L, t)) (\beta + \sigma(L, t)) \Gamma(L, t) \quad (3.15)$$

and

$$\frac{\partial [\sigma(L, t) + \epsilon \Gamma(L, t)]}{\partial t} + \frac{q}{A \phi} \cdot \frac{\partial \Gamma(L, t)}{\partial L} = 0 \quad (3.2)$$

3.4.1 Plugging Process at the Inlet End of the Porous Medium

The form of the plugged oil saturation at the core inlet end ($L = 0$) can be determined from Equation 3.14. For a constant flow rate case, with constant emulsion injection concentration Γ_i

$$\Gamma(0, t) = \Gamma_i = \text{constant} \quad (3.16)$$

and for the porous medium initially saturated with water

$$\sigma(0, 0) = 0 \quad (3.17)$$

then Equation 3.14 can be written as

$$\frac{\partial \sigma(0, t)}{\partial t} = H_o (\sigma_m - \sigma(0, t)) (\beta + \sigma(0, t)) \Gamma_i$$

from which the inlet end plugged oil saturation with time is established:

$$\sigma(0, t) = \sigma_m \frac{\exp(H_o t \Gamma_i (\sigma_m + \beta)) - 1}{\exp(H_o t \Gamma_i (\sigma_m + \beta)) + \sigma_m / \beta} \quad (3.18)$$

A graphical illustration of Equation 3.18 is shown in Figure 3.3. The function demonstrates that the oil saturation at the inlet end of the core does not jump instantaneously to its maximum value when flow begins, but takes some time to reach this value.

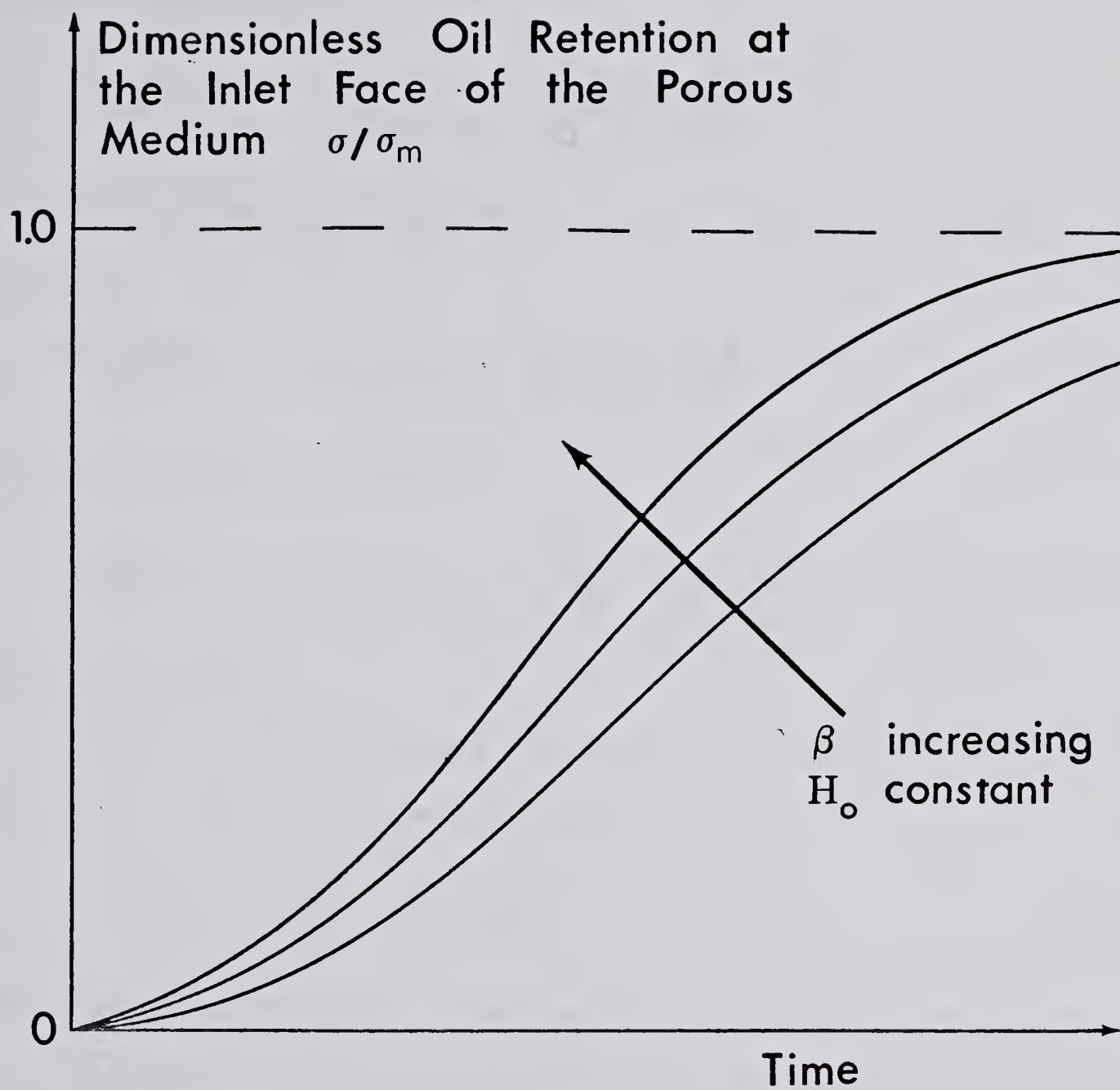


FIGURE 3.3 THE PLUGGING PROCESS AT THE INLET END OF THE POROUS MEDIUM

3.4.2 Solution of the Retained Oil Saturation Equation

Eliminating, in Equation 3.14, the function $\Gamma(L,t)$ and placing the parameter $\sigma(L,t)$ in a differential operator one obtains

$$\Gamma(L,t) = -H_o \frac{1}{[\sigma_m + \beta]} \frac{\partial}{\partial t} \ln \left[\frac{\sigma - \sigma_m}{\sigma + \beta} \right] \quad (3.19)$$

and differentiating Equation 3.19 with respect to time produces

$$\frac{\partial \Gamma(L,t)}{\partial t} = -H_o \frac{1}{[\sigma_m + \beta]} \frac{\partial^2}{\partial t^2} \ln \left[\frac{\sigma - \sigma_m}{\sigma + \beta} \right] \quad (3.20)$$

and with respect to length

$$\frac{\partial \Gamma(L,t)}{\partial L} = -H_o \frac{1}{[\sigma + \beta]} \frac{\partial^2}{\partial t \partial L} \ln \left[\frac{\sigma - \sigma_m}{\sigma + \beta} \right] \quad (3.21)$$

Simplification 1:

Now in order to solve Equations 3.3 and 3.14, Equation 3.3 has to be approximated to

$$\frac{\partial \sigma}{\partial t} + \bar{\epsilon} \frac{\partial \Gamma}{\partial t} + \frac{q}{A \phi} \frac{\partial \Gamma}{\partial L} = 0 \quad (3.22)$$

where $\bar{\epsilon}$ is the average value for the fraction of the pore space occupied by the flowing emulsion within the emulsion front. Without this simplification the equation cannot be solved analytically because in the function $\sigma + \epsilon \Gamma$, ϵ is a function of σ

$$\epsilon = 1 - b\sigma \quad (3.23)$$

The relationship between ϵ , b and σ is unknown. Thus the function $\sigma + \epsilon \Gamma$ is replaced by $\sigma + \bar{\epsilon} \Gamma$ and a solution of

the equation is possible.

Introducing the definition

$$\frac{\sigma - \sigma_m}{\sigma + \beta} = G \quad (3.24)$$

and substituting Equations 3.24, 3.20 and 3.21 into 3.22 one obtains

$$\frac{q}{A \phi} \frac{\partial^2}{\partial t \partial L} \ln G + \bar{\epsilon} \frac{\partial^2}{\partial t^2} \ln G - H_o(\sigma_m + \beta) \frac{\partial}{\partial t} \left[\frac{\sigma_m + \beta G}{1 - G} \right] = 0 \quad (3.25)$$

Integration of Equation 3.25 with respect to time yields

$$\frac{q}{A \phi} \frac{\partial}{\partial L} \ln G + \bar{\epsilon} \frac{\partial}{\partial t} \ln G - H_o(\sigma_m + \beta) \left[\frac{\sigma_m + \beta G}{1 - G} \right] = C_4 \quad (3.26)$$

The constant of integration C_4 is evaluated using the following boundary condition

$$\sigma(L, t) = 0 \quad t < \frac{L}{v_f} \quad (3.27)$$

where $v_f = q / A \phi_e$ = frontal velocity.

This condition states that there is no oil in the core at the position L before the emulsion front has arrived.

Thus for the boundary condition 3.27, C_4 equals zero and Equation 3.26 becomes

$$\frac{q}{A \phi} \frac{\partial}{\partial L} \ln G + \bar{\epsilon} \frac{\partial}{\partial t} \ln G - H_o(\sigma_m + \beta) \left[\frac{\sigma_m + \beta G}{1 - G} \right] = 0 \quad (3.28)$$

A solution to Equation 3.28 in this form is possible, however the resulting equation is too complicated for practical purposes. Thus a simplified solution will be presented which yields a more manageable expression.

Simplification 2:

By linearising the third term in Equation 3.28 around $\sigma(L,t) = 0$ and by introducing the new variable

$$\tau = t - \frac{L}{v_f} \quad (3.29)$$

then Equation 3.28 becomes

$$\frac{q}{A\phi} \frac{\partial G(L,\tau)}{\partial L} - H_o \beta^2 \left(G + \frac{\sigma_m}{\beta} \right) G = 0 \quad (3.30)$$

The integration of Equation 3.30 yields

$$G(L,\tau) = -\sigma_m \left[\beta - C_5 \exp \left\{ -\frac{H_o L A \phi \sigma_m \beta}{q} \right\} \right]^{-1} \quad (3.31)$$

The constant of integration C_5 can be found from Equation 3.18. At $L = 0$, Equation 3.31 becomes

$$\sigma(L,\tau) = \sigma_m (C_5 - \beta)^{-1} \quad (3.32)$$

where from

$$C_5 = \beta \left[1 - \exp \left\{ H_o \Gamma_i (\sigma_m + \beta) \tau \right\} \right] \quad (3.33)$$

On substitution of the expression for C_5 into Equation 3.31 one obtains

$$\sigma(L,\tau) = \sigma_m \frac{\exp t_d - 1}{\exp t_d + \left[1 + \frac{\sigma_m}{\beta} \right] \exp l_d - 1} \quad (3.34)$$

where

$$t_d = H_o \Gamma_i (\sigma_m + \beta) \tau$$

$$l_d = \frac{H_o L A \phi \sigma_m \beta}{q}$$

3.4.3 Solution in Terms of the Flowing Emulsion Concentration

Substituting for $\sigma(L,t)$ and its derivative from Equation 3.34 into Equation 3.15 and solving yields

$$\Gamma(L,\tau) = \Gamma_i \frac{\exp t_d}{\exp t_d + \exp l_d - 1} \quad (3.35)$$

Thus Equations 3.24 and 3.25 are the solutions of the system of Equations 3.3 and 3.15 using the boundary conditions 3.16, 3.17, 3.27 and 3.18 with simplifications 1 and 2.

3.4.4 Comparisons of the Flow Models

The solutions using all three kinetic equations proposed in this study, Equations 3.12, 3.13 and 3.14, are shown below.

$$\text{Kinetic equation} \quad \frac{\partial \sigma}{\partial t} = H_o (\sigma_m - \sigma)(\beta + \sigma)\Gamma \quad (3.14)$$

$$\sigma(L,\tau) = \sigma_m \frac{\exp t_d - 1}{\exp t_d + \left[1 + \frac{\sigma_m}{\beta}\right] \exp l_d - 1} \quad (3.34)$$

$$\Gamma(L,\tau) = \Gamma_i \frac{\exp t_d}{\exp t_d + \exp l_d - 1} \quad (3.35)$$

$$\text{where} \quad t_d = H_o \Gamma_i (\sigma_m + \beta) \tau$$

$$l_d = \frac{H_o L A \phi \sigma_m \beta}{q}$$

$$\text{Kinetic equation} \quad \frac{\partial \sigma}{\partial t} = H_o (\sigma_m - \sigma)\Gamma \quad (3.12)$$

$$\sigma(L, \tau) = \sigma_m \frac{\exp t_d - 1}{\exp t_d + \exp l_d - 1} \quad (3.36)$$

$$\Gamma(L, \tau) = \Gamma_i \frac{\exp t_d}{\exp t_d + \exp l_d - 1} \quad (3.37)$$

where $t_d = H_o \Gamma_i \tau$

$$l_d = \frac{H_o A \phi \sigma_m L}{q}$$

$$\text{Kinetic equation} \quad \frac{\partial \sigma}{\partial t} = H_o (\sigma_m - \sigma)(\beta - \sigma) \Gamma \quad (3.13)$$

$$\sigma(L, \tau) = \sigma_m \frac{\exp t_d - 1}{\exp t_d + \left[1 - \frac{\sigma_m}{\beta}\right] \exp l_d - 1} \quad (3.38)$$

$$\Gamma(L, \tau) = \Gamma_i \frac{\exp t_d}{\exp t_d + \exp l_d - 1} \quad (3.39)$$

where $t_d = H_o \Gamma_i (\beta - \sigma_m) \tau$

$$l_d = \frac{H_o L A \phi \beta \sigma_m}{q} \quad \text{and } \beta > \sigma_m \text{ always}$$

For Kinetic Equation 3.12, only simplification 1 is required, while for Kinetic Equation 3.13 both simplifications 1 and 2 are used. Equations of this type have been derived for the flow of suspensions through porous media (15), (44), (45), (46).

The models stated above are derived for an emulsion consisting of one droplet size, flowing in a linear, homogeneous core previously saturated with water, such that all the droplets in the emulsion have the same probability of capture. The assumption of a linear, homogeneous core was required so that σ_m could be assumed constant along the

core, in order to carry out the integration.

3.4.5 N-Fractional Size Emulsion

An emulsion is generally characterised by droplets of various sizes, the size distribution usually being described by some type of probability distribution, rather than of one narrow size range. Thus the probability of capture for each droplet size is different because there are a greater number of constriction sites available within the core for the larger, rather than smaller droplets.

The above models for the single sized emulsion can thus be extended for a n-fractional sized emulsion by introducing the variables of the system for each size range. The interaction between the droplet sizes is accounted for, as for the permanent semi-permanent capture, by modelling the effective capture rate for each droplet size range.

Extension of the model for Kinetic Equation 3.14 produces

$$\sigma(L, \tau) = \sum_1^j \sigma_{mj} \frac{\exp t_{dj} - 1}{\exp t_{dj} + \left[1 + \frac{\sigma_{mj}}{\beta_j}\right] \exp l_{dj} - 1} \quad (3.40)$$

$$\Gamma(L, \tau) = \sum_1^j \Gamma_{ij} \frac{\exp t_{dj}}{\exp t_{dj} + \exp l_{dj} - 1} \quad (3.41)$$

where $t_{dj} = H_{oj} \Gamma_{ij} (\sigma_{mj} + \beta_j) \tau_j$

$$l_{dj} = \frac{H_{oj} A \phi \beta_j \sigma_j L}{q}$$

and subscript j refers to each fractional size in the emulsion.

3.5 THE EMULSION FLOW MODEL

The equations reported in section 3.4.4 represent the emulsion flow models for the three kinetic equations 3.12, 3.13 and 3.14 using the boundary and initial conditions 3.16, 3.17 and 3.27 and simplifications 1 and 2.

These models assume that the rate of plugging can be modelled by a rate equation and the rate at which the retained oil saturation increases in the system is dependent on the saturation within the system and the concentration of the flowing emulsion. When the coefficients of the model H_0 , β and $\bar{\epsilon}$, have been evaluated from the experimental data, the model can be used to predict the flowing emulsion concentration, Γ and the retained oil concentration, σ profiles within the system at any position and time.

Some of the properties of these models are:

- 1) the models allow the retained oil concentration at the inlet end of the system to increase slowly with time to its maximum concentration. This boundary condition as often proven difficult to define in waterflooding and it is often assumed to jump from zero to the maximum value at the instant flow starts.
- 2) When the plugging rate constant H_0 is large, the model is equivalent to the moving boundary model.

- 3) At early times, the model allows the oil front to move through the porous medium at a velocity greater than the superficial velocity, while at later times, the front can fall behind the position designated by the superficial velocity.
- 4) The shape of the front is controlled by the plugging rate constant H_0 , while the position of the front is controlled by the coefficients $\bar{\epsilon}$ and β .

CHAPTER 4

EXPERIMENTAL EQUIPMENT AND PROCEDURE

4.1 POROUS MEDIA

In this study four types of sandstone porous media were used. The type and general description of each is given below:

1) a 80 - 120 mesh unconsolidated Ottawa sand from Fisher which produced cores of an average porosity of 38%, with a permeability range of 14 - 18 darcies,

2) an unconsolidated Sundance Kinsella sand, which produced an average porosity of 33%, with a permeability range of 155 - 320 millidarcies,

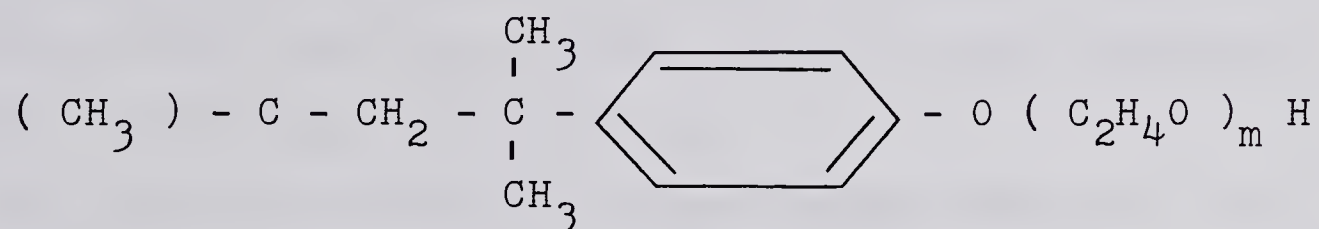
3) an unconsolidated Lloydminster sand, which depending on the average grain size produced an average porosity of 37% and a permeability range of 3.6 - 8.5 darcies and

4) a consolidated Berea sandstone with a porosity of 20% and a permeability of 39 millidarcies.

Due to the quantity of Lloydminster sand available, occasionally the sand had to be cleaned and reused. The sand was initially washed with toluene to remove the oil, then oven dried at 120 °F to evaporate the toluene. Finally the sand was fired at 500 °F for 48 hours to remove any organics which may have been adsorbed onto the sand.

4.2 EMULSION AND EMULSIFIER SYSTEM

The emulsion used in this study was a Triton X-100 surfactant stabilised emulsion of tapwater and Bon Accord oil. Triton X-100 is a water soluble iso-octyl phenoxypolyethoxy ethanol linked to up to ten molecular ethylene oxide units. Its molecular weight is 647 at $m = 10$. Triton X-100 has the formula



where $8 \leq m \leq 10$

and was supplied by Union Carbide and manufactured by Rohm and Haas.

The pertinent properties of Bon Accord oil are summarised in Table 4.1. The viscosities were measured with a reverse flow Cannon-Fenske viscometer, the densities with a Haake Density meter and the interfacial tension with a spinning drop apparatus.

TABLE 4.1

PROPERTIES OF BON ACCORD OIL

Temperature (°F)	70	80	100	120	150
Viscosity (mm ² s ⁻¹)	18.8	15.9	11.2	-	6.0
Density (g/cc)	0.881	0.878	0.870	0.863	0.852
Surfactant Concentration (%)	0	1	2½		
Interfacial Tension (dynes/ cm)	9.0	0.36	0.24		

4.3 FLUID INJECTION, CORE HOLDER AND PRESSURE RECORDING SYSTEMS

A diagram of the flow system is shown in Figure 4.1. Central to the system was a Ruska pump capable of 28 constant rates, varying from 2.5 - 560 cc/hr. Two steel cylinders, one two litre cylinder containing water and a one litre cylinder containing emulsion, were connected to the pump. The pump injected mercury into the cylinder, which in turn displaced the fluid of interest into the core.

The core holder for the unconsolidated sand was a 4.8 cm. I.D. , 30cm long PVC tube with an internal length of 23.2 cm between the end block flanges. The end blocks were made of PVC, contained 400 mesh screens and were attached to the core holder by bolts and sealed with 'O' rings. The internal volumes of the end blocks were known.

The size of the unconsolidated core holder was chosen in order that a number of pore volumes of emulsion could be injected into the core without recharging the pump. The pore volume of the core holder was approximately 170 cc, while the maximum throughput of the pump was 500cc without changing cylinders. This approach was carried out because it was felt, and subsequently established, that stopping and restarting the flow would have a disturbing effect on the conditions within the core.

The core holder for the unconsolidated sand was a rubber sleeve enclosed in a steel vessel, see Figure 4.2. The sleeve was squeezed onto the core by pressuring an oil

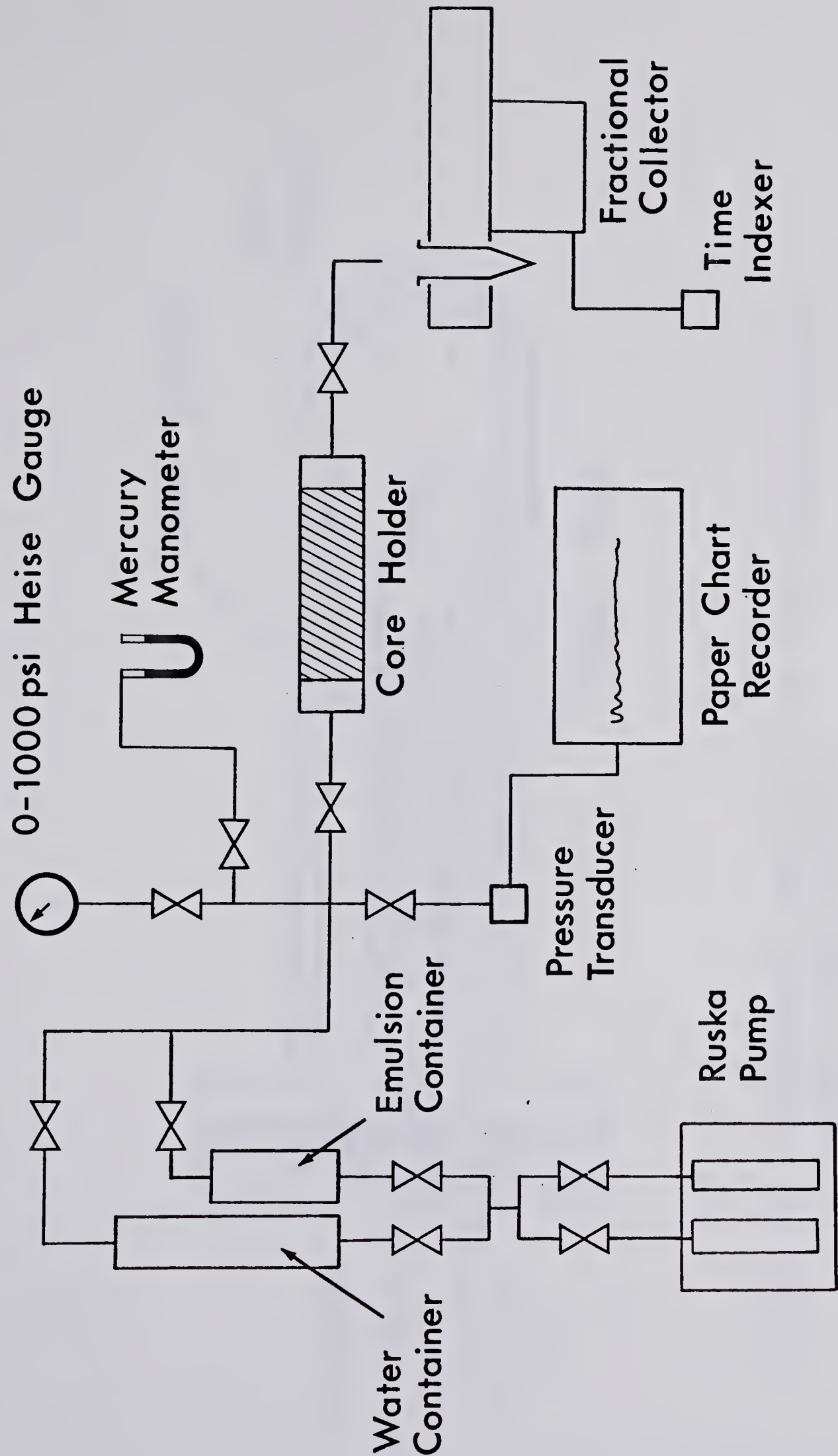


FIGURE 4.1 SCHEMATIC DIAGRAM OF THE EXPERIMENTAL EQUIPMENT

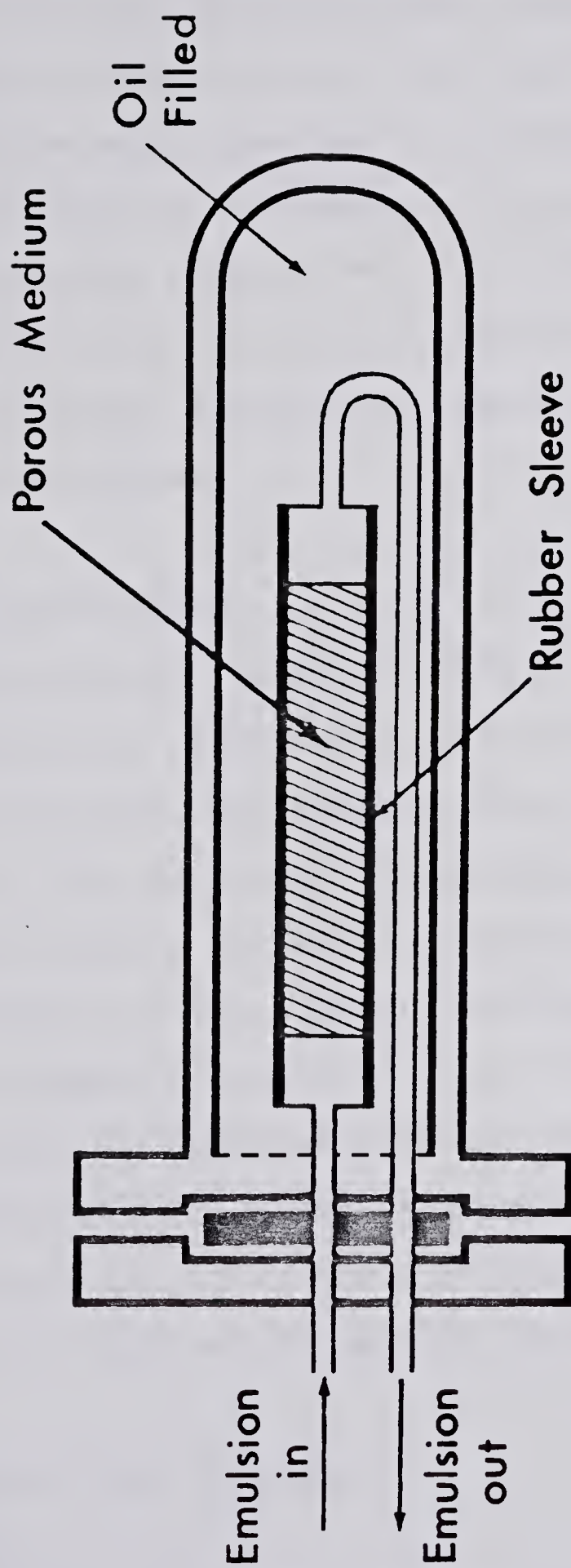


FIGURE 4.2 SCHEMATIC DIAGRAM OF THE CONSOLIDATED SAND CORE HOLDER

enclosed within the vessel.

The pressure drop across the core was measured just prior to the inlet to the core holder. Depending on the expected pressure drop, either a 1000 psi Heise gauge or a mercury manometer was connected to the flowline to provide a direct indication of the pressure. A Validyne differential pressure transducer, either 1, 5, 20 or 1000 psi was also connected to the line to provide a continuous recording of the pressure history. The signals from the transducer were recorded on chart paper.

4.4 EMULSION PREPARATION

The emulsion was prepared in 400 cc batches. Exactly 10 cc of surfactant, constituting 5% of the emulsion prepared in one batch, was added to 270 cc of tapwater and 120 cc of oil. The surfactant concentration used in preparing the emulsion was well in excess of the minimum amount required to obtain a stable emulsion. The whole mixture was subsequently stirred in an Osterizer blender for two minutes. The produced emulsion was then diluted down to the required quality by adding tapwater. In calculating the emulsion quality (Γ), the surfactant Triton X-100 was considered to be part of the aqueous phase.

4.5 PROPERTIES OF THE EMULSION

4.5.1 Density

The density of the emulsion was measured using a

Haake Density meter and was 0.981 g/cc for an emulsion quality of 0.15 and 0.963 g/cc for an emulsion quality of 0.30.

4.5.2 Droplet Size Distribution

The droplet size distribution of the emulsion was measured with a Coulter Counter Model TAIL, using a 130 micron aperture tube. As the measurement of oil-in-water macroemulsion droplet sizes using a Coulter Counter is now a standard procedure and found in a number of papers (12), (36) and (37), the operation of this device will not be described. It will however be noted that the diluent used was Isoton and the procedure used was that described in the Coulter Counter Manual (47). As primary interest was placed on the large droplets in the emulsion, a 130 micron aperture tube was chosen so that the maximum droplet size was measureable within the range of the tube, which was 2.0 - 40.3 microns.

4.5.3 Emulsion Stability

Prior to the emulsion flow study, a preliminary study was carried out to find a stable emulsion by changing the parameters of oil type, surfactant type, concentration and mixing time. During this experiment it was found that the Zeta meter, a device for establishing emulsion stability, gave different conclusions to those from the degree of separation during centrifugation of the emulsion. It was

therefore assumed that for some reason, the Zeta meter was producing erroneous results. Thus no quantitative estimate of emulsion stability was obtained.

For the emulsion used in this study, no oil phase separation occurred over a period of weeks when stored in an air tight container. However, if left open to the atmosphere, within days, oil separated out from the emulsion. When left over a period of time in an air tight container, the emulsion did tend to cream, but it was easily redispersed upon shaking.

4.5.4 Viscosity

The viscosity of the emulsion was measured using a reverse flow Cannon-Fenske viscometer. The viscosity correlations were obtained by accurately diluting down the original emulsion with tapwater to produce a viscosity oil concentration profile, producing the seven data points for $\Gamma = 0.15, 0.12, 0.09, 0.075, 0.06, 0.03$ and 0.0 . Using the seven data points, the viscosity correlation

$$\nu_e = \nu_w (1 + C_1\Gamma + C_2\Gamma^2) \quad (2.1)$$

was fitted to the data on the computer, by evaluating the best values for the constants C_1 and C_2 . In all cases, the error in the correlation was smaller than the degree of scatter within the experimental evaluation of the emulsion viscosity.

The viscosity correlation was then used to evaluate the concentration of the produced emulsion in the

displacement tests.

4.6 TYPICAL RUNS

4.6.1 Core Preparation

Prior to each run, a sieve analysis of the sand was carried out, followed by recombining the sand. The cores were packed by tamping the core holders with a hammer until no visible settlement occurred while obtaining a core length of 23.4 cm. The mass of the core holder was determined before and after it was packed.

The cores were then evacuated, saturated with tapwater and reweighed. From the series of weighings, the sand weight, the water weight and thus the volume of water within the core holder were determined. From the volume of water within the core holder, the pore volume and porosity of the core were determined by subtracting the value for the water enclosed in the core holder end blocks. The absolute permeability was determined routinely by the flow of tapwater, at which time the transducer calibration was checked.

4.6.2 The Emulsion Flood

Two types of emulsion flood were carried out in this study. Type 1 was carried out to investigate objectives 1 and 2 of this study and type 2 to investigate objectives 3 and 4. The conditions of these floods are described

separately below:

Type 1 :

In these experiments, the emulsion was flooded at a constant rate through the core until steady state conditions were achieved. Steady state was designated by no further change in the pressure drop across the core. When steady state conditions were achieved, the pressure drop, flow rate and emulsion viscosity were recorded, from which the permeability of the core to emulsion was determined.

The flow rate was then lowered and the flooding continued until a new steady state condition was obtained. This procedure of lowering the flow rate and evaluating the core permeability to emulsion at steady state was continued until a predetermined lower flow rate was reached. The procedure was then reversed and the permeability was evaluated through a series of increasing flow rates, back to the original flow rate. This procedure was carried out to establish that the core properties, such as wettability, had not changed due to the adsorption of organics from the oil or the surfactant. The net result of this procedure was to determine the effect of emulsion flow rate or the pressure gradient, on the permeability of the core to the emulsion.

The lower limit of the flow rate was determined by the accuracy with which the pressure drop could be evaluated using the transducers. At low rates, the error in the measurement was large in comparison to the magnitude of the pressure drop and thus could give a misleading estimate of

the core permeability to the emulsion.

Homogeneity of the emulsion throughout the run was assured by:

- 1) producing all the emulsion before the run and storing this emulsion in one storage container and
- 2) at the end of the run for each flow rate, the emulsion cylinder in the flow system was replenished with new emulsion, which was kept thoroughly mixed in the storage container.

This technique, rather than using one large cylinder in the flow system, ensured the homogeneity of the emulsion, because in a large cylinder some droplet size segregation does occur over a period of time. Thus the droplets would be slightly larger than average at the beginning of the run, becoming progressively smaller with time.

In these experiments the produced emulsion was collected in one large container until steady state occurred, when a small sample was collected from the core outlet and used to evaluate the viscosity.

Type 2 :

In this experiment, the unsteady state time period for emulsion flow was investigated. After the absolute permeability evaluation, the emulsion was injected through the auxiliary lines and transducers on the equipment up to the valve upstream of the core holder, in order that a material balance could be carried out on the core.

For a constant injection flow rate, the produced emulsion was collected in 50 cc tubes which were placed in a fractional collector. The viscosity of the produced emulsion was then evaluated for each tube and in one experiment, the droplet size distribution.

From the emulsion viscosity, the emulsion concentration was calculated, from which a material balance was carried out on the system to evaluate the retention of the oil within the core. The results were then converted to refer to the ends of the porous medium, rather than the inlet and outlet of the core holder. From these results, the outlet emulsion concentration history and the oil saturation within the core were evaluated.

From the results of:

- 1) maximum oil saturation within the core,
- 2) produced emulsion concentration history and
- 3) flow rate, inlet emulsion concentration, core porosity, length and area

the mathematical models described in Chapter 3 were fitted to the experimental results in order to evaluate the constants H_o , β and $\bar{\epsilon}$. A computer program COMPLX was used to find the best values for these constants. The computer program minimises the error in the fitting of the model to the results using the Simplex method of Box (48) and Nelder and Mead (49). From the evaluated constants for the model, the saturation history of the core was calculated using the model.

CHAPTER 5

RESULTS AND DISCUSSION

5.1 SAND, CORE AND EMULSION PROPERTIES

A sieve analysis of the sands used in this study is presented in Table 5.1. The core properties of porosity and permeability for each run are presented in Table 5.2. The emulsion properties of viscosity and concentration for each run are also shown in Table 5.2.

Tables 5.3 and 5.4 show the particle size distribution data as obtained from the Coulter Counter for the 15 and 30 percent concentration emulsions, respectively. Examination of these results, shows that channels 1 and 2 were cut-off and this procedure was carried out to overcome background noise which effects the results of the lower channels. Therefore channel 3 represents the droplet size range, 0 - 2.52 microns rather than the range 2 - 2.52 microns. Figures 5.1 and 5.2, represent a correlation of this data on semi-log paper, equivalent to the paper provided by Coulter Electronic Inc. (form 4221030). The curves have the typical form of the bell shaped distribution curve.

Figure 5.3 shows a representation of the cumulative frequency curves on log-probability paper. A straight line on this type of paper demonstrates that the emulsion particle diameter is log-normally distributed. The correlation, Figure 5.3, demonstrates that the emulsions used in this study were not log-normally distributed but

TABLE 5.1

CORE SAND PROPERTIES

RUN	SAND TYPE	WEIGHT FRACTION EACH SIZE					SAND WEIGHT GRAMS		
		<45	>100	<100	>140	<140		>325	<325
		MESH	MESH	MESH	MESH	MESH		MESH	
		<354	>149	<149	>105	<105		>44	<44
		MICRONS	MICRONS	MICRONS	MICRONS	MICRONS	MICRONS		
1	B	-	-	-	-	-	-		
100	SK	-	-	-	-	-	716.7		
101	SS	-	-	-	-	-	746.0		
102	SS	-	-	-	-	-	746.4		
103	SK	-	-	-	-	-	742.4		
104	SS	-	-	-	-	-	741.4		
106	SK	0.402	0.220	0.307	0.071	0.071	733.8		
109	LM	0.780	0.120	0.090	0.010	0.010	712.4		
110	LM	-	-	-	-	-	691.8		
111	LM	0.780	0.120	0.090	0.010	0.010	711.2		
112	LM	0.780	0.120	0.090	0.010	0.010	711.5		
113	LM	0.780	0.120	0.090	0.010	0.010	711.2		
114	LM	0.780	0.120	0.090	0.010	0.010	711.1		
115	LM	0.780	0.120	0.090	0.010	0.010	710.4		
119	LM	0.780	0.120	0.090	0.010	0.010	711.1		
120	LM	0.780	0.120	0.090	0.010	0.010	711.3		
121	LM	0.780	0.120	0.090	0.010	0.010	711.1		
123	LM	0.780	0.120	0.090	0.010	0.010	711.3		
124	LM	0.780	0.120	0.090	0.010	0.010	709.5		
125	LM	0.562	0.240	0.180	0.018	0.018	711.1		
126	LM	0.343	0.361	0.285	0.011	0.011	710.5		
127	LM	0.0	0.651	0.313	0.038	0.038	688.8		
128	LM	0.092	0.408	0.473	0.027	0.027	701.1		
129	LM	0.497	0.134	0.348	0.021	0.021	717.8		

TABLE 5.2

CORE AND EMULSION PROPERTIES

Run	Porosity -	Permeability darcies	Emulsion Concentration -	Emulsion Viscosity mPa.s	Core Length cm	Core Area cm ²
1	0.205	0.039	0.30	2.15	62.4	20.2
100	0.359	0.320	0.30	2.1	23.4	18.1
101	0.352	18.9	0.30	2.3	23.4	18.1
102	0.346	15.9	0.30	2.3	23.4	18.1
103	0.338	0.155	0.30	2.1	23.4	18.1
104	0.343	14.25	0.30	2.08	23.4	18.1
106	0.333	0.217	0.30	2.03	23.4	18.1
109	0.366	6.45	0.15	1.46	23.4	18.1
110	0.368	7.32	0.15	1.46	23.4	18.1
111	0.369	7.64	0.15	1.50	23.4	18.1
112	0.376	7.87	0.15	1.48	23.4	18.1
113	0.372	8.11	0.15	1.49	23.4	18.1
114	0.375	8.83	0.15	1.49	23.4	18.1
115	0.371	8.06	0.15	1.50	23.4	18.1
119	0.377	8.12	0.15	1.48	23.4	18.1
120	0.371	9.50	0.15	1.50	23.4	18.1
121	0.352	6.50	0.15	1.51	23.4	18.1
123	0.379	8.55	0.15	1.47	23.4	18.1
124	0.376	8.22	0.15	1.46	23.4	18.1
125	0.375	5.23	0.15	1.49	23.4	18.1
126	0.387	5.46	0.15	1.49	23.4	18.1
127	0.399	3.03	0.15	1.46	23.4	18.1
128	0.397	3.64	0.15	1.51	23.4	18.1
129	0.379	4.22	0.15	1.52	23.4	18.1

TABLE 5.3

DROPLET SIZE DISTRIBUTION
15 PERCENT EMULSION CONCENTRATION

CHANNEL	MINIMUM DROPLET DIAMETER Microns	SIZE DISTRIBUTION PERCENT GREATER THAN	
		DIFFERENTIAL	CUMULATIVE
1	1.26	-	-
2	1.59	-	-
3	2.00	18.8	100.0
4	2.52	21.4	81.2
5	3.17	23.5	59.8
6	4.00	19.6	36.3
7	5.04	10.5	16.7
8	6.35	2.6	6.2
9	8.00	0.6	3.6
10	10.08	0.5	3.0
11	12.7	0.5	2.5
12	16.0	0.7	2.0
13	20.2	0.7	1.3
14	25.4	0.6	0.6
15	32.0	0.0	0.0
16	40.3	0.0	0.0

TABLE 5.4

DROPLET SIZE DISTRIBUTION
30 PERCENT EMULSION CONCENTRATION

CHANNEL	MINIMUM DROPLET DIAMETER Microns	SIZE DISTRIBUTION PERCENT GREATER THAN	
		DIFFERENTIAL	CUMULATIVE
1	1.26	-	-
2	1.59	-	-
3	2.00	20.4	100.0
4	2.52	22.5	79.6
5	3.17	21.4	57.1
6	4.00	14.4	35.7
7	5.04	6.6	21.3
8	6.35	2.6	14.7
9	8.00	1.4	12.1
10	10.08	3.0	10.7
11	12.7	2.7	7.7
12	16.0	2.0	5.0
13	20.2	2.0	3.0
14	25.4	1.0	1.0
15	32.0	0.0	0.0
16	40.3	0.0	0.0

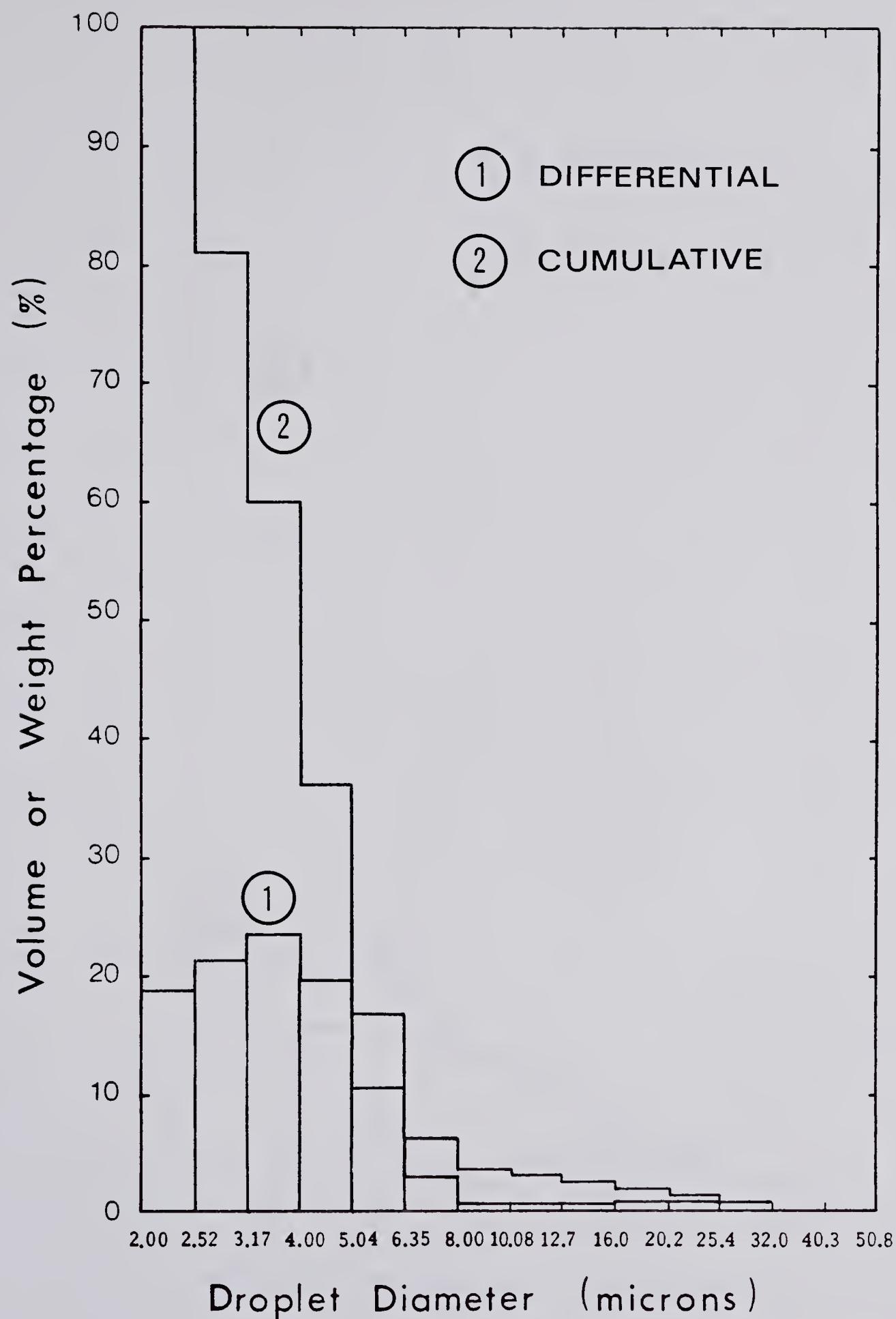


FIGURE 5.1 DROPLET SIZE DISTRIBUTION FOR THE 15% QUALITY EMULSION

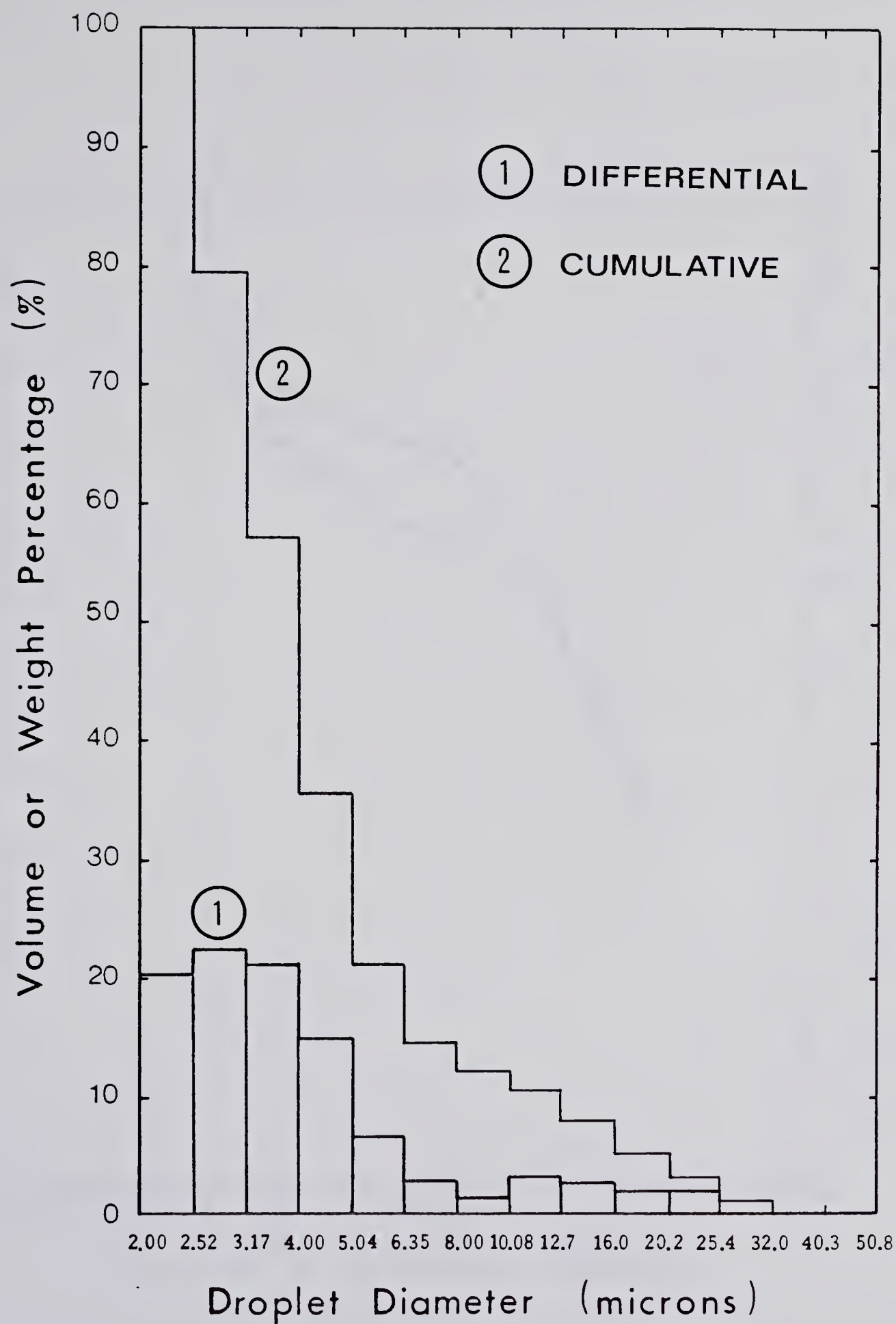


FIGURE 5.2 DROPLET SIZE DISTRIBUTION FOR THE 30% QUALITY EMULSION

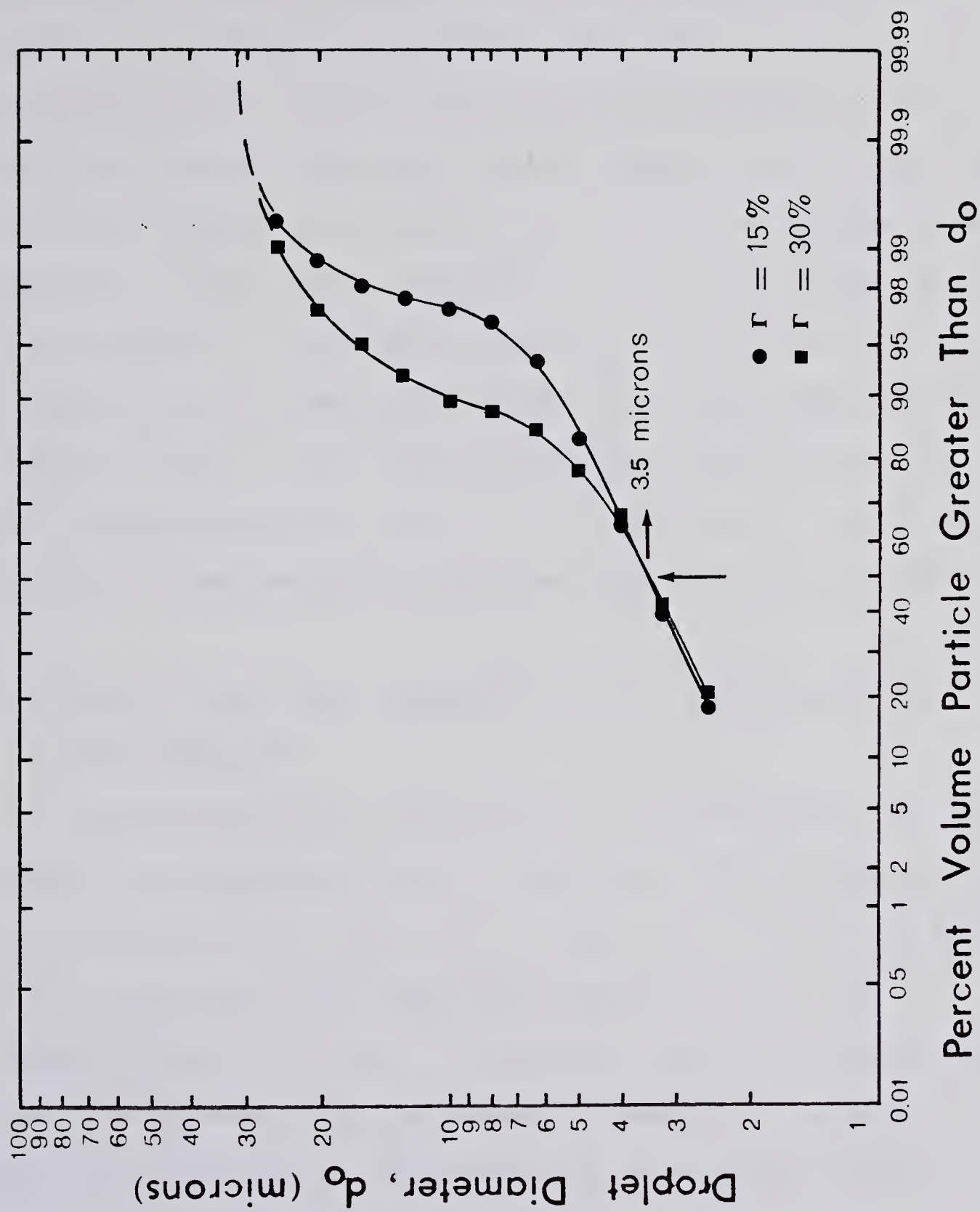


FIGURE 5.3 EMULSION DROPLET SIZE DISTRIBUTION

had a higher frequency of the larger droplets than that characterised by a log-normal distribution.

From Figure 5.3, the value for the emulsion median diameter is easily identifiable. The median diameter is the value of the droplet size about which the volume of particles in the distribution is divided equally. The two emulsions had an identical median diameter of 3.45 microns. Although the median diameters for the two emulsions were identical, there were a higher proportion of larger droplets in the higher concentration emulsion. The values for the 99 percent less than emulsion droplet size were estimated from Figure 5.3 to be 25.4 and 21 microns for the 30 and 15 percent concentration emulsions, respectively. For both emulsions there were no droplets larger than 32 microns.

5.2 STEADY STATE FLOW CHARACTERISTICS OF EMULSIONS IN A POROUS MEDIUM

Twenty runs were carried out to investigate the steady state flow characteristics of emulsions in a porous medium. The permeability of the core to emulsion is shown in Table 5.5 for each run. The fractional permeability, the permeability of the core to emulsion as a fraction of the absolute permeability, is shown in Table 5.6. A number of phenomena relating to emulsion flow in a porous medium can be observed from these results.

TABLE 5.5

PERMEABILITY OF THE CORE TO EMULSION

RUN	CORE		PERMEABILITY @ FLOW RATE (cc/hr)											
	PERMEABILITY	darcies	560	400	320	240	200	160	120	100	80	60	40	30
101	18.9	18.9	18.9	-	18.9	18.9	-	-	-	18.9	-	-	-	-
102	15.9	15.9	15.9	-	15.9	15.9	-	-	-	15.9	-	-	-	-
104	14.25	14.25	14.25	-	14.25	14.25	-	-	-	14.25	-	-	-	-
120	9.50	7.27	-	-	-	-	-	-	-	-	-	-	-	-
114	8.83	-	-	-	-	-	7.66	-	-	-	-	-	-	-
123	8.55	8.07	8.05	8.07	7.99	7.96	7.87	7.83	7.84	7.67	7.57	7.46	7.21	7.21
124	8.22	-	6.68	6.50	6.36	6.23	6.05	-	5.76	5.49	5.14	-	-	4.65
119	8.12	6.71	-	-	-	-	-	-	-	-	-	-	-	-
113	8.11	-	-	-	-	-	-	-	-	6.54	-	-	-	-
112	7.87	-	-	-	-	-	-	-	-	-	-	6.05	-	-
111	7.64	-	-	-	-	-	-	-	-	6.69	-	-	-	-
110	7.32	-	-	-	-	-	-	-	-	5.10	-	-	-	3.56
121	6.53	5.22	-	-	-	-	-	-	-	-	-	-	-	-
109	6.45	-	4.78	4.76	4.70	4.65	4.63	4.62	4.58	-	-	-	-	-
126	5.46	-	4.28	4.28	4.26	4.20	4.15	4.12	3.98	-	-	-	-	-
125	5.23	-	4.24	4.20	-	4.15	-	-	-	4.10	-	3.99	-	3.86
129	4.14	-	-	-	-	-	-	-	-	2.26	-	-	-	-
128	3.64	-	-	-	-	-	-	-	-	1.90	-	-	-	-
127	3.02	-	1.20	-	1.04	-	-	-	-	1.00	-	-	-	-
100	0.32	-	-	-	-	<0.005	-	-	-	-	-	-	-	-
106	0.217	-	-	-	-	-	-	-	-	-	-	<0.007	<0.005	-
103	0.155	-	-	-	-	-	-	-	-	-	<0.002	-	-	-
1	0.039	-	-	-	-	<0.001	-	-	-	-	-	-	-	-

TABLE 5.6

FRACTIONAL PERMEABILITY OF THE CORE TO EMULSION

CORE PERMEABILITY		FRACTIONAL PERMEABILITY @											
		FLOW RATE (cc/hr)											
RUN	darcies	560	400	320	240	200	160	120	100	80	60	40	30
101	18.9	1.0	-	1.0	1.0	-	-	-	1.0	-	-	-	-
102	15.9	1.0	-	1.0	1.0	-	-	-	1.0	-	-	-	-
104	14.25	1.0	-	1.0	1.0	-	-	-	1.0	-	-	-	-
120	9.50	0.765	-	-	-	-	-	-	-	-	-	-	-
114	8.83	-	-	-	-	0.867	-	-	-	-	-	-	-
123	8.55	0.944	0.942	0.944	0.935	0.932	0.921	0.916	0.917	0.898	0.886	0.873	0.844
124	8.22	-	0.812	0.790	0.773	0.758	0.736	-	0.701	0.668	0.625	-	0.566
119	8.12	0.826	-	-	-	-	-	-	-	-	-	-	-
113	8.11	-	-	-	-	-	-	-	-	0.806	-	-	-
112	7.87	-	-	-	-	-	-	-	-	-	0.769	-	-
111	7.64	-	-	-	-	-	-	-	0.875	-	-	-	-
110	7.32	-	-	-	-	-	-	-	0.697	-	-	-	0.486
121	6.53	0.799	-	-	-	-	-	-	-	-	-	-	-
109	6.45	-	0.741	0.737	0.728	0.718	0.718	0.715	0.710	-	-	-	-
126	5.46	-	0.785	0.784	0.780	0.770	0.760	0.755	0.730	-	-	-	-
125	5.23	-	0.810	0.803	-	0.794	-	-	0.783	-	0.763	-	0.739
129	4.14	-	-	-	-	-	-	-	0.545	-	-	-	-
128	3.64	-	-	-	-	-	-	-	0.522	-	-	-	-
127	3.02	-	0.396	-	0.344	-	-	-	0.331	-	-	-	-
100	0.32	-	-	-	-	<0.017	-	-	-	-	-	-	-
106	0.217	-	-	-	-	-	-	-	-	-	<0.045	<0.032	-
103	0.155	-	-	-	-	-	-	-	-	<0.013	-	-	-
1	0.039	-	-	-	<0.025	-	-	-	-	-	-	-	-

5.2.1 Reduction of the Core Permeability by Emulsion Flow

It was postulated earlier in Section 2.2 of this study, that the flow of an emulsion through a porous medium could reduce the permeability of the medium. The results reported in Tables 5.5 and 5.6, show that this was true for the emulsions used in this study, when the permeability of the core was less than 9.5 darcies. Two parameters which can provide an estimate of whether and when an emulsion can reduce the permeability of the core, are discussed later in Section 5.3 of this study.

5.2.2 Degree of Core Permeability Reduction by Emulsion Flow

McAuliffe (12) reported that, in no case did the emulsion completely plug the porous materials used in his study. The core retained one to ten percent of the initial permeability and the emulsion continued to flow through the core.

In this study for runs 1, 106, 100 and 103, where the core permeabilities ranged from 39 millidarcies to 320 millidarcies, the permeabilities were reduced to below 7 millidarcies in all cases. These values represent a fractional permeability of less than 5 percent of the initial permeability. For all these runs, steady state was never attained because the pressure drop across the cores approached 400 psi for runs 100, 103 and 106 and 1000 psi

for run 1, with these pressures representing the limits of the respective core holders used in the runs. The number of pore volumes flowed through the cores before the pressure limit of the core holders were reached were 1.0, 1.5, 3.1 and 1.5 for runs 1, 100, 103 and 106, respectively.

Therefore, because the steady state core permeability to the emulsion was never attained and the core permeabilities were so low that extremely high pressure gradients, hundreds of psi/ft, were required for flow at reservoir rates, then the condition of the core can be termed as completely plugged.

It can therefore be postulated from the results of this study, that there are three possible degrees of core permeability reduction due to the flow of an emulsion through a porous medium.

Firstly, and characterised in runs 101, 103 and 104 for which the core permeabilities ranged from 14.25 to 18.9 darcies, the emulsion does not plug the porous medium and reduce the permeability. In these runs, the permeability of the porous medium was not reduced because the emulsion droplets were too small to plug the pore throats.

Secondly, and characterised in runs 109 through 129, for which the core permeabilities ranged from 3 to 9.5 darcies, the emulsion plugged the core, partially reducing the permeability of the core.

Thirdly, and characterised in runs 1, 100, 103 and 106 the emulsion completely plugs the core, reducing the permeability to such an extent that there was essentially no

flow at normal reservoir pressure gradients.

A parameter for predicting the degree of permeability reduction, whether zero, partial or complete, is discussed in Section 5.3 of this study.

Examination of the results shown in Table 5.5, some of which are shown in Figure 5.4, demonstrates that in general, for an unconsolidated porous medium, a core with an higher initial permeability will retain a higher permeability after emulsion flow, than a core with a lower initial permeability. This observation is not true in every case because permeability is an average property of the porous medium, while it is the particular combination of the pore sizes that determines the permeability of the core to an emulsion.

Although there is a general relationship between the permeability of the core to emulsion and the initial core permeability, the results which are shown in Figure 5.5 demonstrate that there is no simple relationship between the degree of pore plugging or permeability reduction and the core permeability. A comparison of the data for runs 109, 125 and 126 shown in Figure 5.5, demonstrates that the fractional permeability of the core to emulsion flow was higher for the lower permeability cores.

The results of runs 109, 125 and 126 demonstrate that the core with the higher initial permeability retained a higher permeability after emulsion flow, but this

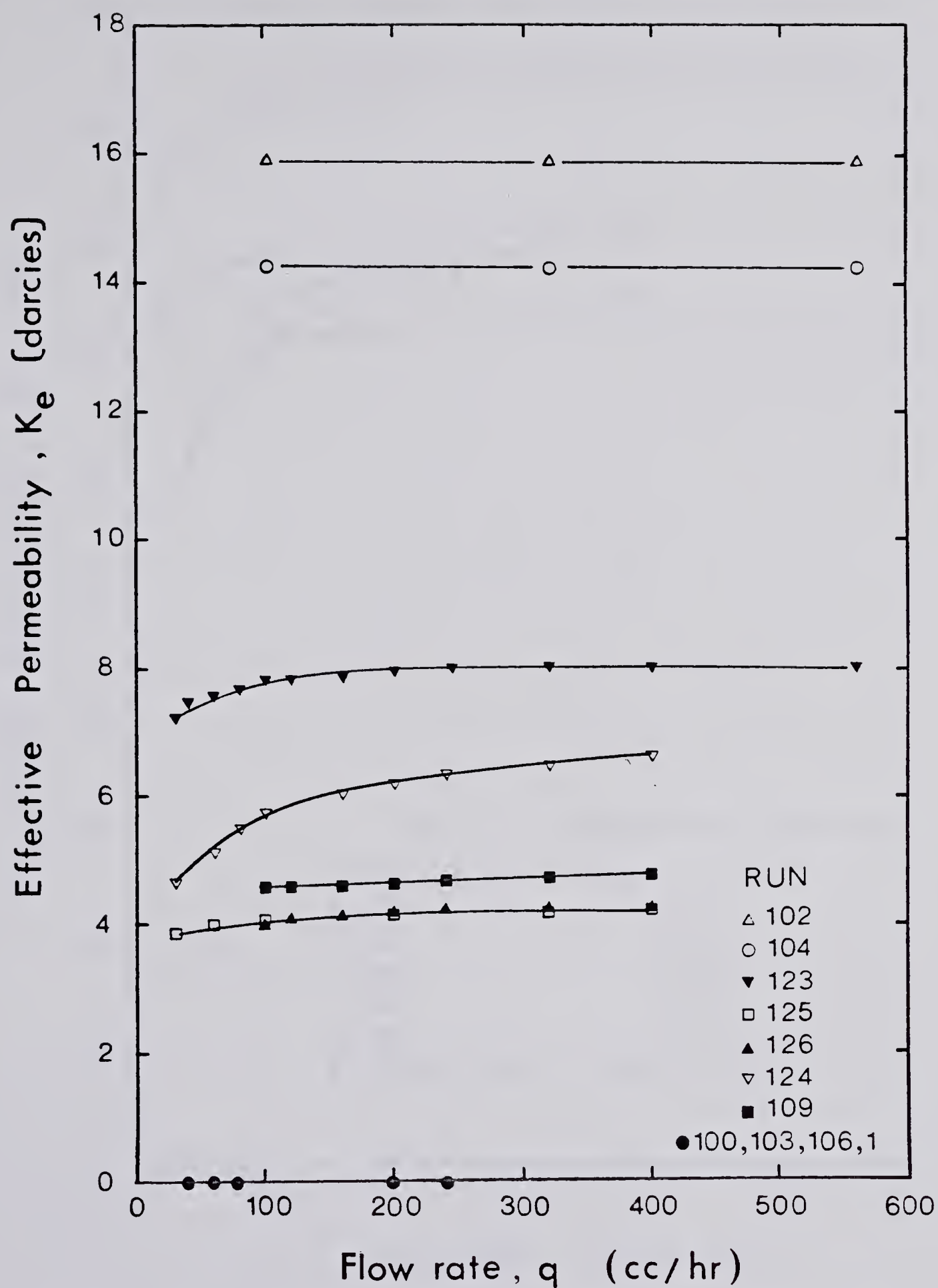


FIGURE 5.4 EFFECTIVE PERMEABILITY VERSUS FLOW RATE

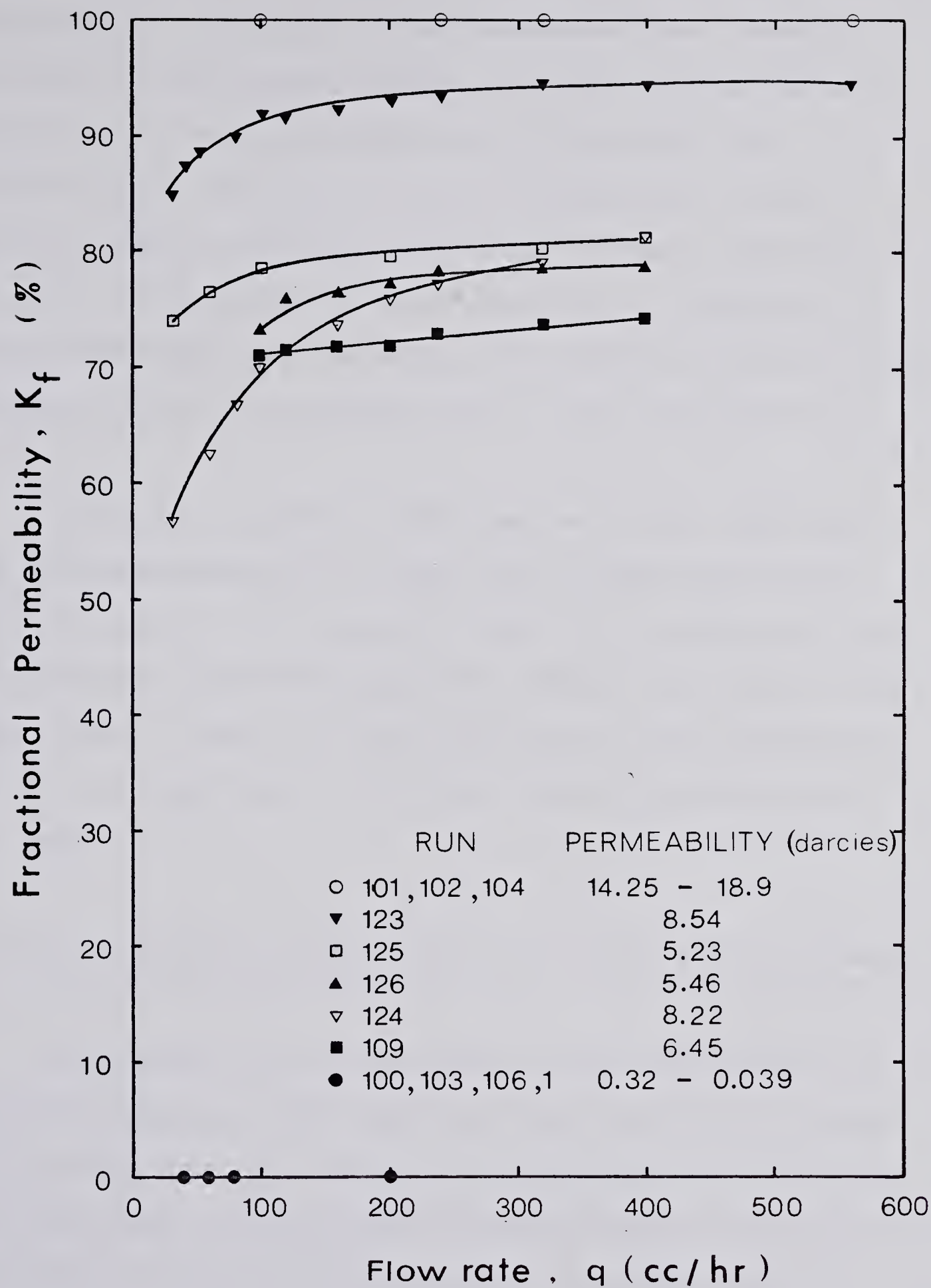


FIGURE 5.5 FRACTIONAL PERMEABILITY VERSUS FLOW RATE

represented a lower fractional permeability of the initial permeability. Therefore it was postulated that there is no simple relationship between the degree of permeability reduction and the core properties of porosity and permeability. There is no simple relationship because porosity and permeability are volume averaged qualities of the pore sizes, while it is the particular combination of these pore sizes that determines the shape of the fractional permeability versus pressure drop or flow rate profile.

The smooth nature of the results of the fractional and actual permeability of the core to emulsion versus flow rate, shown in Figures 5.4 and 5.5, demonstrates that no changes in the rock properties occurred during the runs. These results imply that the adsorption of the surfactant or oil, if they occurred, did not affect the plugging of the core.

5.2.3 Non-Darcy Flow Nature of Emulsions in a Porous Medium

In section 2.2 of this study it was postulated, by examining Equation 2.17, that emulsion flow is a non-Darcy flow process when the emulsion can plug the porous medium. This phenomena was postulated because emulsion droplets are deformable and for a higher pressure gradient they will deform to a greater extent and pass through a smaller constriction. Therefore as the pressure gradient is reduced,

the pore throat which can be plugged will increase and the permeability of the core to emulsion will decrease.

The relationship between the pressure drop and the flow rate for run 124, which is a representative example of a core which was plugged by emulsion flow in this study, is shown in Figure 5.6. The circular data points represent the flow of water through the porous medium. The linear relationship indicates the flow of water obeyed Darcy's Law, with the permeability of the core being 8.22 darcies. The dashed line on Figure 5.6 represents the pressure - flow rate relation for a liquid of equal viscosity to the emulsion and which obeys Darcy's Law. The triangular data points represent the pressure - flow rate profile for the emulsion used in the run. The non-linearity of the line through the triangular data points indicates that emulsion flow is a non-Darcy flow process when the emulsion plugs the porous medium. The results for this run, reported in Table 5.6, show that the fractional permeability of the core changed from 0.566 to 0.812 as the flow rate increased from 30 to 400 cc/hr.

This non-Darcy flow process for emulsions was originally demonstrated by McAuliffe (12). This phenomenon was not observed by Alvarado (34), who reported that the reduction of the core permeability was independent of the flow rate and the flow of an emulsion in a porous medium was classified as a Darcy flow process.

The degree of this non-Darcy flow process for

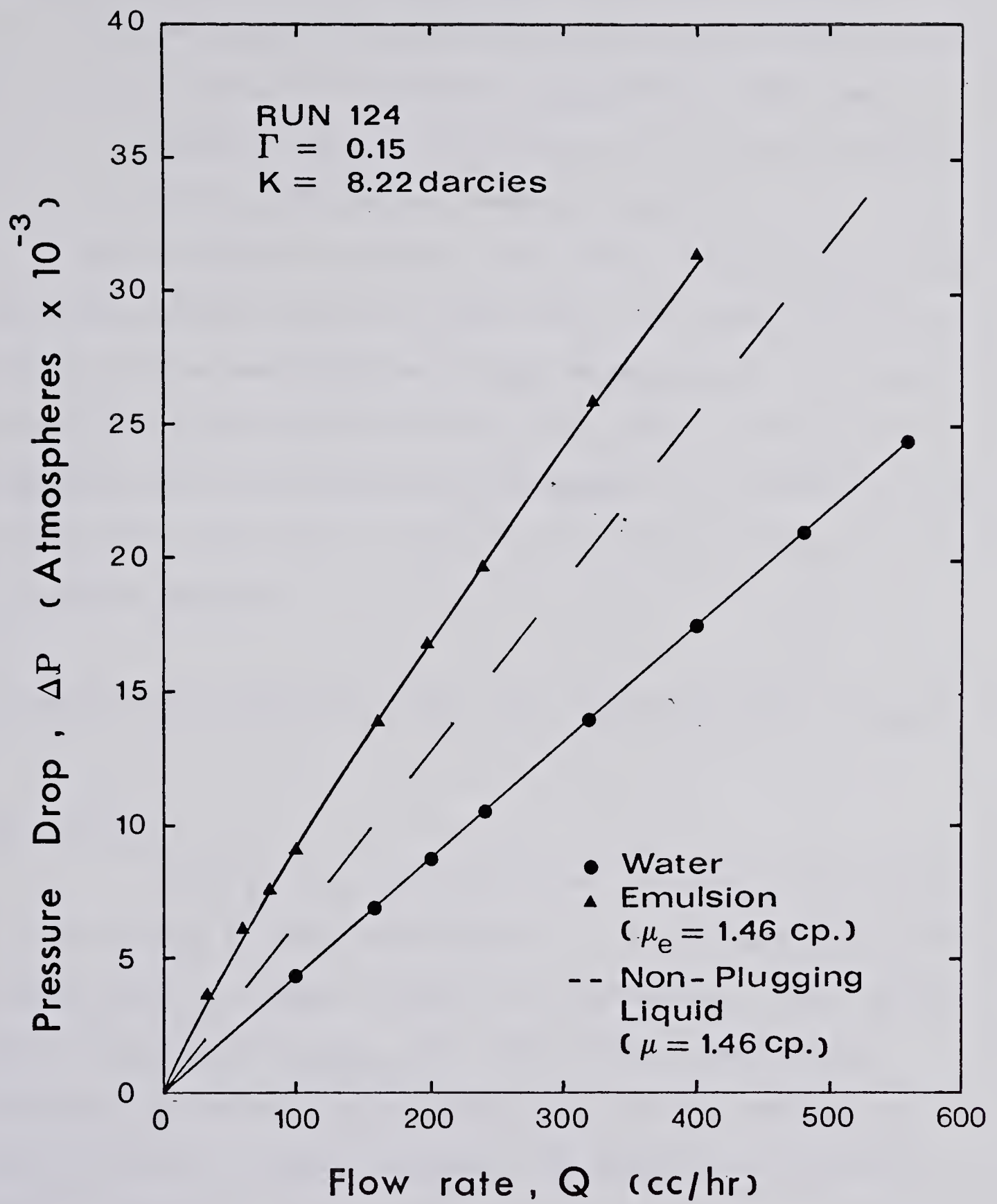


FIGURE 5.6 EXAMINATION OF DARCY'S LAW

emulsions is a function of the pore size distribution of the porous medium and the size of the droplets in the emulsion.

Properties conducive to observing this phenomenon are:

- 1) a sharply-distributed pore size distribution and
- 2) an emulsion containing large rather than small droplets because they deform to a greater extent under a particular pressure gradient.

The results of runs 101, 102 and 104 demonstrate that when the emulsion does not plug the porous medium, then the flow of an emulsion is a Darcy flow process. The non-Darcy flow characteristic of emulsion flow, described by McAuliffe (12) as 'pseudo non-Newtonian', is therefore only evident when the emulsion droplets are large enough to plug the porous medium.

5.3 PREDICTION TECHNIQUES FOR THE DEGREE OF CORE PLUGGING

d_g/d_e Ratio

Herzig et al (15) and Sakthivadivel (46) worked on the process of deep filtration, in which suspensions are mechanically entrapped within a porous medium. They showed that the parameter d_g/d_s , the ratio of the sand grain diameter to the maximum particle size in the suspension, could be used to predict whether the porous medium would become plugged.

Their analysis can be extended to predict whether an emulsion can plug a porous medium by using the parameter

d_g/d_e , the ratio of the sand grain size to the deformed size of the largest droplet in the emulsion. The parameter d_g/d_d , the ratio of the sand grain size to the maximum oil droplet size in the emulsion might be used, however, this ratio would not be truly valid as emulsion droplets are deformable. The use of the ratio d_g/d_d , rather than d_g/d_e , would provide a more optimistic estimate of whether an emulsion could plug the porous medium.

The ratio d_g/d_e can be used to predict whether a core will be plugged by an emulsion by comparing this ratio with the ratio d_g/d_p , the ratio of the sand grain size in the porous medium to the pore throat size.

For a porous medium consisting of uniformly sized spherical particles, the ratio of the grain size to the minimum pore throat and maximum pore opening in the porous medium, for the various packing schemes of cubic, hexagonal and rhombohedral has been evaluated. The values for the various packing schemes are shown in Table 5.7.

TABLE 5.7
CRITICAL d_g/d_p RATIOS

Packing	Minimum Pore Throat Diameter	Maximum Pore Opening Diameter
	d_g/d_p	d_g/d_p
Cubic	2.415	1.366
Hexagonal	6.493	1.894
Rhombic	6.493	2.415

Thus for spherical grains in a random pack, the minimum pore throat size is given by 0.154 ($1/6.493$) of the grain size and this represents the easiest pore which can be plugged. Therefore for plugging to occur in a random pack, the ratio d_g/d_e has to be smaller than 6.493, for a single droplet to plug the pore constriction.

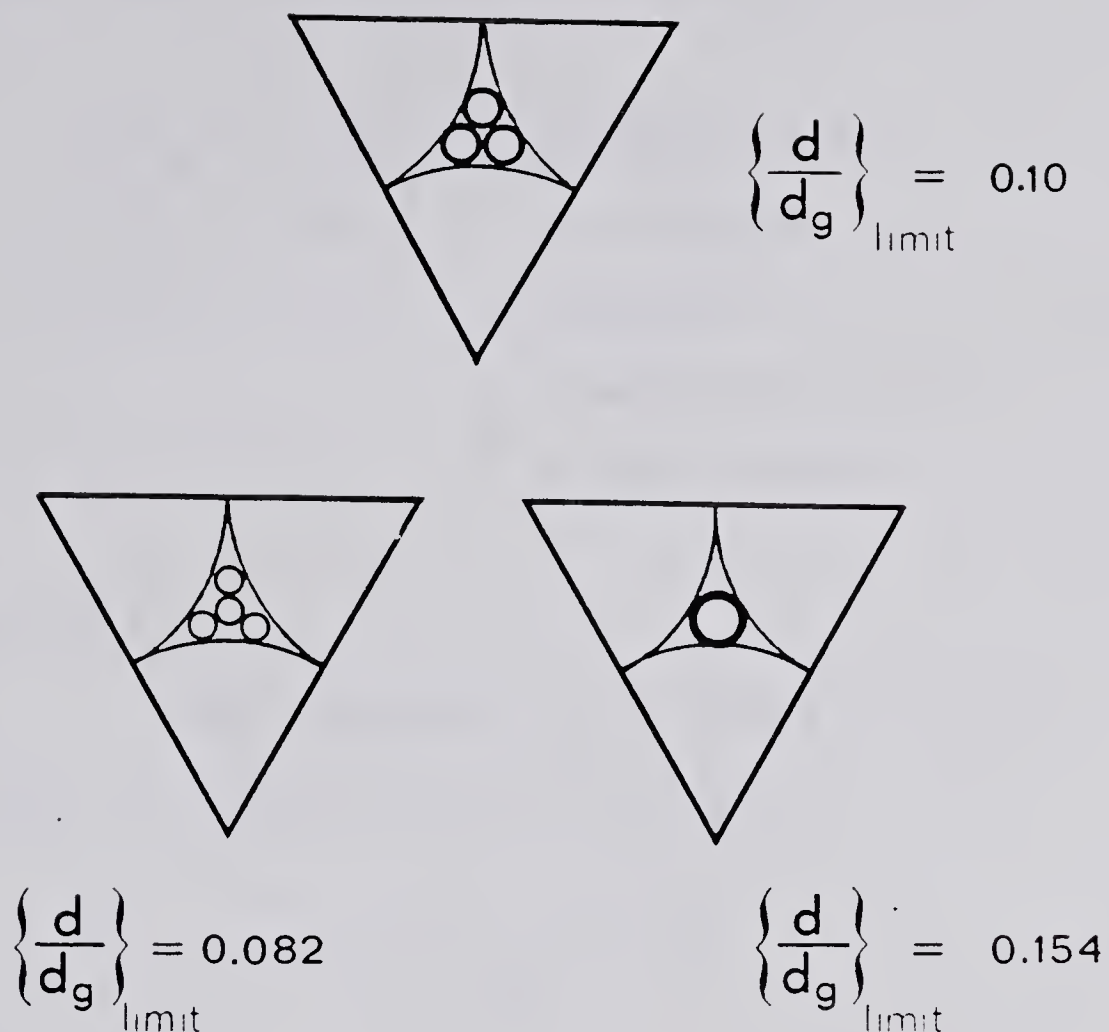
In a random pack, the maximum pore throat size is characterised by the pore throat for cubic packing. Therefore, for complete plugging, the ratio d_g/d_e has to be smaller than 2.415. Therefore theoretically, in a random core pack consisting of cubic, hexagonal and rhombohedrally packed spherical grains, then for

$$\begin{aligned} d_g/d_e &> 6.493 && : \text{no plugging} \\ 2.415 < d_g/d_e &< 6.493 && : \text{partial plugging} \\ d_g/d_e &< 2.415 && : \text{complete plugging} \end{aligned} \quad (5.1)$$

Herzig et al (15) stated that for plugging to begin

$$\begin{aligned} d_g/d_e &< 6.493 && : \text{plugging with one} \\ &&& \text{droplet capture} \\ d_g/d_e &< 10.0 && : \text{plugging with three} \\ &&& \text{droplet capture} \\ d_g/d_e &< 12.2 && : \text{plugging with four} \\ &&& \text{droplet capture} \end{aligned} \quad (5.2)$$

A representation of their theory is illustrated in Figure 5.7.



d : Diameter of Emulsion Droplet

d_g : Diameter of Sand Grain

FIGURE 5.7 SIZE OF EMULSION DROPLET
RELATED TO TRIANGULAR
CONSTRICTION SITE (15)

Sakthivadivel (46) in his work stated that for

$$\begin{aligned}
 d_g/d_e < 5.0 & : \text{plugging occurs} \\
 d_g/d_e > 14.0 & : \text{no plugging} \\
 5.0 < d_g/d_e < 14.0 & : \text{plugging or no plugging dependent} \\
 & \text{on the porosity}
 \end{aligned} \tag{5.3}$$

Calculation of d_g :

The value for d_g , for each core, was evaluated using the modified Kozeny equation

$$d_g = \frac{180 (1 - \phi)^2 K}{\phi^3}$$

where K : permeability (cm^2)

d_g : grain size (cm)

ϕ : porosity

which is valid for an unconsolidated porous medium made from spherical particles of one distinct size. The values of d_g evaluated for each run are shown in Table 5.8.

Calculation of d_e :

In suspension flow, the value for the maximum particle size is constant, however because emulsion droplets are deformable, the value for the deformed size of the largest emulsion droplet must be evaluated at a specific pressure gradient. In this study, the value of d_e and the

TABLE 5.8

PARAMETER d_g/d_e

RUN	r_o microns	d_g microns	r_o/d_g	d_g/d_e @			Plugging Type
				0 psi/ft	1 psi/ft	5 psi/ft	
101	12.7	180	0.141	7.08	7.20	7.65	NP
102	12.7	171	0.148	6.73	6.84	7.26	NP
104	12.7	164	0.154	6.48	6.58	6.99	NP
120	10.5	118	0.178	5.62	5.68	5.92	PP
114	10.5	108	0.194	5.14	5.20	5.42	PP
123	10.5	104	0.202	4.95	5.00	5.22	PP
124	10.5	103	0.204	4.90	4.96	5.17	PP
119	10.5	106	0.198	5.05	5.10	5.32	PP
113	10.5	105	0.200	5.00	5.05	5.27	PP
112	10.5	101	0.208	4.81	4.86	5.07	PP
111	10.5	104	0.202	4.95	5.00	5.22	PP
110	10.5	102	0.206	4.86	4.91	5.12	PP
121	10.5	106	0.198	5.05	5.10	5.32	PP
109	10.5	97	0.216	4.62	4.67	4.86	PP
126	10.5	79	0.266	3.76	3.80	3.96	PP
125	10.5	83	0.253	3.95	3.99	4.16	PP
129	10.5	65	0.323	3.10	3.13	3.26	PP
128	10.5	61	0.344	2.90	2.94	3.06	PP
127	10.5	59	0.356	2.81	2.84	2.96	PP
100	12.7	22	1.154	0.88	0.90	0.95	PP
106	12.7	22	1.154	0.848	0.86	0.92	PP
103	12.7	18	1.411	0.70	0.71	0.75	PP

ratio d_g/d_e were evaluated for the pressure gradients of 0 psi/ft, 1 psi/ft and 5 psi/ft. The value of d_e was evaluated using the equation

$$\Delta P = \frac{dP}{dL} L_d = 2 \gamma \cos \theta \left\{ \frac{2}{d_e} - \frac{1}{r_m} \right\} \quad (5.5)$$

where

r_m : maximum emulsion droplet radius

θ : wetting angle, assumed to be 90°

γ : interfacial tension

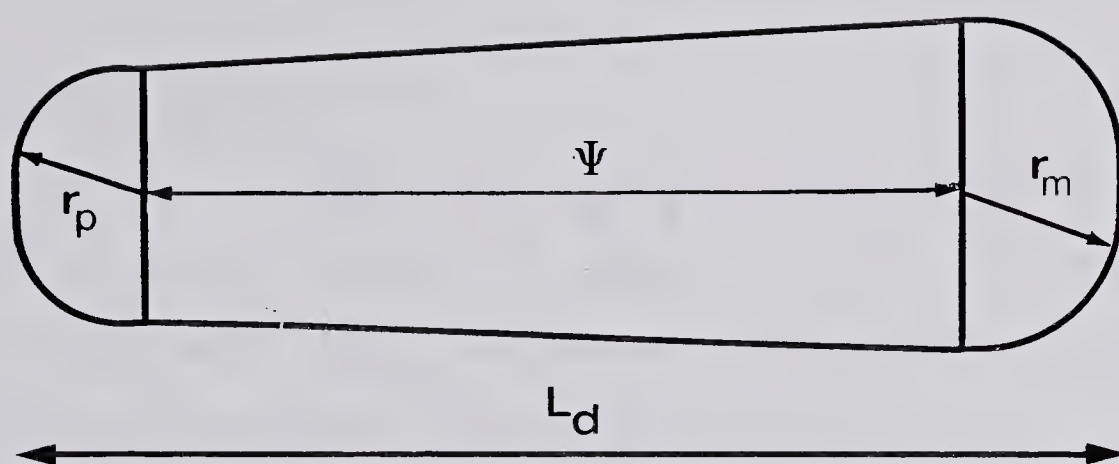
L_d : length of the droplet over which the pressure gradient applies

$\frac{dP}{dL}$: pressure gradient

ΔP : pressure differential

d_e : the diameter of the deformed emulsion droplet of radius r_m , under the applied pressure gradient.

In order to evaluate the deformed droplet diameter, d_e the length over which the pressure gradient applies has to be estimated. In this study, the pressure gradient was assumed to apply over the total length of the deformed droplet. The deformed droplet length was evaluated as the addition of the minimum and maximum radii of the droplet plus the length of a conical shape between the end radii. Figure 5.8 shows a schematic diagram of the deformed emulsion droplet. The calculation methods for the deformed droplet length and diameter and the value of d_g/d_e are



$$\Psi = 2 \frac{r_m^3 - r_p^3}{r_m^2 + r_p^2 + r_m r_p}$$

$$L_d = r_m + r_p + 2 \frac{r_m^3 - r_p^3}{r_m^2 + r_p^2 + r_m r_p}$$

FIGURE 5.8 SCHEMATIC DIAGRAM OF THE DEFORMED EMULSION DROPLET

reported in Appendix A. The value for the deformed emulsion droplet length for each run is recorded in Table 5.9.

The value of the maximum emulsion droplet diameter used in the calculation of the parameter d_g/d_e , was the 99 percent less than size, evaluated in Section 5.1. This value was used because the exact maximum droplet size could not be evaluated from the Coulter Counter analysis.

The Parameter d_g/d_e :

The ratio d_g/d_e for the pressure gradients 0, 1 and 5 psi/ft is shown in Table 5.8. From the values of the ratio d_g/d_e calculated, the type of plugging expected was determined using inequality 5.1.

The values of the ratio d_g/d_e for the 1 psi/ft pressure gradient, shows that for runs 101, 102 and 104 the values were greater than 6.493, which implies the porous medium should not become plugged. For runs 100, 103 and 106, the ratio d_g/d_e was less than 2.415, which implies the porous medium should be completely plugged. While for runs 109 - 129, the ratio was between the values of 2.415 and 6.493, which implies the porous medium should be partially plugged. Therefore the degree of plugging determined from the ratio d_g/d_e showed a perfect correlation with the experimentally observed results.

The correlation parameter d_g/d_e , therefore yields a simple technique for estimating whether an emulsion will plug an unconsolidated core by having knowledge of:

TABLE 5.9

CRITICAL CAPILLARY NUMBER

RUN	PORE RADIUS r_p	DROPLET RADIUS r_o	DROPLET LENGTH l_d	CRITICAL CAPILLARY NUMBER
101	13.85	12.7	-	-
102	13.15	12.7	-	-
104	12.66	12.7	25.4	8.02×10^{-4}
120	9.08	10.5	22.4	3.36×10^{-2}
114	8.31	10.5	23.2	5.03×10^{-2}
123	8.01	10.5	23.5	5.61×10^{-2}
124	7.93	10.5	23.6	5.65×10^{-2}
119	8.16	10.5	23.3	4.98×10^{-2}
113	8.08	10.5	23.4	5.24×10^{-2}
112	7.77	10.5	23.7	5.83×10^{-2}
111	8.01	10.5	23.5	5.15×10^{-2}
110	7.85	10.5	23.6	5.34×10^{-2}
121	8.16	10.5	23.3	4.27×10^{-2}
109	7.47	10.5	24.0	5.60×10^{-2}
126	6.10	10.5	25.4	7.53×10^{-2}
125	6.38	10.5	25.1	6.74×10^{-2}
129	4.98	10.5	26.5	8.76×10^{-2}
128	4.71	10.5	26.8	7.91×10^{-2}
127	4.54	10.5	27.0	6.95×10^{-2}
100	1.73	10.5	36.4	2.41×10^{-2}
106	1.66	10.5	36.4	1.85×10^{-2}
103	1.36	10.5	36.7	1.62×10^{-2}

- 1) the core permeability and porosity
- 2) maximum oil droplet size in the emulsion and
- 3) the interfacial tension.

Care however should be taken around the inequality values because of the errors and assumptions made in the analysis:

- 1) the estimation of the maximum droplet size in the emulsion,
- 2) estimation of the length L_d , over which the pressure gradient applies and
- 3) assuming the value for d_g calculated from the permeability and porosity using Equation 5.4 is valid for the core.

Examination of the values for the ratio d_g/d_e shown in Table 5.8, demonstrates that a change in the applied pressure gradient does have a moderate effect on the ratio d_g/d_e . This change in the deformed emulsion droplet size is the basis of the non-Darcy flow characteristic of emulsions described earlier.

Evaluation of the parameter d_g/d_d for the work of other researchers, shows that for Uzoigwe's work (36) on glass bead packs, the ratio varied from 35 to 126, which implies the experimentally observed result of no plugging. The value of the ratio for Cartmill's work (38) is 24 to 59, which predicts no plugging should occur. However, Cartmill observed that the $\frac{1}{2}$ to $1\frac{1}{2}$ micron sized emulsion droplets were screened out by the 37 to 88 micron glass beads. The ratios d_g/d_e and d_g/d_d are, however, only valid for plugging

due to capillary forces, while Cartmill suggested electrostatic rather than capillary forces were the reason for the plugging.

The experimental results of this study and the parameter d_g/d_e , further demonstrate that a core with any permeability can be plugged as long as the emulsion droplets are large enough. McAuliffe (12) stated that emulsions could effectively reduce the permeability of the core when the initial permeability was two darcies or less.

Capillary Number

The capillary number, N_c is most often defined as

$$N_c = \frac{v \mu}{\gamma} \quad (5.6)$$

which on combining with equations 2.17 and 2.18 can be written as

$$N_c = \frac{q \mu}{A \phi \gamma} = \frac{K K_r dP}{\gamma \phi dL} = \frac{K K_r 2 \cos \theta}{\phi L_d} \left\{ \frac{1}{r_p} - \frac{1}{r_o} \right\} \quad (5.7)$$

The values of the capillary number at which plugging of the porous medium commences can be calculated using the equation

$$N_c = \frac{K K_r 2 \cos \theta}{\phi L_d} \left\{ \frac{1}{r_p} - \frac{1}{r_o} \right\} \quad (5.8)$$

In this analysis, the value of the length over which the pressure gradient applies was calculated as before, the relative permeability is taken to be one, because there is no plugging and the contact angle is assumed equal to 90

degrees. Equation 5.8 can therefore be written

$$N_c = \frac{2 K}{\phi L_d} \left\{ \frac{1}{r_p} - \frac{1}{r_o} \right\} \quad (5.9)$$

The value for the pore throat size was taken as $0.077 d_g$ and the value for the maximum droplet size was again taken as the 99 percent less than size. The values of the capillary number calculated using this equation represent the value at which plugging of the porous medium will commence. When the capillary number exhibited in the flow system is less than this critical capillary number, then the oil droplets in the emulsion will plug the porous medium.

The values of the critical capillary number calculated using Equation 5.9 are reported in Table 5.9. A representation of the critical capillary number versus the core permeability, with a cross plot of the core porosity, calculated using the analysis of Equation 5.9, is shown in Figure 5.9. The results calculated from this simple model study, show that the critical capillary number necessary for pore plugging is lower for the low and high permeability cores and thus pore plugging will commence at a lower flow rate. Although the critical capillary number is lower for the low and high permeability cores, the pressure drop necessary for no plugging, increases as the permeability decreases. The critical pressure drop and flow rate necessary for no plugging to occur, are reported in Table 5.10. The capillary number concept might therefore be a useful parameter for determining whether an emulsion will

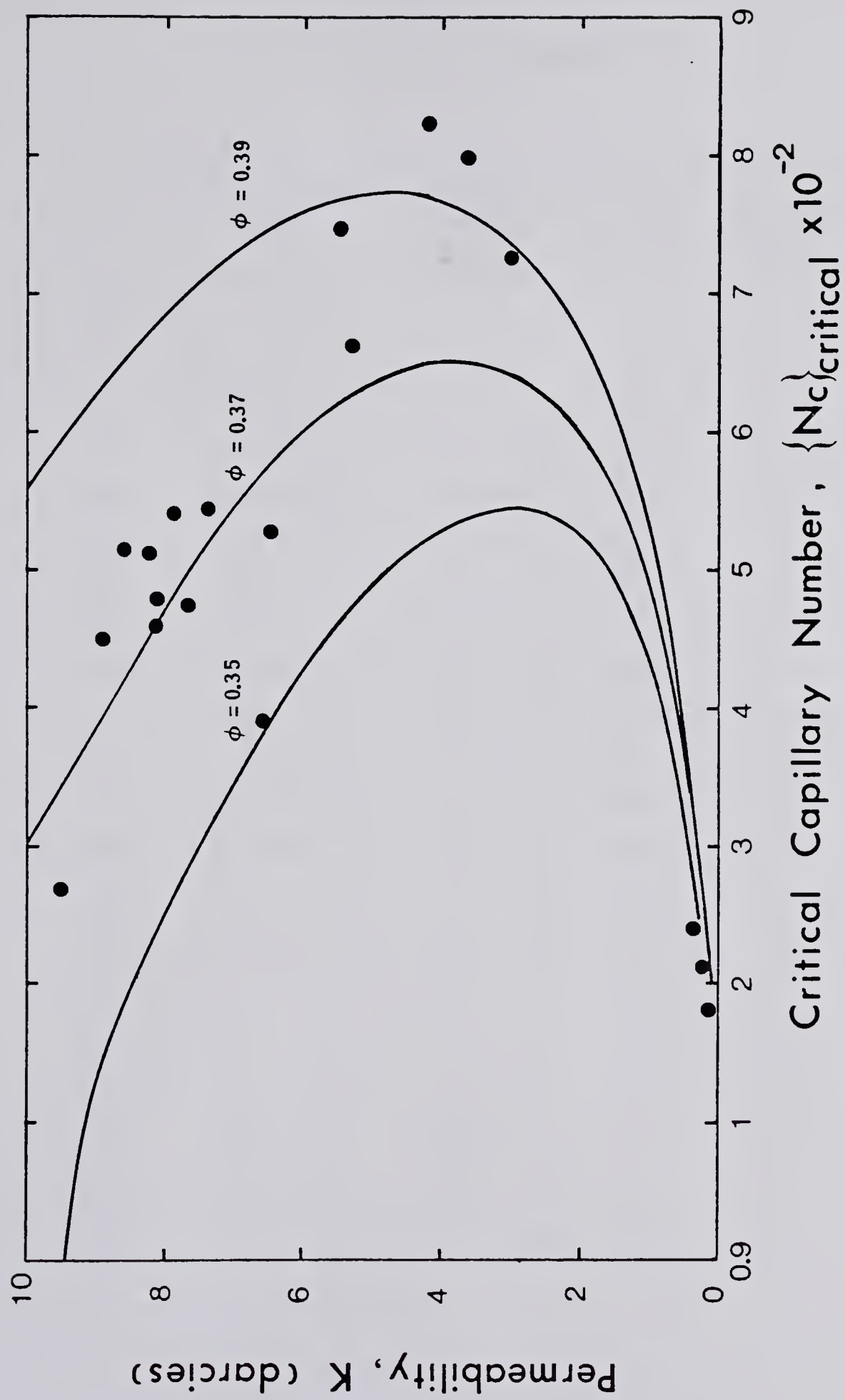


FIGURE 5.9 CRITICAL CAPILLARY NUMBER FOR PERMEABILITY REDUCTION

TABLE 5.10

CRITICAL BLOCKAGE PARAMETERS

RUN	CRITICAL CAPILLARY NUMBER	CRITICAL FLOW RATE cc/hr	CRITICAL VELOCITY ft/day	PRESSURE GRADIENT psi/ft
101	-	-	-	-
102	-	-	-	-
104	8.02×10^{-4}	207	26.2	0.2
120	3.56×10^{-2}	1.3×10^4	1530	14.1
114	5.03×10^{-2}	1.98×10^4	2290	22.9
123	5.61×10^{-2}	2.26×10^4	2600	26.7
124	5.65×10^{-2}	2.28×10^4	2640	27.8
119	4.98×10^{-2}	1.99×10^4	2290	24.8
113	5.24×10^{-2}	2.05×10^4	2390	25.8
112	5.83×10^{-2}	2.32×10^4	2680	29.9
111	5.15×10^{-2}	1.98×10^4	2340	26.7
110	5.34×10^{-2}	2.10×10^4	2490	28.8
121	4.27×10^{-2}	1.55×10^4	1910	24.8
109	5.60×10^{-2}	2.19×10^4	2610	34.1
126	7.53×10^{-2}	3.05×10^4	3430	57.4
125	6.74×10^{-2}	2.65×10^4	3080	51.9
129	8.76×10^{-2}	3.51×10^4	4030	84.5
128	7.91×10^{-2}	3.25×10^4	3560	92.7
127	6.96×10^{-2}	2.97×10^4	3230	98.4
100	2.41×10^{-2}	6.46×10^4	7830	291
106	1.85×10^{-2}	4.74×10^4	6190	305
103	1.62×10^{-2}	4.07×10^4	5240	379

plug a porous medium at a particular flow rate.

The values for the critical capillary number calculated in this study varied from 1.81×10^{-2} to 8.24×10^{-2} for the cores which were plugged. Morrow (32) in his study on the mobilisation of residual oil reported capillary numbers of 1.43×10^{-2} to 1.68×10^{-2} for similar oil droplet to grain size ratios.

For runs 101 and 102, the capillary number was not calculated because the emulsion droplet was smaller than the pore throat size and therefore the core could not be plugged. For run 104, the capillary number was evaluated to be 7.02×10^{-4} . This capillary number predicts that the core would be plugged for flow rates less than 180 cc/hr. Within the experimental accuracy of measuring the pressure drop across the core, there was no plugging of the core for the flow rates of 560, 320 and 100 cc/hr. However, when the pore throat radius and the emulsion droplet radius are similar, the evaluation of the critical capillary number and thus the critical flow rate, are very sensitive to the input data. A sensitivity analysis on the critical capillary number is reported in Appendix B, along with the conditions when the capillary number concept is reliable for predicting the plugging of a core.

For runs 109 to 129, the capillary number during the displacement tests varied from 5.5×10^{-5} to 1.4×10^{-3} , while the capillary numbers varied from 1.81×10^{-2} to 8.24×10^{-2} . Therefore for the runs 109 to 129, the capillary

number was lower than the critical, verifying that plugging should occur.

Thus although there are errors and assumptions made in evaluating the capillary number and measuring the permeability of the core to emulsion, the concept of using the critical capillary number for predicting whether a core will be plugged by an emulsion would appear to be a useful concept.

5.4 EMULSION VISCOSITY CORRELATION

In this study, the emulsion viscosity correlation

$$\nu_e = \nu_w (1 + C_1 \Gamma + C_2 \Gamma^2) \quad (2.1)$$

was used to evaluate the produced emulsion concentration. From the produced emulsion concentration, a material balance was carried out, from which the oil retention in the core was established. The use of a viscosity correlation for establishing a material balance was used by Holm (50), in the investigation of the retention of polymers during a flood.

The values of the constants C_1 and C_2 for the runs 119, 120, 128 and 129, for which the correlation was used, are reported in Table 5.11. A representative figure of the correlation versus the experimental data is shown in Figure 5.10 for run 119. In all cases, the error in the correlation was less than the error associated with measuring the emulsion viscosity.

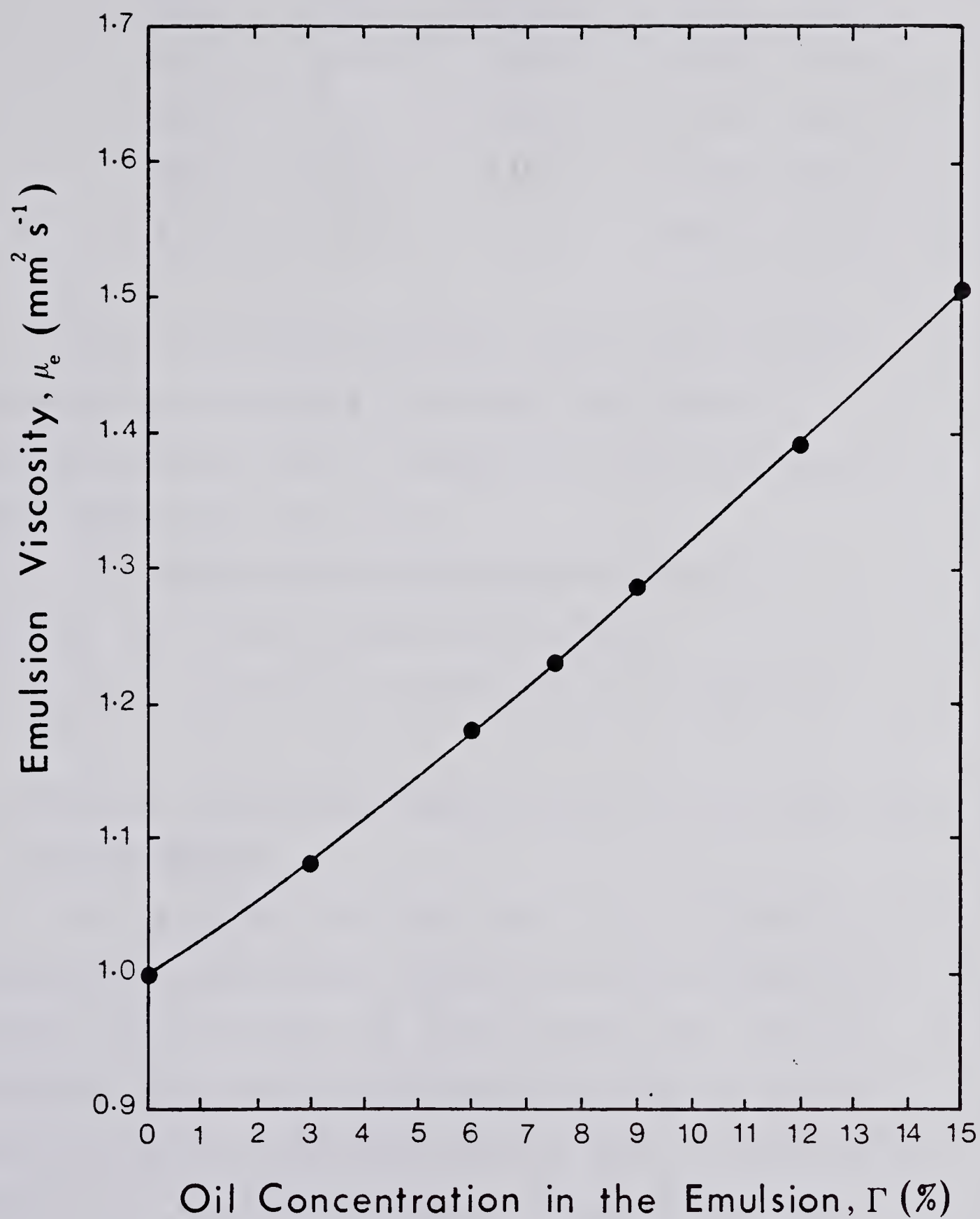


FIGURE 5.10 EMULSION VISCOSITY CORRELATION
RUN 119

TABLE 5.11
CONSTANTS FOR THE VISCOSITY CORRELATION

Run	Viscosity		Constants	
	mPa.s	mm ² s ⁻¹	C ₁	C ₂
119	1.48	1.50	2.738	4.444
120	1.50	1.53	2.967	3.556
128	1.51	1.54	2.920	4.622
129	1.52	1.55	2.843	5.649

It was therefore believed that the use of the viscosity correlation to calculate the emulsion concentration was more accurate than the other methods which might have been used:

- 1) distillation of the produced emulsion,
- 2) use of the Coulter Counter and
- 3) the electrical resistivity of the solution.

5.5 UNSTEADY STATE FLOW CHARACTERISTICS OF EMULSIONS IN A POROUS MEDIUM

Four runs 119, 120, 128 and 129 were carried out to investigate the unsteady state flow characteristics of emulsion flow through the porous medium. The raw and processed data used to calculate the produced emulsion concentration profiles for the four runs, is reported in Appendix C. A summary of some of the pertinent data collected in these runs is shown in Tables 5.12 and 5.13. The produced emulsion concentration profiles for the runs

TABLE 5.12

SUMMARY OF PERTINENT EXPERIMENTAL DATA
UNSTEADY STATE FLOW CHARACTERISTIC RUNS

	119	120	128	129
Maximum Oil Saturation	0.171	0.176	0.198	0.167
Plugged Oil Saturation	0.0835	0.0987	0.152	0.120
Fractional Porosity To Flow	0.583	0.515	0.308	0.325
Blockage Coefficient	4.99	4.91	4.56	5.61
Breakthrough Time (Pore Volumes)	0.727	0.745	0.638	0.659
Injection Rate (cc/hr)	560	560	100	100
Core Permeability (darcies)	8.12	9.50	3.64	4.24
Fractional Permeability	0.810	0.765	0.521	0.544

TABLE 5.13

SUMMARY OF EXPERIMENTAL DATA FOR RUN 129

CHANNEL	INLET CONCENTRATION	RETAINED		PLUGGED		PLUGGED OIL SAT. INLET CONC.		RETAINED OIL SAT. INLET CONC.	
		OIL	SATURATION	OIL	SATURATION				
3 + 4	0.0603	0.0585		0.0394		0.968		0.97	
5	0.03525	0.0353		0.0241		1.10		1.00	
6	0.0294	0.0353		0.0253		1.27		1.18	
7+	0.02525	0.04		0.032		1.88		1.58	

are shown in Figures 5.11 to 5.14.

Explanations based upon the current emulsion and immiscible flow theories are proposed to describe the findings of this study. The interpretations are however limited to general concepts due to the wide differences in the properties of the porous media and the flow rates used in the runs.

5.5.1 Produced Emulsion Concentration Profile

Although it was not possible to ascertain the exact breakthrough time for each run in this study, it was observed that breakthrough occurred earlier in those experiments conducted at lower flow rates. An exact breakthrough time could not be evaluated because the produced fluids passed from clear, to cloudy, to a distinct colouration over a period of a few cetilitres. For all the runs, the oil phase breakthrough occurred before one pore volume of emulsion was injected. It is believed that one criterion for the oil phase breakthrough time, is the relationship between the maximum oil phase saturation in the core and the injected emulsion concentration.

In the low concentration emulsion floods of Devereux (39) the maximum oil saturation in the porous medium was many times the inlet concentration. In these runs, initially only the original water phase in the core and the external water phase of the emulsion were produced. The oil phase of the emulsion did not breakthrough until a number of pore

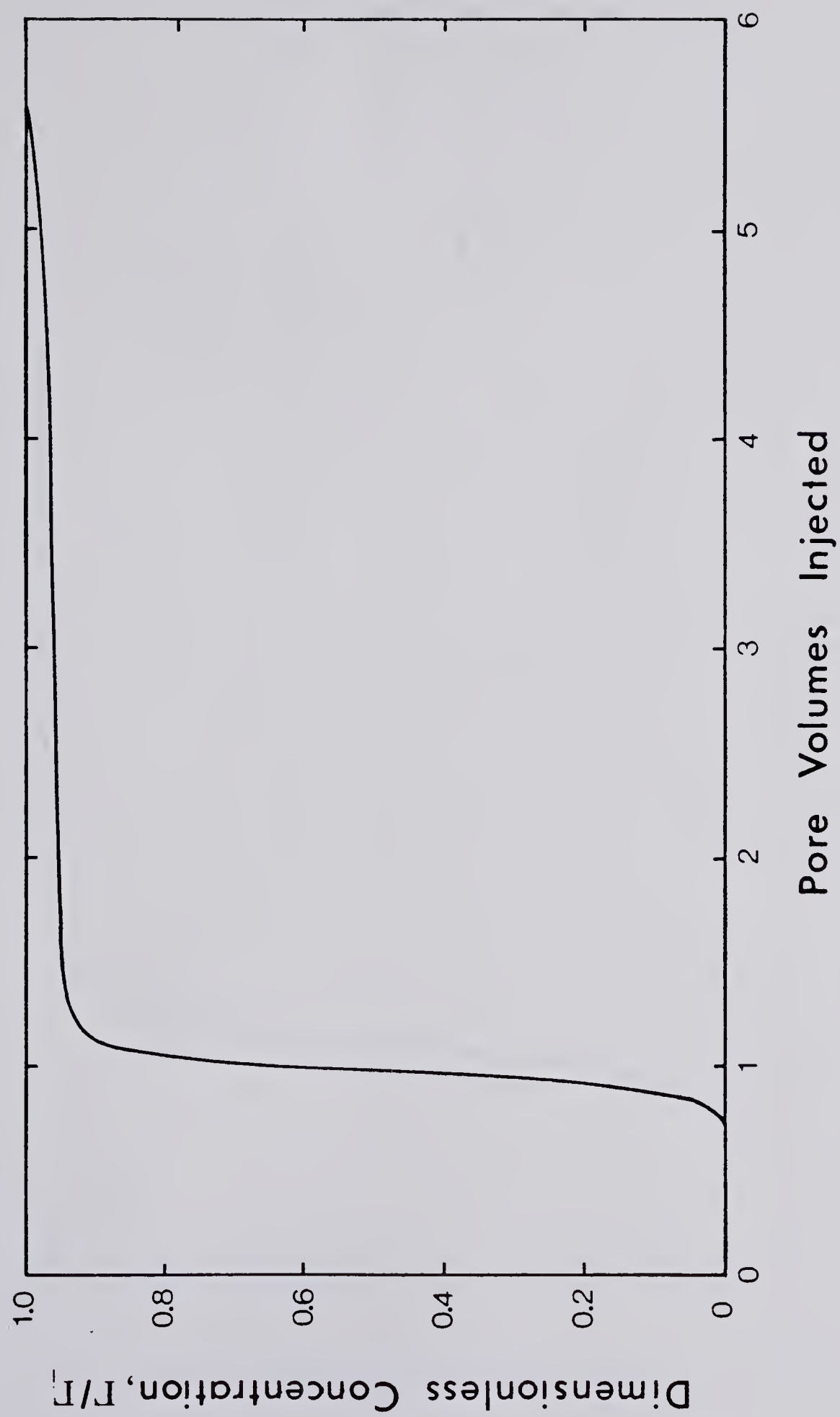


FIGURE 5.11 PRODUCED EMULSION CONCENTRATION : RUN 119

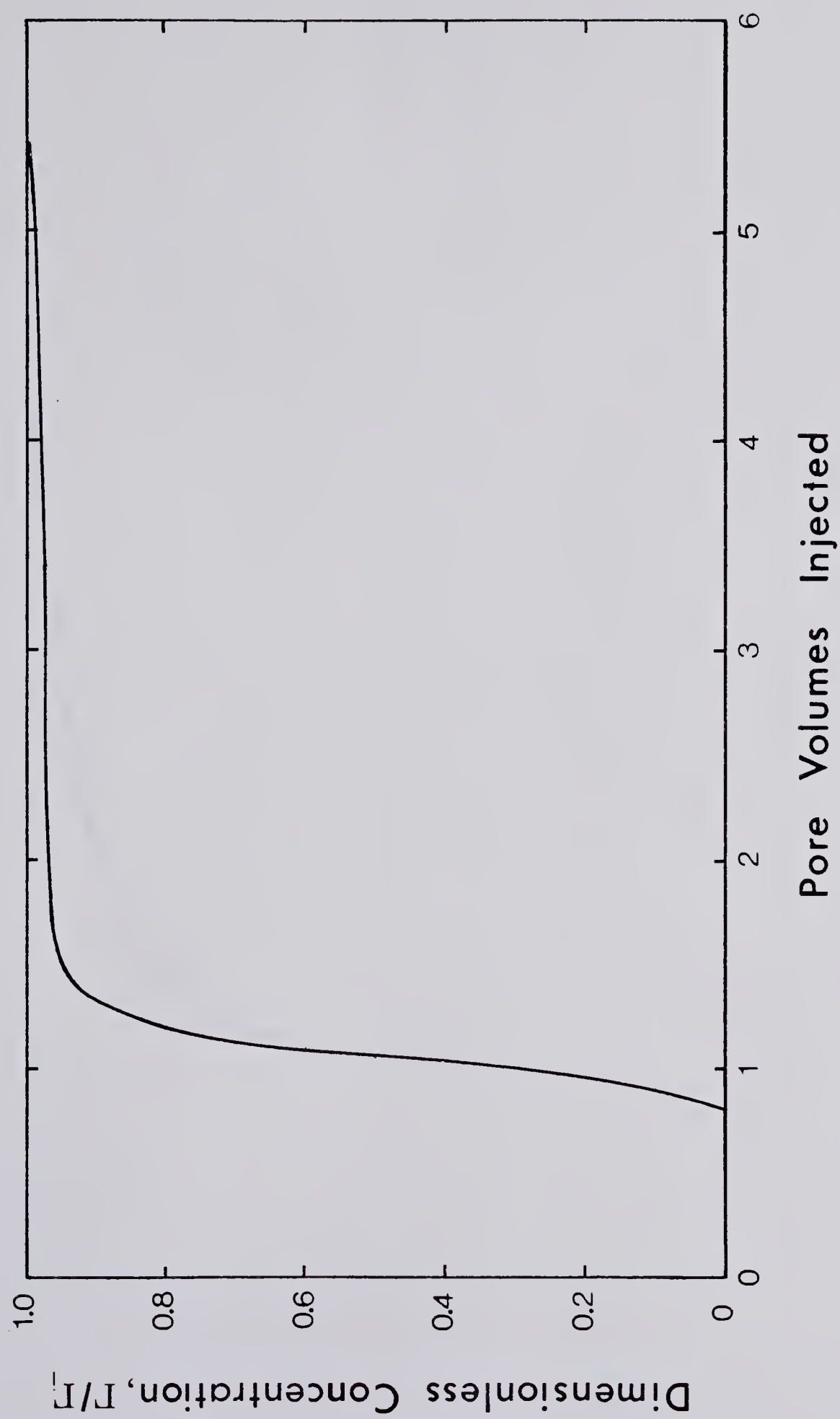


FIGURE 5.12 PRODUCED EMULSION CONCENTRATION : RUN 120

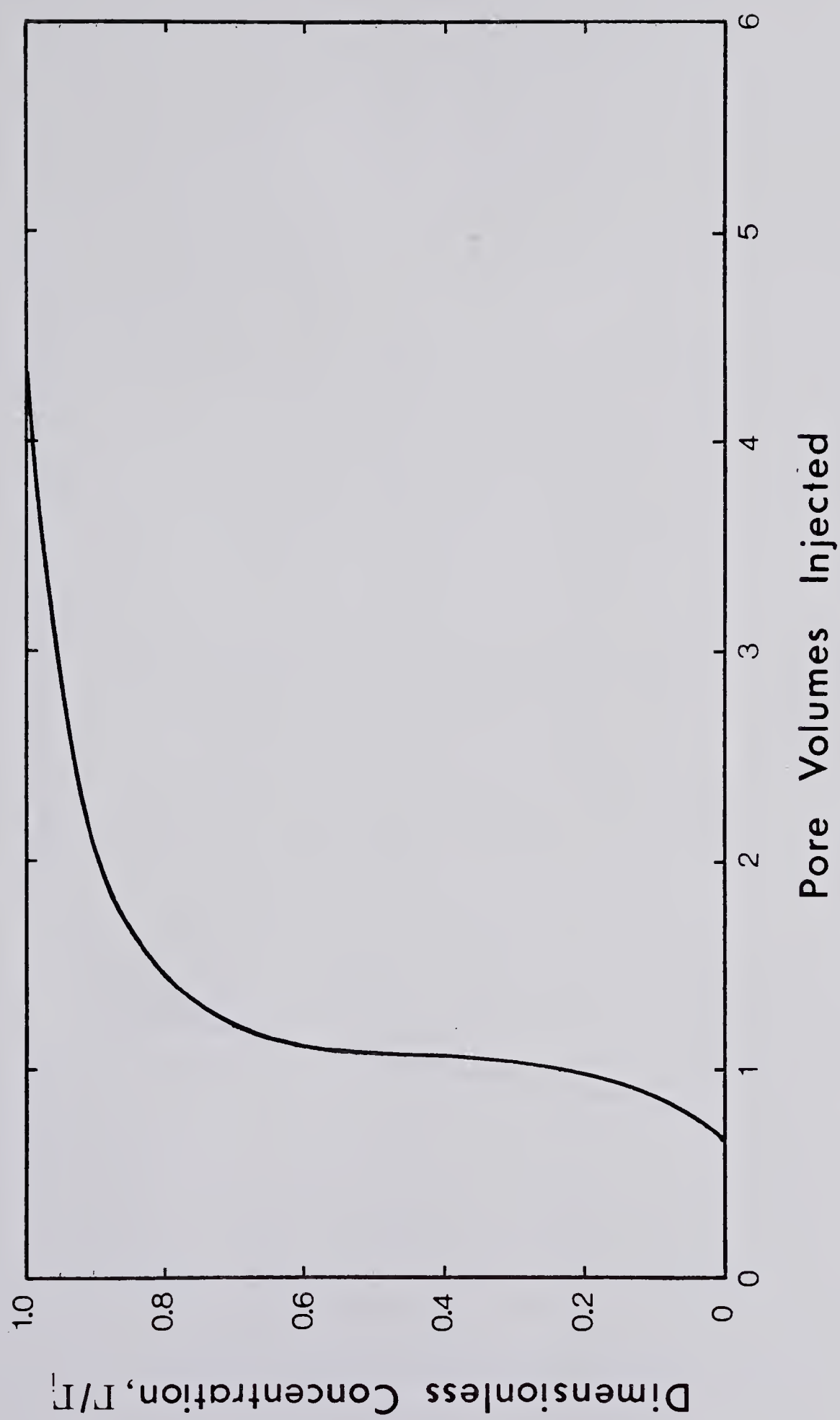


FIGURE 5.13 PRODUCED EMULSION CONCENTRATION : RUN 128

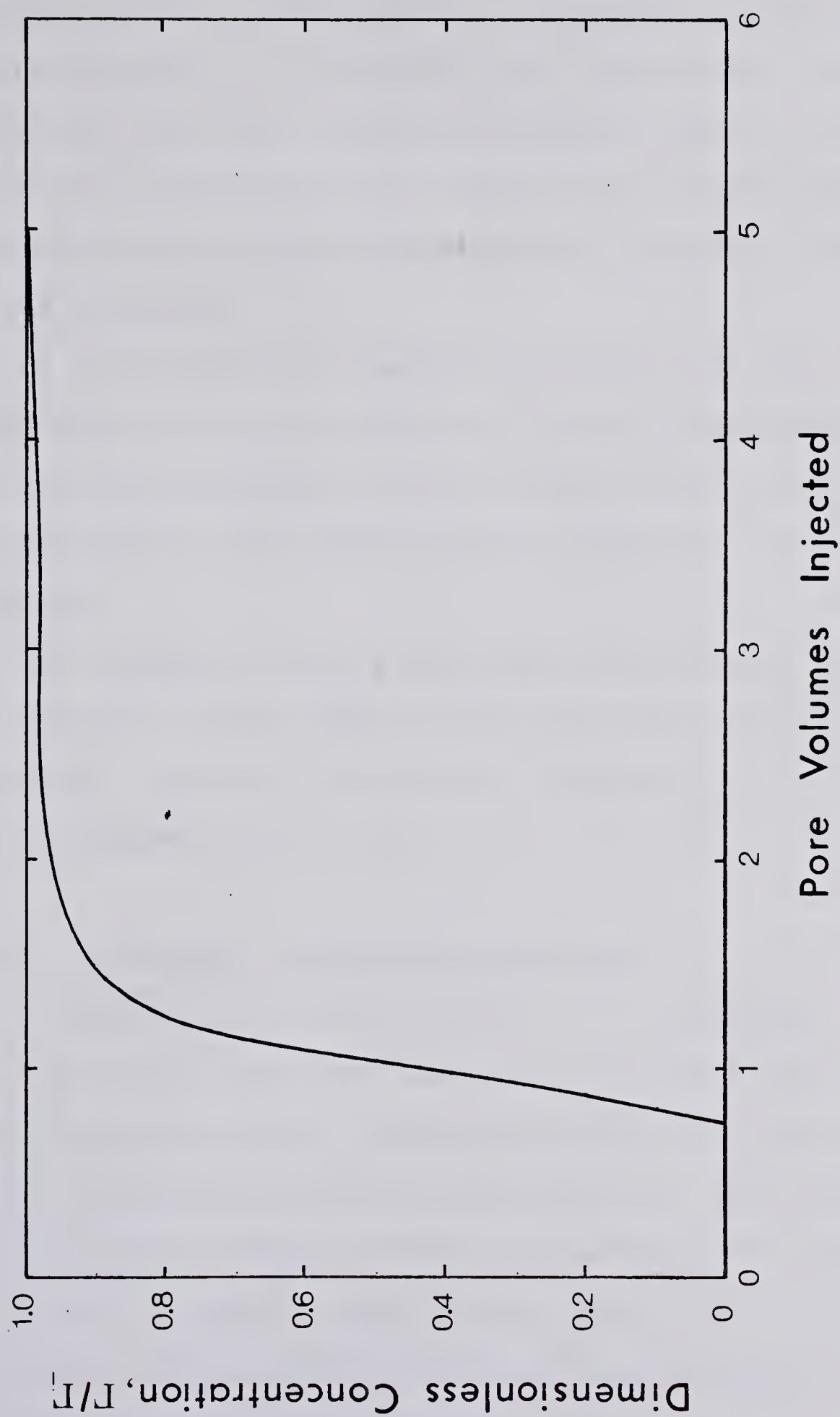


FIGURE 5.14 PRODUCED EMULSION CONCENTRATION : RUN129

volumes of emulsion were injected. A possible explanation for the delayed oil phase breakthrough is the high efficiency of the porous medium at screening out the emulsion droplets. In this study, see Table 5.12, the oil saturation S_o was only marginally greater than the inlet concentration of the emulsion and the lower screening efficiency of the porous medium led to an earlier oil phase breakthrough.

It is believed that another criterion for the number of pore volumes injected before oil phase breakthrough occurs in the laboratory, is the length of the core. This criterion will be discussed further in Section 5.6.3 of this study.

The results of this study also showed that a steeper front occurred in the higher flow rate runs. This can be observed by comparing the produced emulsion profiles shown in Figures 5.11 to 5.14.

5.5.2 Oil Retention in the Porous Medium

A comparison of the magnitudes of the maximum oil saturation within the cores for each run is not justifiable, as the properties of the porous medium and the flow rates varied for each run. However, the results do show that the oil accumulation in the core for all the runs was slightly greater than the inlet concentration, see Table 5.12. Thus the blockage coefficient (b) for each run was always less than $1/\Gamma$, which for these runs was 6.667.

The results of this study also confirm the observation of McAuliffe (12) that emulsified oil is more efficient at reducing the permeability than oil left after waterflooding. The results for run 129, reported in Appendix C, show that a plugged oil saturation of 12 percent reduced the core permeability by 45.6 percent, while for residual oil it would be approximately 25 percent using McAuliffe's analysis (12).

In order to investigate the plugging capability of the emulsion, a droplet size distribution was carried out on the produced emulsion in run 129. The results of this analysis are reported in Appendix D, and a smoothed graph of the droplet size versus pore volumes injected is shown in Figure 5.15. The size distribution of the emulsion was divided up into four sizes in order to simplify the manipulation and presentation of the data.

Comparison of the produced emulsion droplet size distribution near the end of the run and the inlet size distribution, shows that the characteristics of the produced emulsion were approaching the inlet conditions. This trend of the produced emulsion droplet size towards the inlet size distribution, implies that for steady state conditions, the conservation of droplet size within the emulsion would occur. This phenomenon of no aggregation or breaking up of the droplets at steady state flow conditions in a porous medium, for low concentration emulsions, was also observed by Uzoigwe (36).

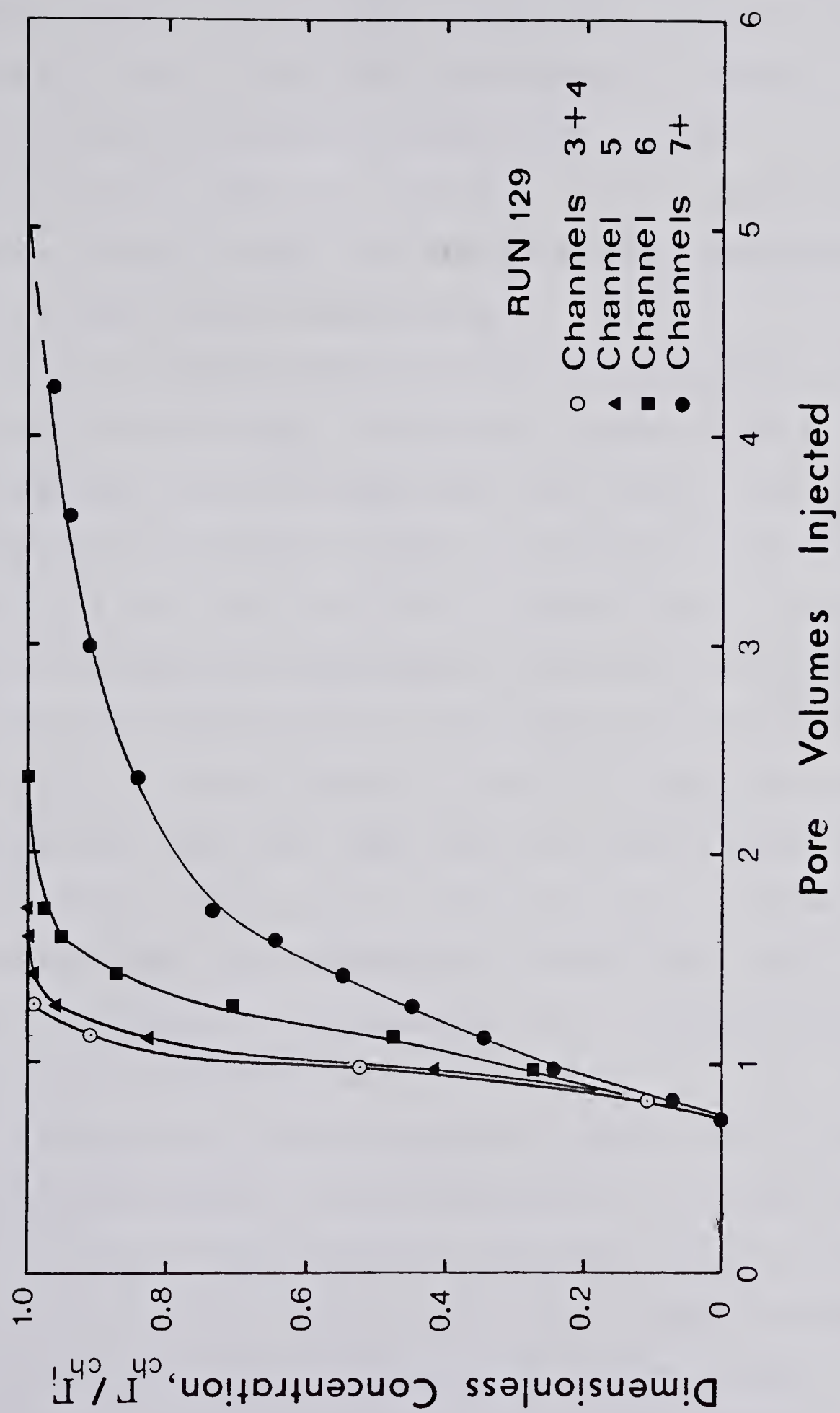


FIGURE 5.15 DROPLET SIZE DISTRIBUTION OF PRODUCED EMULSION

The results reported in Table 5.13 show that there were different degrees of retention in the core for the different droplet size ranges. Within the limits of the evaluation, the oil droplets represented in channels 6 and 7+ of the Coulter Counter analysis had a higher concentration in the core than their inlet concentration. Channels 3+4 and 5 were both retained with a concentration close to their inlet concentration.

One explanation for the different retentions, for each droplet size range, is that the larger droplets have more plugging sites to occupy than the smaller droplets. Considering the parameter d_g/d_d , described earlier in section 5.3, then the droplets of channels 3+4, 5 and 6 would not normally be retained in the core if they were the only droplets flowing in the core. The value of the ratio d_g/d_d for each channel is shown in Table D4. Thus it is postulated that the larger droplets plug off the constrictions and the smaller droplets which would normally not be retained, are retained in cavern sites behind the larger droplets or in combination with the larger droplets to plug off a constriction.

Although the smaller droplets reached their inlet concentration rapidly, it is believed that they were still being trapped in constrictions along with larger droplets throughout the run. However, the droplets were breaking away from other sites and because the droplets were retained at a concentration similar to their inlet

concentration, their concentration in the core remained approximately constant.

Examination of the results for channels 7 and 8 near the end of the run, see Table D2, shows that these channels had a larger concentration of droplets leaving the core than were being injected. A possible explanation for why these droplets were leaving the core at a higher rate than their injection rate, is that the pressure drop had increased sufficiently to squeeze the droplets through the constrictions and because the droplets were retained within the core at a concentration higher than their inlet concentration, they were produced at a higher concentration.

Thus for droplets within a certain size range, such as was exhibited by channels 7 and 8, their concentration at steady state conditions may not represent their highest concentration recorded throughout the run. Their maximum concentration is reached prior to steady state conditions and the concentration then becomes smaller as the droplets leave their constriction sites. Thus for each droplet size there is an equilibrium concentration at steady state conditions and a maximum concentration and these conditions do not have to be equal. Thus superimposed on the rate at which droplets are plugged, is the rate at which the droplets are released from their capture sites.

Thus the results of run 129, shown in Tables D2 and 5.13 and in Figure 5.15, show that:

- 1) each droplet size takes a different time for the

produced concentration to reach the inlet concentration,

- 2) there are different degrees of retention for each droplet size range,
- 3) the maximum concentration for a particular droplet size does not have to be equal to the concentration at steady state conditions and
- 4) the produced concentration for a particular droplet size can be greater than the inlet concentration.

5.5.3 Pressure Profiles

The pressure profiles for the runs 119, 120, 128 and 129 are shown in Figure 5.16. These profiles show two characteristics of liquid-liquid displacements in a porous medium:

- 1) the curved pressure profile after breakthrough and before steady state conditions are reached and
- 2) the curved nature of the pressure drop profile versus time, prior to breakthrough, which designates that a stabilised front had not formed.

5.5.4 Effect of Interrupting the Flow on the Equilibrium of the Flow System

Three parameters, the pressure drop, the produced emulsion concentration and the droplet size distribution were examined to establish the effect of interrupting the emulsion flow on the system equilibrium.

The pressure profiles shown in Figure 5.16, demonstrate that after interrupting the flow, it took approximately one third of a pore volume (50 cc.) in the small core holders, to reattain the pressure drop present before interrupting the flow. This phenomenon could be due to the emulsion droplets breaking away from their plugging sites when the flow was stopped and on restarting the flow, some of the droplets flowed out of the area by a route other than their plugging site. It then takes some time for the droplet to find another plugging site.

A similar disturbance was not observed in the emulsion viscosity or droplet size distribution data, although this could have been masked due to the influence of the end blocks and the size of the samples taken.

5.6 EMULSION FLOW MODEL

5.6.1 Emulsion Flow Model

The curves on Figure 5.17 to 5.20 represent the best fit of emulsion flow model 3, Equation 5.14, to the experimental data for runs 119, 120, 128 and 129, respectively. The best fit values for the coefficients H_0 , β and \bar{e} for the model are shown in Table 5.14. The results demonstrated that the model can effectively describe the early time periods of the experimental curves. However, the model did predict an earlier time to reach steady state conditions.

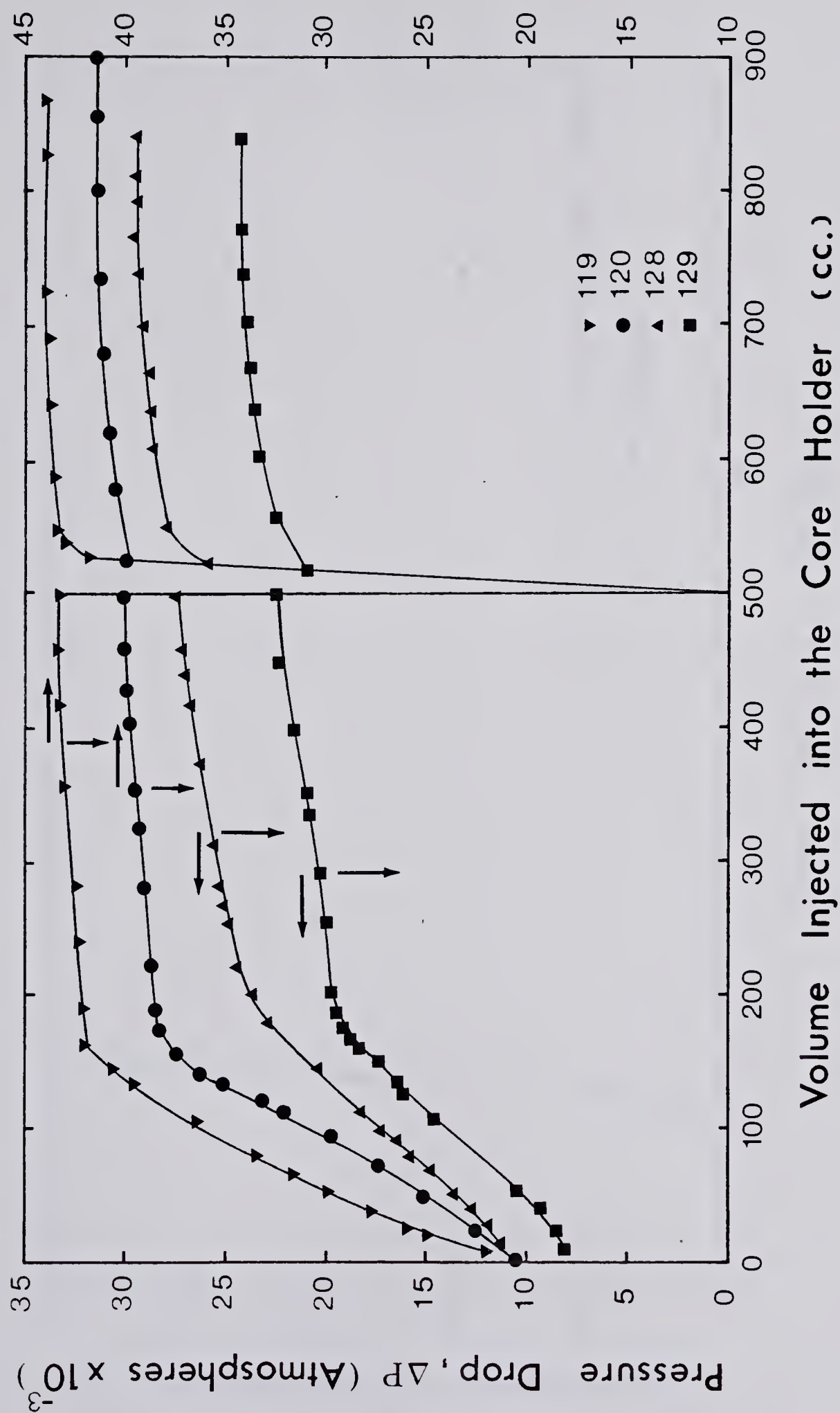


FIGURE 5.16 PRESSURE DROP PROFILES FOR RUNS 119,120,128 AND 129

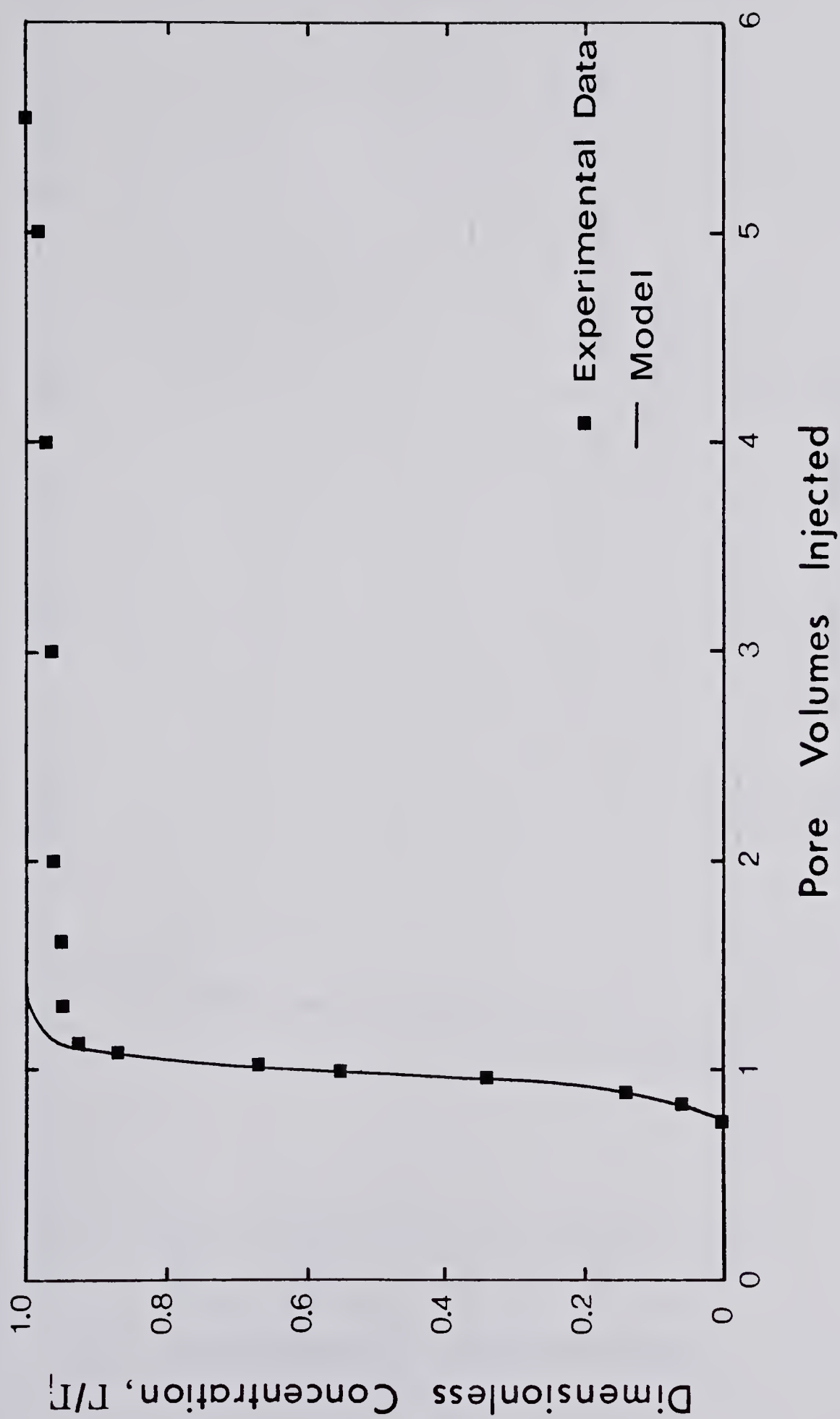


FIGURE 5.17 EXAMINATION OF MODEL 3 : RUN '119

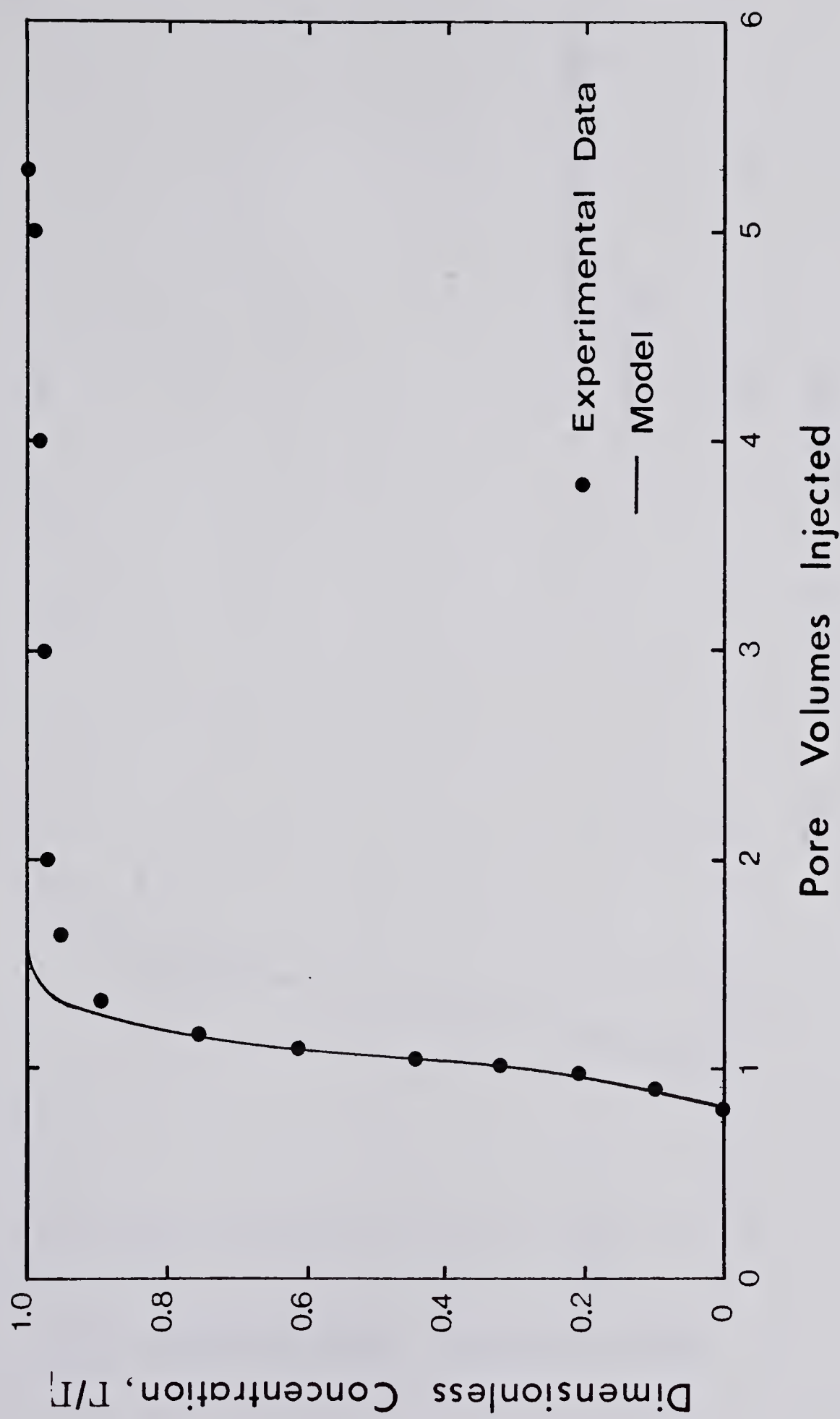


FIGURE 5.18 EXAMINATION OF MODEL 3 : RUN 120

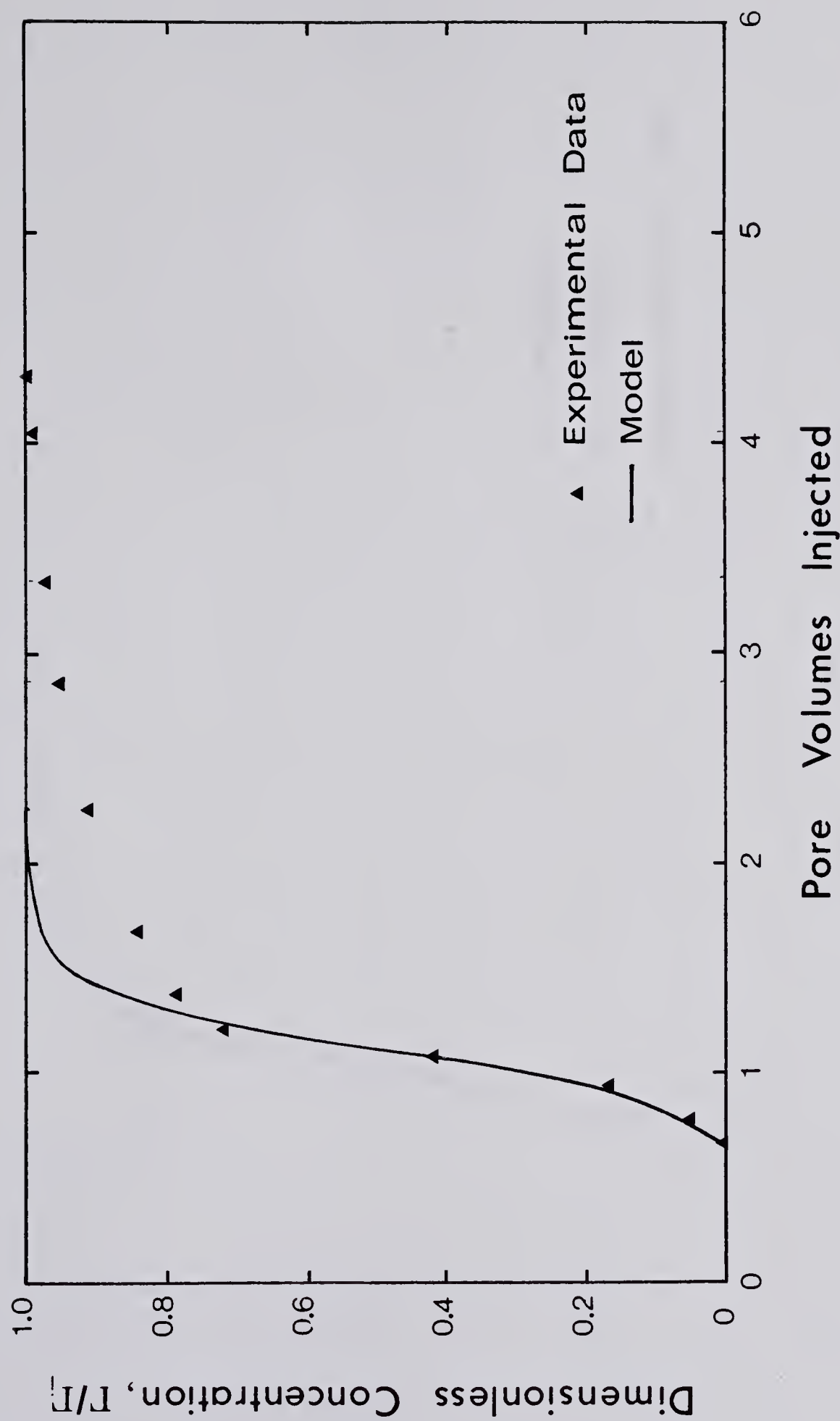


FIGURE 5.19 EXAMINATION OF MODEL 3 : RUN 128

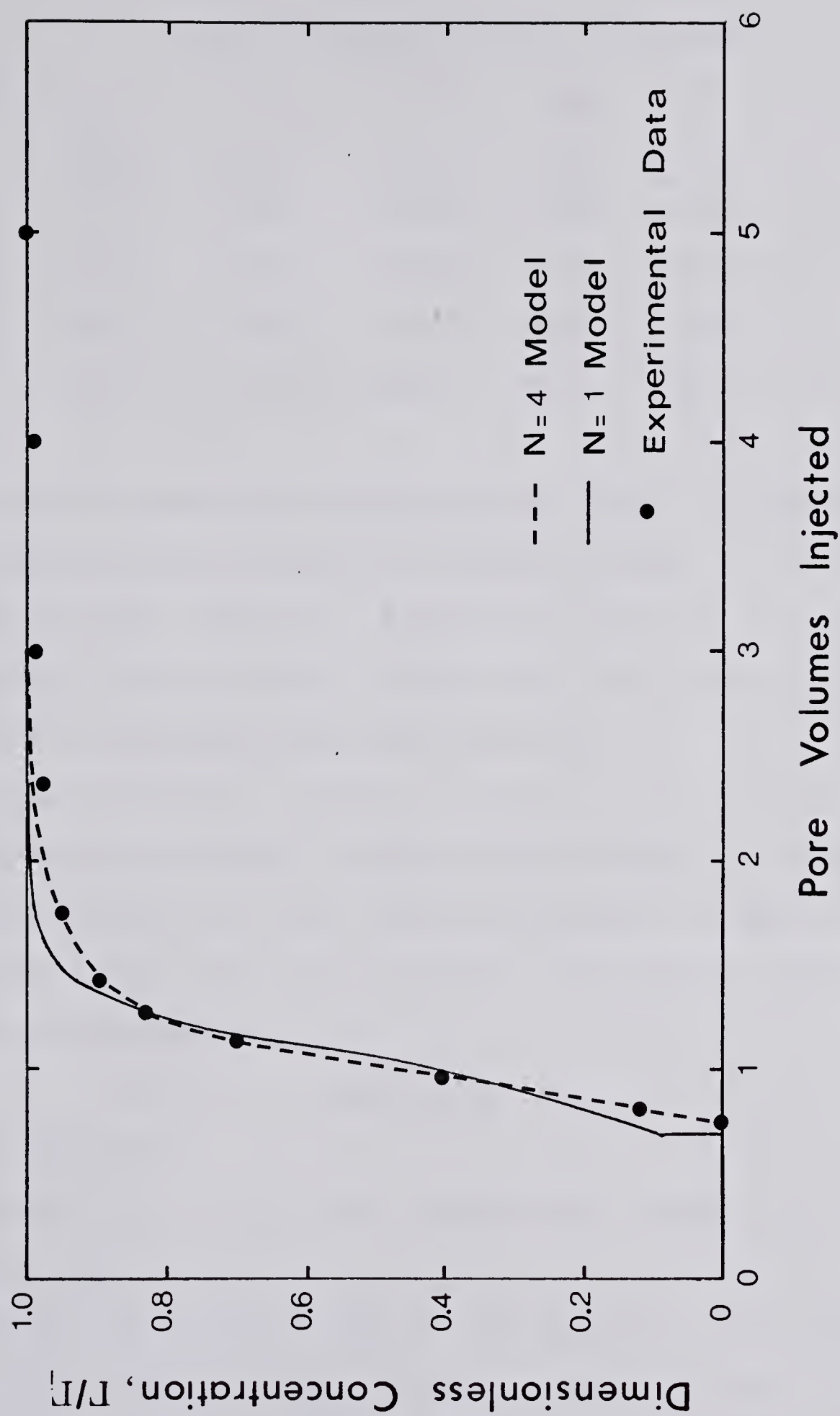


FIGURE 5.20 EXAMINATION OF MODEL 3 : RUN 129

TABLE 5.14

BEST FIT COEFFICIENTS FOR MODEL 3

RUN	H_0 sec^{-1}	β -	t_{bt} sec	$\bar{\epsilon}$ -	α cm^{-1}
119	0.812	0.0764	746	0.727	35.6
120	0.422	0.0979	753	0.745	18.2
128	0.033	0.136	3859	0.638	8.5
129	0.029	0.116	3807	0.659	7.3

It was found in this study that model 3 fitted the experimental data the best, followed by model 1, then 2 and because of this, the fits of models 1 and 2 are not shown. An insight into why model 3 fitted the data the best can be obtained by examining the coefficient β .

When comparing the fits of models 1 and 2 together, the value of β in model 2 always increased to the upper limiting value set in the computer program. In model 2, as β becomes larger, the form of model 2 approaches model 1, because the variable

$$(\beta - \sigma) \text{ approaches } \beta$$

and the function

$$\text{const.} (\sigma_m - \sigma)(\beta - \sigma) \text{ approaches } \text{const.} (\sigma_m - \sigma)$$

which is model 1.

Comparing models 3 and 1, the values of β in model 3 were always similar to σ_m . If model 1 was the better model, then β in model 3 would try to be as large as possible in order that the form of model 3 would approach model 1.

However, β was similar to σ_m , and as such the form of the rate equation is convex in shape, rather than linear. Figure 3.2 shows the comparative shapes of the different kinetic rate equations.

The method by which the model is fitted to the experimental data is described in Appendix E. In evaluating the best fit coefficients of the model, it was found that there was not one unique set of constants which produced the best fit to the data. Due to the interrelation between H_0 and β in the model, there were a series of similar values of H_0 and β which provided an identical fit. Although these coefficients gave the same fit to the experimental data, it was found that for later times, some of these sets of coefficients seriously violated the material balance for the system. Thus for further work in this area, longer cores should be used because the evaluation of the coefficients of the model is more sensitive on a fully developed front.

The rate coefficient α is defined as $H_0 A \phi / q$ and Trzaska (45), in his work on filtration, stated that an increase in the flow rate resulted in an increase in the value of the rate coefficient α . This observation states that for a higher flow rate, the rate of plugging increases and a steeper front exists within the core. Although the core properties of each run were different in this study, it can be seen in Table 5.14 that the value of the rate coefficients α were higher for the higher flow rate runs.

For run 128, the model did not provide a good fit to

the experimental data. One possible reason for the poor fit, is that emulsions are made up of droplets of different sizes and the model assumed droplets of one distinct size. The results reported in Table 5.13 show that for the four size ranges, each range was retained in different amounts and thus the poor fit of the model could be associated with the nature of the model. If the emulsion droplet size ranges are retained in different amounts, then the model should allow for this phenomenon. Also a different form of the model to those used in this study, may produce a better fit to this type of produced oil concentration profile. A model that may produce a better fit will be discussed in Section 5.6.5

5.6.2 N-Fractional Size Emulsion

The model for a n-fractional size emulsion is described because emulsions are made up of droplets of different sizes, rather than of one size and each size has a different probability of capture.

The raw and processed data of the produced emulsion droplet size distribution profile is reported in Appendix D. A summary of some of the pertinent data collected in run 129 is shown in Table 5.13. The fit of the model, for each size range, to the experimental data is shown in Table D8 and Figure 5.21. The fit of the model of the combined size range data, to the produced emulsion concentration profile, is shown in Table D9 and Figure 5.20. The best fit

values for the coefficients H_0 , β and $\bar{\epsilon}$ for each size range are shown in Table 5.15.

TABLE 5.15
COEFFICIENTS FOR N=4 EMULSION MODEL

Channel	H_0 sec^{-1}	β -	$\bar{\epsilon}$ -	σ_m -
3 + 4	0.587	0.0311	0.679	0.0389
5	1.162	0.0244	0.662	0.0238
6	0.640	0.033	0.666	0.0251
7+	0.227	0.048	0.662	0.032

The results shown in Table D8 and Figure 5.21 demonstrate that the model can effectively describe the experimental curves for the individual droplet size ranges. Comparison of the data shown in Table D9 and Figure 5.20 shows that the n-fractional sized emulsion model fitted the experimental data better than emulsion flow model 3. The n-fractional model provided a better fit because with the nature of this model, it could allow for each size range of the emulsion to be retained in different concentrations.

Examination of the data shown in Table 5.15, shows that for all the channels, the value of β was similar to σ_m and this further confirms the validity of model 3, Equation 5.11, over the other two models used in this study. Although the n-fractional model effectively fitted the data presented in the four size ranges, the nature of

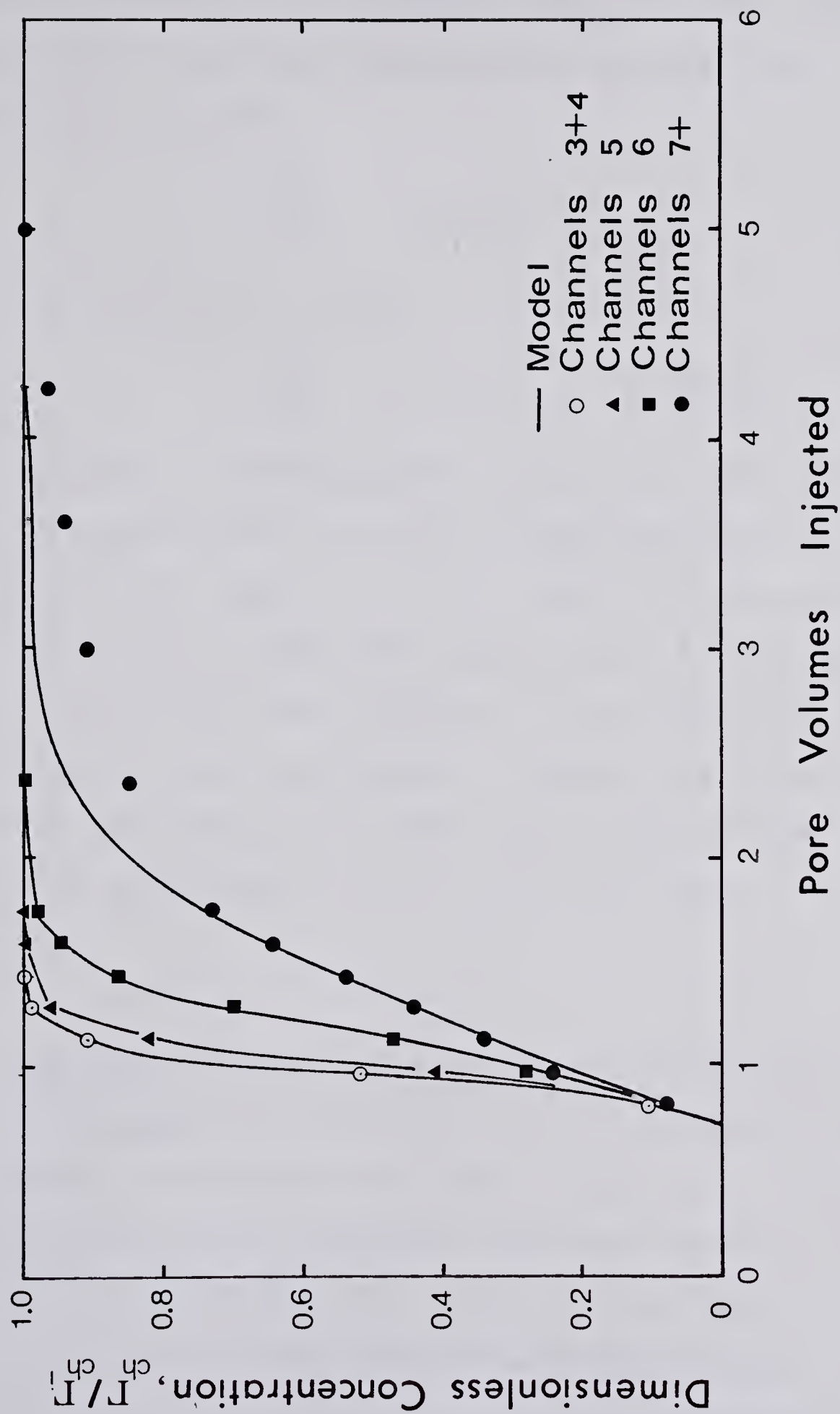


FIGURE 5.21 EXAMINATION OF MODEL 3 FOR EACH SIZE RANGE : RUN129

the kinetic equation is not of the correct form. As explained in Section 5.5.2, the concentration for a certain size range may be greater during the run, than when steady state conditions are attained. As such, the kinetic equation of the form

$$\frac{\partial \sigma}{\partial t} = H_o f(\sigma)$$

should be replaced by a form

$$\frac{\partial \sigma}{\partial t} = H_o f(\sigma) - H_r f(\sigma)$$

where the first term designates the rate at which the emulsion concentration tends to its maximum saturation and the second term, the rate at which the particles leave their constriction sites. The combination of these two rates, yielding the rate at which the concentration tends to its equilibrium concentration. However, in these early stages of modelling this highly complicated process, the simplified model seems to be to a certain extent justified.

5.6.3 Emulsion Saturation and Concentration Profiles

The plugged oil saturation and the flowing emulsion concentration variation with time and position, in the porous medium, can be evaluated using the emulsion flow model. Figure 5.22 shows the change in the plugged oil saturation with time for run 129 using the n=1 size ranged emulsion flow model. Figure 5.23 shows the concentration of

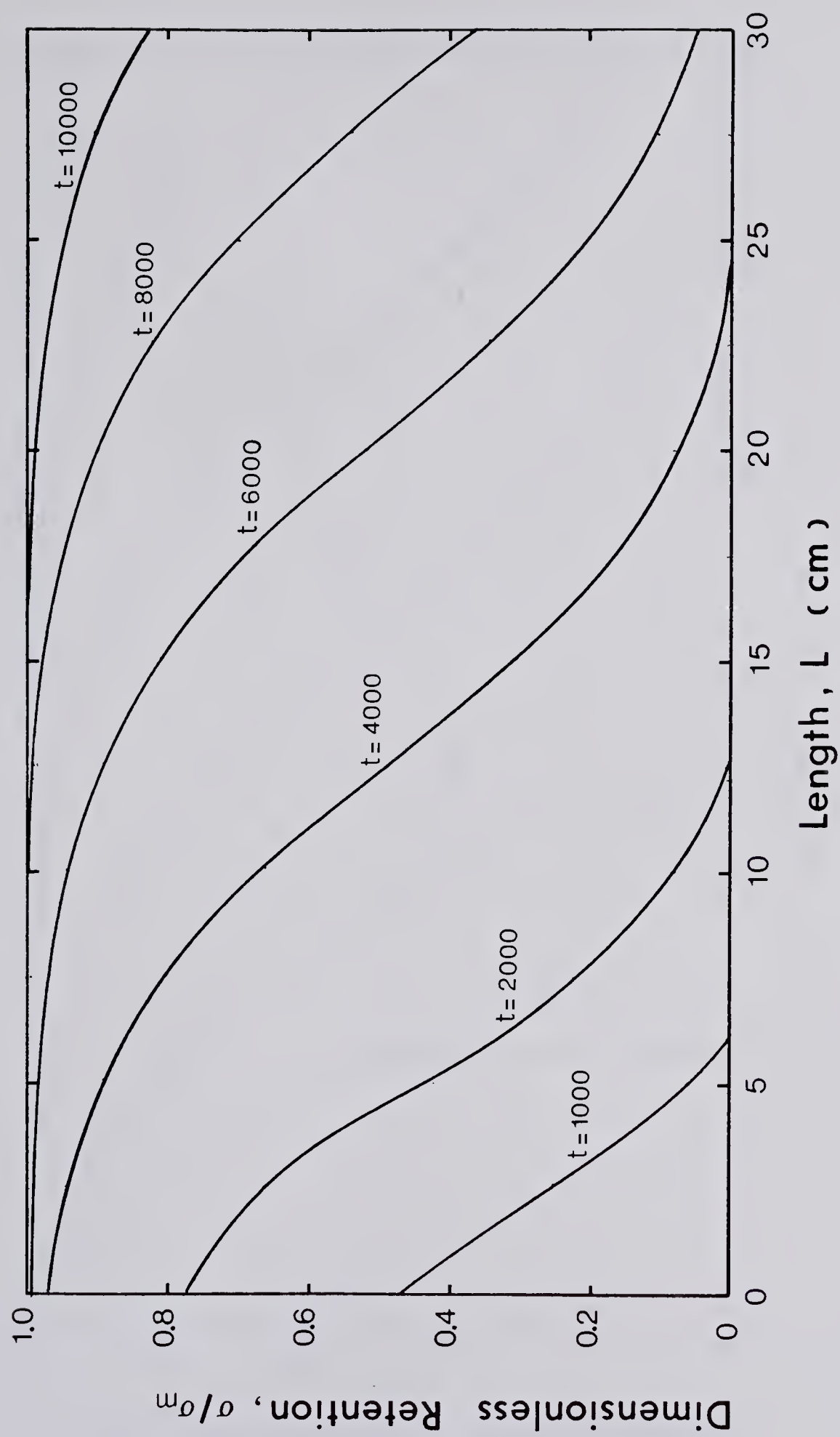


FIGURE 5.22 RETAINED OIL CONCENTRATION PROFILE

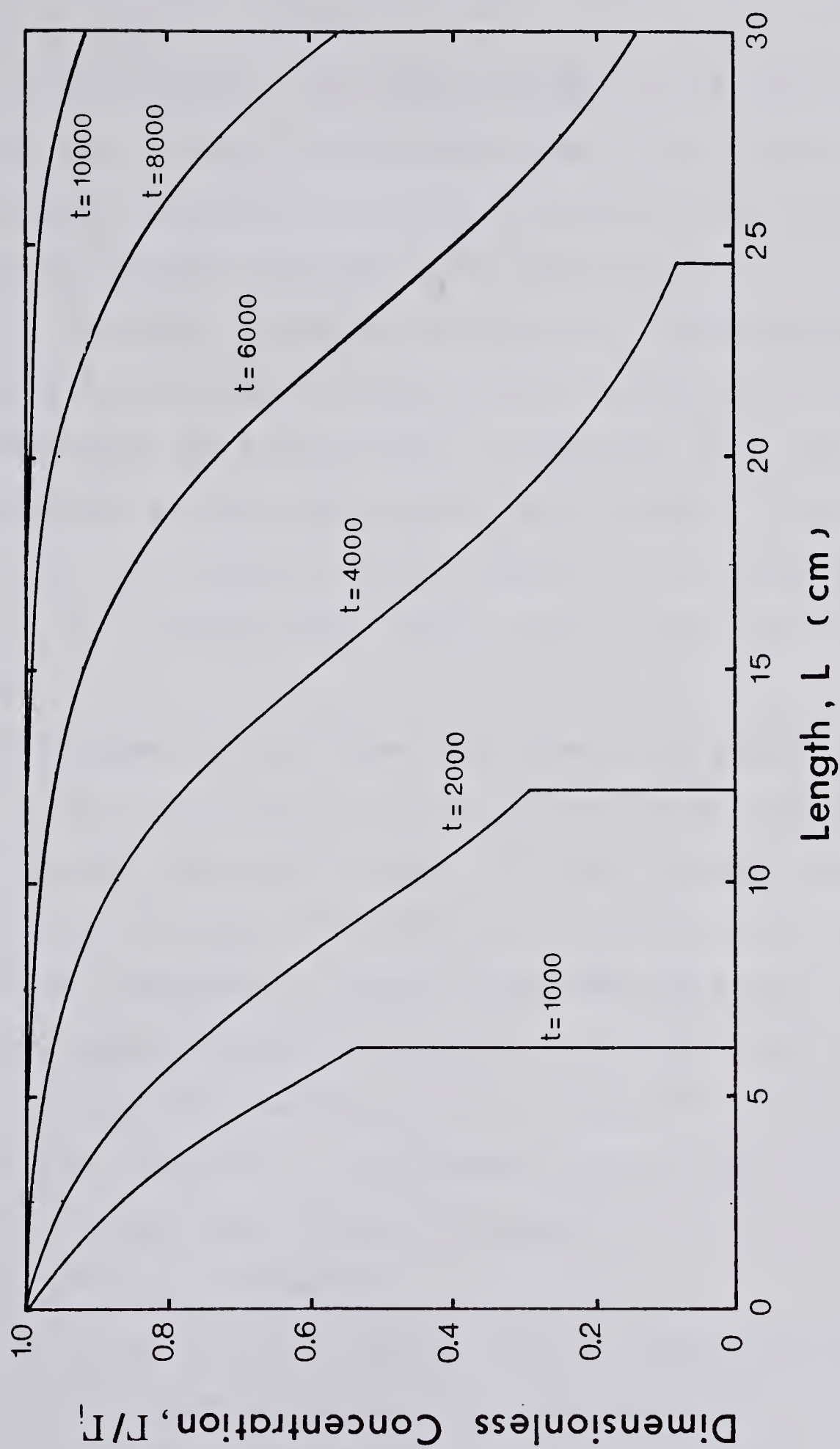


FIGURE 5.23 FLOWING EMULSION CONCENTRATION PROFILE

the flowing emulsion for run 129.

The properties exhibited by the model and shown in Figures 5.22 and 5.23 are:

1) the retained oil concentration at the inlet end of the core can increase slowly with time to its maximum concentration. This relationship is solely based upon the form of the kinetic equation, see Section 3.3.1.

2) the model shows the continually changing shape of the plugged and flowing concentration profiles. If the model predicts the flood front is unstable, then the concentration profile will continually change. If the flood front is stable, then the shape of the concentration profiles will change until steady state conditions are achieved.

A property of the model not shown in Figures 5.22 and 5.23, is the rate at which the oil front moves through the porous medium. For early times, the model allows the oil front to move through the system at a rate greater than the superficial velocity. At later times, when the form of the oil front has developed further, the oil front can fall behind the position designated by the superficial velocity. Thus in the laboratory, the measured breakthrough time can be a function of the frontal development and therefore a function of the core length.

The model should, however, only be used to provide concentration profiles within the core, when the fit of the model to the experimental data is satisfactory, because

in the derivation of the model, the material balance equation was approximated to obtain a solution to the differential equations. Thus when the fit of the model is poor, the material balance for the system is violated.

For further work in this area, it may be better to define the rate equation in terms of the total oil saturation in the core, rather than the plugged saturation. In that way, the material balance equation and the plugging rate equation could be solved without having to approximate the material balance equation. If the model were derived in terms of the total oil saturation and the flowing emulsion concentration, then the model could be used to evaluate:

- 1) the fractional flow curve,
- 2) whether the flood is stable or unstable,
- 3) approximate time for the flood front to become 'stabilised and
- 4) change of the fractional flow curve with time.

The present models can only provide an estimate of whether the front will stabilise and the time to stabilise, by examining the relationship between σ_n and Γ with time and position

5.6.4 Pressure Drop Model

The predicted pressure drop profile for run 129 is shown in Figure 5.24. The pressure drop across the core was predicted by numerically integrating Darcy's Law

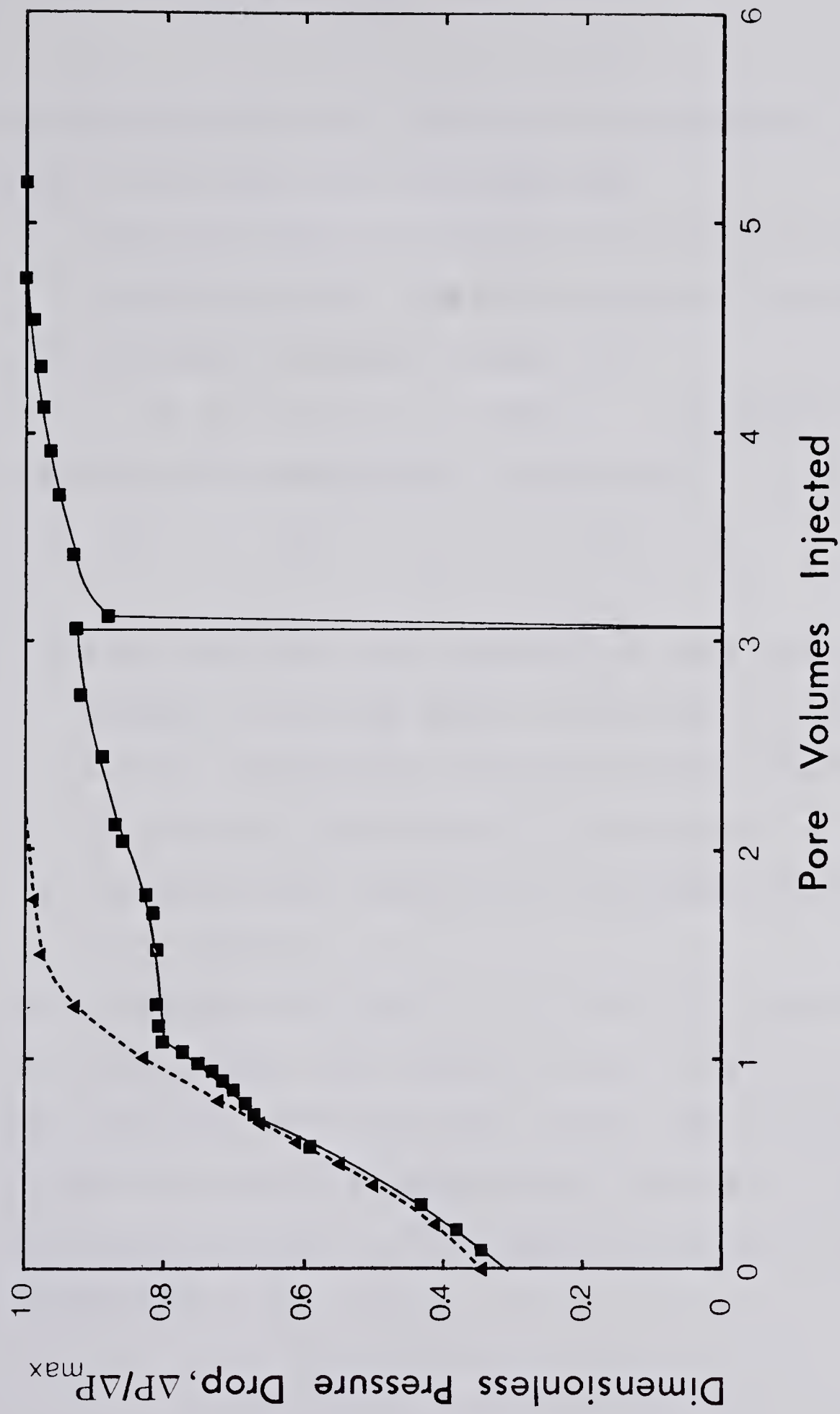


FIGURE 5.24 PRESSURE DROP MODEL FOR RUN 129

$$\Delta P = \frac{q}{A} \int \frac{\mu(\Gamma)}{K(\sigma)} dl \quad (5.10)$$

The relationships for the viscosity and permeability at any position and time were evaluated by:

- 1) using the model to predict the flowing emulsion concentration Γ , and the plugged oil concentration
- 2) using the viscosity correlation

$$\mu_e = \mu_w (1 + 2.666 \Gamma + 5.333 \Gamma^2) \quad \text{and}$$

- 3) using the permeability relationship

$$K(\sigma) = K_w - (1 - K_e) \frac{\sigma}{\sigma_m}$$

This model was used because each pore size is assumed to have an equal probability of being plugged. Therefore, the permeability reduction is directly proportional to the plugged oil concentration, assuming the blockage coefficient b is constant.

The pressure drop model showed a satisfactory correlation with the experimental data until one pore volume of emulsion had been injected. After one pore volume, the pressure drop model could not provide a satisfactory correlation because the flow model on which it is dependent, also provided a poor correlation.

5.6.5 Applicability, Capability and Deficiencies of the Model

The emulsion flow model is obviously a rough simplification of the whole set of physical and mechanical phenomena which accompany the emulsion plugging and flow process in a porous medium. However, as we are only in the initial stage of the investigation on this highly complicated process, the use of such a simplified model seems to be to a certain extent justified.

The model can predict the plugged oil saturation and the concentration of the flowing emulsion within the core by fitting the model to the produced emulsion concentration profile. The model is only valid when it provides a satisfactory fit to the produced emulsion concentration profile because the material balance equation was approximated to obtain a solution to the differential equations. The model overcomes the need for:

- 1) knowledge of the relative permeability, in order to predict the concentration profiles,
- 2) a capillary pressure - saturation relationship, and
- 3) the inlet concentration changing from zero to the maximum concentration at the instant flow begins.

This latter requirement is replaced by an equation that describes the saturation change in the system is dependent on the plugged oil saturation within the system and the concentration of the flowing emulsion. This system rate equation is allied to the rate of formation of a product

in a chemical reaction.

The deficiencies of the model in its present form are:

- 1) the model can only predict the variation in the plugged oil concentration and the flowing emulsion concentration with time and position, and not the overall oil saturation S_o .
- 2) the correct form of the kinetic equation has to be found by trial and error. Model 3 in this study provided a satisfactory fit to the early time data in runs 119, 120 and 129, but not 128.
- 3) the model is only valid for a linear system because σ_m is assumed constant along the system length. In a radial system, because the pressure drop per unit length is always decreasing with length away from the wellbore, the oil retention would be increasing with length away from the wellbore.
- 4) the material balance equation has to be approximated to obtain a solution to the differential equations.

The latter deficiency could be rectified by defining the kinetic rate equation in terms of the overall oil saturation S_o , rather than the plugged oil saturation. In this way, the material balance equation

$$\frac{\partial S_o}{\partial t} + \frac{q}{A \phi} \frac{\partial \Gamma}{\partial L} = 0 \quad (3.4)$$

could be used in the model, rather than the approximated form of Equation 3.3, Equation 3.19

$$\frac{\partial \sigma}{\partial t} + \bar{\epsilon} \frac{\partial \Gamma}{\partial L} + \frac{q}{A \phi} \frac{\partial \Gamma}{\partial L} = 0 \quad (3.19)$$

A kinetic rate equation that might provide a better correlation with the experimental data, than model 3 of this study, is

$$\frac{\partial \sigma}{\partial t} = H_0 (\sigma - \sigma_m)(\lambda - \sigma)(\beta + \sigma)\Gamma \quad (5.12)$$

A comparison of the form of the above model, with model 3, is shown in Figure 5.25. This new model exhibits the same high rate of plugging at low concentrations of σ , as does model 3 of this study. This model might, however, provide a better fit to the experimental data than model 3, because at concentrations of σ approaching σ_m , the model predicts a lower plugging rate. This lower plugging rate would increase the time required for the system to reach steady state conditions. Therefore, the new model has the same form as model 3, over the range where model 3 effectively fitted the experimental data, and has an improved form over the range where model 3 deviated away from the experimental data.

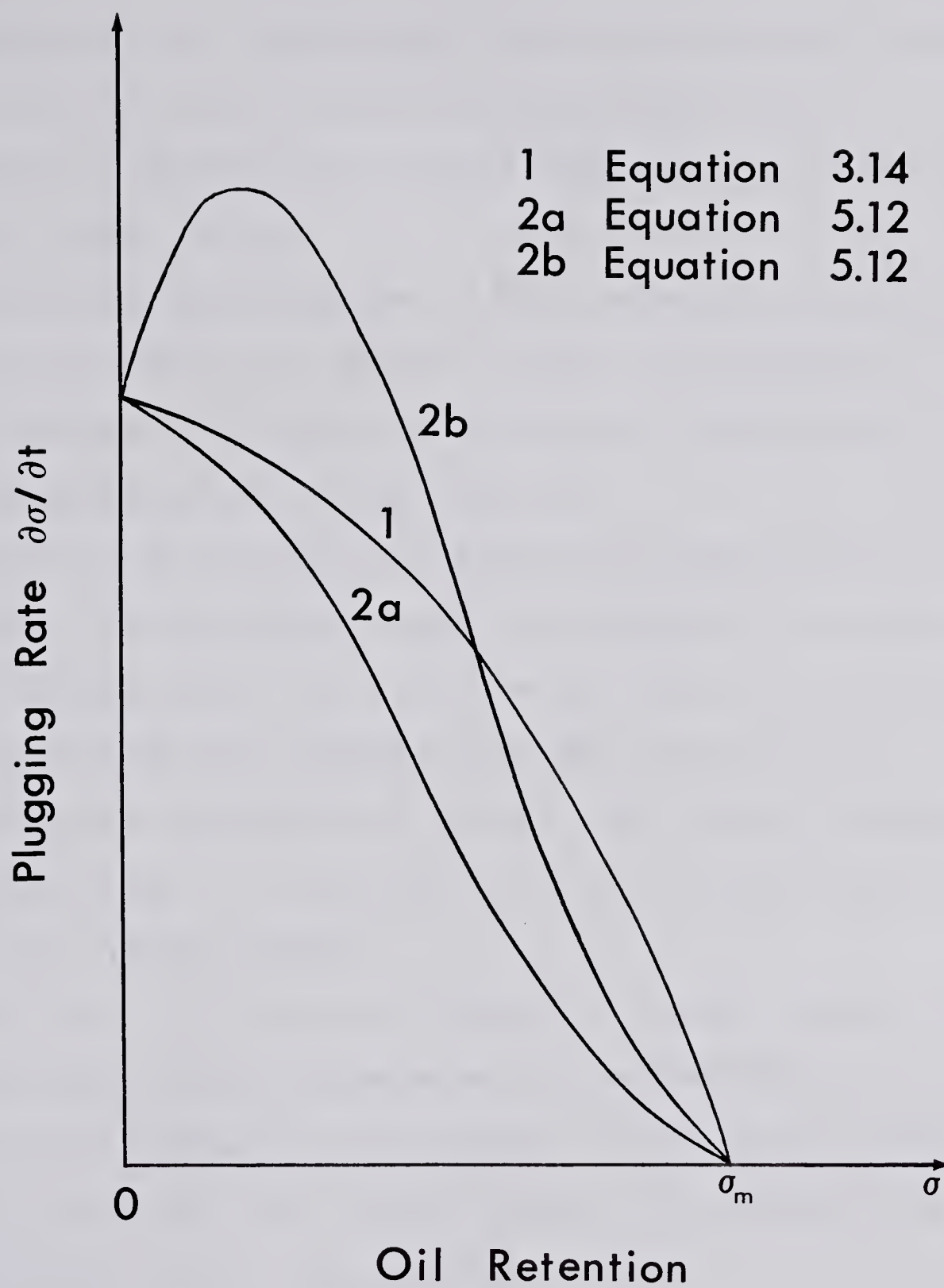


FIGURE 5.25 ILLUSTRATION OF THE FORM OF THE NEW KINETIC EQUATION

CONCLUSIONS

1. Emulsions can effectively reduce the permeability of a core, with any initial permeability, if the emulsion droplets are larger than the pore throats in the porous medium.
2. There are three degrees of core permeability reduction, zero, partial and complete, which are dependent on the relationship between the pore size in the porous medium and the droplets in the emulsion.
3. When the permeability is partially reduced there is no simple relationship between the fractional permeability of a core after emulsion flow and the core properties of porosity and permeability. The shape of the fractional permeability versus flow rate or pressure drop curve is a function of the pore size distribution in the porous medium.
4. The flow of an emulsion through a porous medium is a non-Darcy flow process when the permeability of the core is reduced by the emulsion flow. When the emulsion does not plug the core and reduce the permeability, the flow is a Darcy flow process.
5. For a porous medium that is plugged by an emulsion, the fractional permeability of the porous medium increases with an increase in the flow rate or pressure drop.
6. The parameter d_g/d_e , the ratio of the sand grain size to the deformed size of the largest droplet in the

emulsion, can be used to predict whether the porous medium will be plugged by emulsion flow.

7. The capillary number, N_c can be used to estimate the flow rates over which an emulsion can plug a porous medium.
8. The concentration of the larger droplets retained in the core is larger than for the smaller droplets, possibly because there are more plugging sites available within the core for the larger droplets.
9. The maximum concentration for a particular droplet size does not have to be equal to the concentration at steady state conditions.
10. Model 3 of the three models investigated in this study, provided the best fit to the experimental data. This model was able to effectively describe the experimental outlet emulsion concentration profiles for early times.

RECOMMENDATIONS

1. To evaluate the kinetic equation

$$\frac{\partial \sigma}{\partial t} = H_o (\sigma_m - \sigma)(\lambda - \sigma)(\beta + \sigma)\Gamma$$

where $\lambda \geq \sigma_m$

β less than, equal to or greater than σ_m

2. To develop a kinetic rate equation in terms of the overall oil saturation, S_o , rather than the plugged oil concentration, σ .
3. To use a microwave attenuation instrument, to obtain the oil saturation profiles within the core during emulsion flow. In this way, the model can be compared with both the outlet emulsion concentration and the profiles within the core.
4. To use long cores, of the order of one metre long, so that the emulsion front can develop further and the model can be fitted to the experimental data more accurately.

REFERENCES

1. Subkow, P. : "Process For The Removal Of Bitumen From Bituminous Deposits", U.S.Patent 2 288 857 July 7th. 1942
2. Cooke, C.E.Jr., Williams, R.E. & Kolodzie, P.A. : "Oil Recovery By Alkaline Waterflooding", J. Pet. Tech. December 1974, 1365 - 1374
3. Jennings, H.Y.Jr., Johnson, C.E.Jr. & McAuliffe, C.D. : "A Caustic Waterflooding Process For Heavy Oils", J. Pet. Tech., December 1974, 1344 - 1352
4. Reisberg, J. & Doscher, T.M. : "Interfacial Phenomena In Crude Oil Water Systems", Prod. Monthly, November 1965, 43 - 50
5. Scott, J.D. : "Controlled Chemical Waterflooding Of Viscous Crude Oils", M.Sc. Thesis, University Of Alberta, 1971
6. Flock, D.L., Elmaryergi, H., Baird, H. & Chan, P. : "The Effect Of Emulsions On Recovery Of Heavy Viscous Crude Oils", Paper Presented At 28th. Canadian Chemical Engineering Conference, Halifax, Nova Scotia, 22 - 25th. October 1978
7. Binder, G.G.Jr., Clark, N.A. & Russel, C.D. : "Method Of Secondary Recovery" U.S.Patent 3 208 517 September 28th. 1965
8. Meadors, V.G. : "Method Of Recovering Oil From Underground Reservoirs" U.S.Patent 3 208 515 September 28th. 1965
9. Hardy, W.E., Shephard, J.C. & Reddick, K.L. : "Secondary Recovery Of Petroleum With A Preformed Emulsion In Slug Drive" U.S.Patent 3 294 164 December 24th. 1966
10. McAuliffe, C.D. : "Crude Oil-In-Water Emulsions To Improve Fluid Flow In A Oil Reservoir", J. Pet. Tech., June 1973, 721 - 726
11. Johnson, C.E.Jr. : "Status Of Caustic And Emulsion Floods", J. Pet. Tech., January 1976, 85 - 92
12. McAuliffe, C.D. : "Oil-In-Water Emulsions And Their Flow Properties In Porous Media", J. Pet. Tech., June 1973, 721 - 726

13. D'Elia, R. & Ferrer, J. : "Emulsion Flooding Of Viscous Oil Reservoirs", SPE Paper 4674, Presented At 48th. Annual Fall Meeting OF SPE, Las Vegas, September 30th. - October 3rd. 1973
14. Farouq Ali, S.M., Figueroa, J.M., Azuaje, E.A. & Farquharson, R.G. : "Recovery Of Lloydminster And Morichal Crudes By Caustic, Acid And Emulsion Floods", J. Can. Pet. Tech., January - March 1979, 53 - 59
15. Herzig, J.P., Leclerc, D.M. & Le Goff, P. : "Flow Of Suspensions Through Porous Media - Application To Deep Filtration", Ind. Eng. Chem., 62 (5), 8(1970)
16. Becher, P. : "Emulsions : Theory And Practice" Reinhold Publishing Corp. New York 1957, 61 - 85
17. Sherman, P. : "Emulsion Science" Academic Press 1968 London, 285 - 329
18. Sherman, P.: Ref. 16 page 59
19. Einstein, A.: Ref. 16 page 62, Ref. 17 page 287
20. Guth, E., Gold, O. & Simha, R. : Ref. 16 page 62, Ref. 17 page 287
21. Oliver, D. & Ward, S. : Ref. 16 page 63
22. Hatschek, E. : Ref. 16 page 65, Ref. 17 page 292
23. Sibree, J.O. : Ref. 16 page 65, Ref. 17 page 292
24. Taylor, G.I. : Ref. 16 page 67, Ref. 17 page 292
25. Toms, B.A. : Ref. 16 page 70, Ref. 17 pages 292 & 295
26. Smoluchowski, M. : Ref. 16 page 84, Ref. 17 page 325
27. Richardson, E.G. : Ref. 16 page 78, Ref. 17 page 306
28. Roscoe, R. : Ref. 16 page 78, Ref. 17 page 302
29. Sherman, P. : Ref. 16 page 79
30. Abrams, A. : "The Influence Of Fluid Viscosity, Interfacial Tension, and Flow Velocity On Residual Oil Saturation Left By Waterflood", Soc. Pet. Eng. Jour., October 1975, 437 - 447

31. Stegemeier, G.L. : "Mechanisms Of Entrapment And Mobilisation Of Oil In Porous Media", Improved Oil Recovery By Surfactant And Polymer Floods, Edited By D.O.Shah and R.S.Schechter, Published By Academic Press, Inc, 1977
32. Morrow, N. : "Interplay Of Capillary, Viscous, And Buoyancy Forces In The Mobilisation Of Residual Oil", Paper No. 78-29-24 Presented At 29th. Annual Technical Meeting Of Petroleum Society Of CIM In Calgary, June 13 - 16th, 1978
33. Batychy, J.P. & Singhal, A.K. : "Mobilisation Of Entrapped Ganglia", Research Report RR-35 Petroleum Recovery Institute, October 1977
34. Lefebvre du Prey, E.J. : "Factors Affecting Liquid-Liquid Relative Permeabilities Of A Consolidated Porous Medium", Soc. Pet. Eng. Jour., February 1973, 39 - 47
35. Taber, J.J. : "Dynamic And Static Forces Required To Remove A Discontinuous Oil Phase From Porous Media Containing Both Oil And Water", Soc. Pet. Eng. Jour., March 1969, 3 - 12
36. Uzoigwe, A.C. & Marsden, S.S.Jr. : "Emulsion Rheology And Flow Through Unconsolidated Synthetic Porous Media", Paper SPE 3004 Presented At SPE-AIME 45th. Annual Fall Meeting, Houston, October 4 - 7th, 1970
37. Alvarado, D.A. : "The Flow Of Macroemulsions Through Porous Media ", Ph.D. Dissertation, Petroleum Engineering Department, Stanford University, 1975
38. Cartmill, J.C. & Dickey, P.A. : "Flow Of A Disperse Emulsion Of Crude Oil In Water In Porous Media", SPE Paper 2481 Presented At 48th. Annual Fall Meeting Of Society Of Petroleum Engineers Of AIME, Denver Colorado, 28th. September - 1st. October 1969
39. Devereux, O.F. : "Emulsion Flow In Porous Solids - Experiments With A Crude Oil In Water Emulsion In Porous Sandstone", Chemical Engineering Journal 7, 129 - 136, 1976
40. Spielman, L.A. & Goren, S.L. : Indust. and Eng. Chem., 62(1970) 10

41. Devereux, O.F. : "Emulsion Flow In Porous Solids - A Flow Model", Chemical Engineering Journal 7, 121 - 128, 1974
42. Buckley, S.E. & Leverett, M.C. : "Mechanism Of Fluid Displacement In Sands", Trans. AIME, Vol.146 (1942) 107 -116
43. Koval, E.J. : "A Method For Predicting The Performance Of Unstable Miscible Displacement In Heterogeneous Media", Petroleum Transactions Reprint Series, Miscible Processes No. 8 173 - 182, Published By The Society Of Petroleum Engineers Of AIME
44. Gruesbeck, C. & Collins, R.E. : "Entrainment And Deposition Of Fine Particles In Porous Media", SPE Paper 8430
45. Trzaska, A. : "New Kinetics Equations Of The Colmatage Process And Their Applications", Archiwum Gornicta 1972, 361 - 383
46. Sakthivadivel, R. : "Theory And Mechanisms Of Filtration Of Non-Colloidal Fines Through A Porous Medium", Tech. Rep. HEL 15-5, Hydraulic Eng. Lab, University Of California, Berkeley 1966
47. Coulter Counter Manual : Reference Manual For The Coulter Counter Model TAI
48. Box, M.J. : "A New Method Of Constrained Optimisation And A Comparison With Other Methods", The Computer Journal 8, 42 1965
49. Nelder, J.A. & Mead, R. : "A Simplex Method For Function Minimisation", Computer Journal 7, 308 1965
50. Holm, L.W. : "Soluble Oils For Improved Oil Recovery", Improved Oil Recovery By Surfactant And Polymer Floods, Edited By D.O.Shah and R.S.Schechter, Published by Academic Press, Inc, 1977

APPENDIX A

PARAMETER EVALUATION

The Characteristic Emulsion Droplet Length:

The length of the deformed emulsion droplet was calculated using Equation 5.4

$$L_d = r_p + r_m + 2 \times \frac{r_m^3 - r_p^3}{r_m^2 + r_p^2 + r_p r_m}$$

The equation provides an approximate estimate of the emulsion droplet length provided the droplet length is not greater than the diameter of the sand grain.

Thus the equation is probably valid for all the runs of this study except runs 100, 103 and 106. For all these runs, the deformed length is too small, which leads to high estimates for the critical capillary number, a high value for the deformed emulsion droplet radius and a low estimate of the parameter d_g/d_e . Thus a low estimate for the length of the deformed emulsion droplet, produces an optimistic impression of whether a droplet will plug a pore constriction.

The Deformed Emulsion Droplet Radius:

The deformed emulsion droplet radius was calculated using the equation

$$\Delta P = \frac{\Delta P}{\Delta L} \times L_d = 2 \gamma \cos \theta \left\{ \frac{1}{r_e} - \frac{1}{r_o} \right\}$$

which can be written as

$$\frac{68942}{30.48} \times \frac{\Delta P}{\Delta L} \times L_d = 2 \times 0.24 \times 1 \left\{ \frac{1}{r_e} - \frac{1}{r_o} \right\}$$

in consistent units,

where 68942 dynes/cm² per psi
30.48 cm per foot.

Thus the equation solved by trial and error was

$$4712.25 \frac{\Delta P}{\Delta L} \left[r_o + r_e + \frac{2(r_o^3 - r_e^3)}{r_o^2 + r_e^2 + r_o r_e} \right] = \left\{ \frac{1}{r_e} - \frac{1}{r_o} \right\}$$

where $\frac{\Delta P}{\Delta L}$ Pressure gradient (psi / ft)

r_o Emulsion droplet size (microns)

r_e Deformed emulsion droplet size (microns)

γ Interfacial tension (dynes / cm)

Critical Capillary Number:

The critical capillary number was calculated using the equation

$$[N_c]_{\text{critical}} = \frac{K}{\phi} \frac{2}{1.013} \frac{1}{L_d} \left\{ \frac{1}{r_p} - \frac{1}{r_o} \right\}$$

where K permeability (darcies)

r_p pore throat size ($r_g / 6.493$) (microns)

r_o emulsion droplet size (microns)

L_d deformed droplet length for the system, calculated
using r_p and r_o in equation 5.4 (microns)
porosity (-)

APPENDIX B

SENSITIVITY ANALYSIS ON THE
CRITICAL CAPILLARY NUMBER

Sensitivity Analysis on the Critical Capillary Number:

The critical capillary number was calculated using the equation

$$N_c = \frac{K}{\phi} \cdot \frac{2}{1.013} \cdot \frac{1}{L_d} \cdot \left\{ \frac{1}{r_p} - \frac{1}{r_o} \right\} \quad (5.10)$$

Examination of this equation shows that for an emulsion droplet with a radius similar to the pore throat radius, then a small error in either size leads to a significant error in the capillary number because of the sensitivity associated with evaluating the group:

$$\left\{ \frac{1}{r_p} - \frac{1}{r_o} \right\}$$

While, when the emulsion droplet size is significantly different from the pore throat size, a small error in either reading only produces a small error in the capillary number. This phenomenon is demonstrated in the analysis shown in Table B1.

Therefore when the emulsion droplet size and the pore throat size are similar, the capillary number is very sensitive to the input data and the analysis should not be used to predict the flow rate at which no plugging will occur. When the droplet size and the pore throat size are significantly different, the errors associated with the analysis are minimal and the concept can be used to predict

the flow rate at which no plugging will occur.

TABLE B1
Sensitivity Analysis on the Critical Number

Pore radius r_p microns	Droplet radius r_o microns	Droplet length L_d microns	N_c		Critical flow rate q_c cc/hr	Percent change in r_p %	Percent change in N_c %
RUN 104							
12.66	12.7	25.44	8.02	10	207	-	-
12.67	12.7	25.43	6.01	10	155	+0.08	-25
12.68	12.7	25.42	4.01	10	103	+0.16	-50
12.69	12.7	25.41	2.00	10	52	+0.24	-75
12.65	12.7	25.45	1.00	10	259	-0.08	+25
12.6	12.7	25.5	2.01	10	518	-0.47	+150
RUN 110							
7.85	10.5	23.65	5.34	10	2.1 10	-	-
7.86	10.5	23.64	5.31	10	2.09 10	+0.1	-0.2
7.84	10.5	23.66	5.36	10	2.11 10	-0.1	+0.5
7.9	10.5	23.6	5.22	10	2.06 10	+0.6	-1.9
7.8	10.5	23.7	5.46	10	2.15 10	-0.6	+2.4

APPENDIX C

EXPERIMENTAL DATA

C1.1 Outlet End Emulsion Concentration

The outlet end emulsion concentration profile and the maximum oil saturation for the core were evaluated from the emulsion viscosity and the viscosity correlation. Use of the viscosity correlation for the series of collected emulsion samples yielded a stepwise outlet end emulsion concentration profile from which a smoothed line was drawn to produce a continuous profile.

The maximum oil saturation within the core was evaluated using the stepwise emulsion concentration of the produced emulsion. This saturation was calculated by applying a correction for the volume of emulsion in the end blocks to the volume of oil retained within the core holder.

The raw and processed data for runs 119, 120, 128 and 129 is shown in tables C.1 - C.3, C.4 - C.6, C.7 - C.9 and C.10 - C.12, respectively.

RUN 119

Core pore volume	159.6 cc
Inlet end block volume	6.3 cc
Outlet end block volume	7.4 cc
Outlet tube volume	2.3 cc
Total fittings volume	16.0 cc
Oil volume in the core holder	29.7 cc
Oil volume in the core	27.3 cc
Maximum oil saturation in the core	0.171

After emulsion breakthrough, the pore volumes injected into the core is given by:

$$\begin{array}{l} \text{Pore volumes injected} \\ \text{into the core} \end{array} = \frac{Q - 16.0}{159.6}$$

where Q = Cumulative emulsion injected into the core holder (cc)

The stepwise and smoothed outlet end emulsion profile is shown in Figure C1. The experimentally recorded data for this run is shown in Table C1, with the smoothed outlet end profile shown in Table C2. The theoretically determined profile evaluated using the model is recorded in Table C2. A summary of the pertinent experimental data and the values for the coefficients of the model are shown in Table C.3.

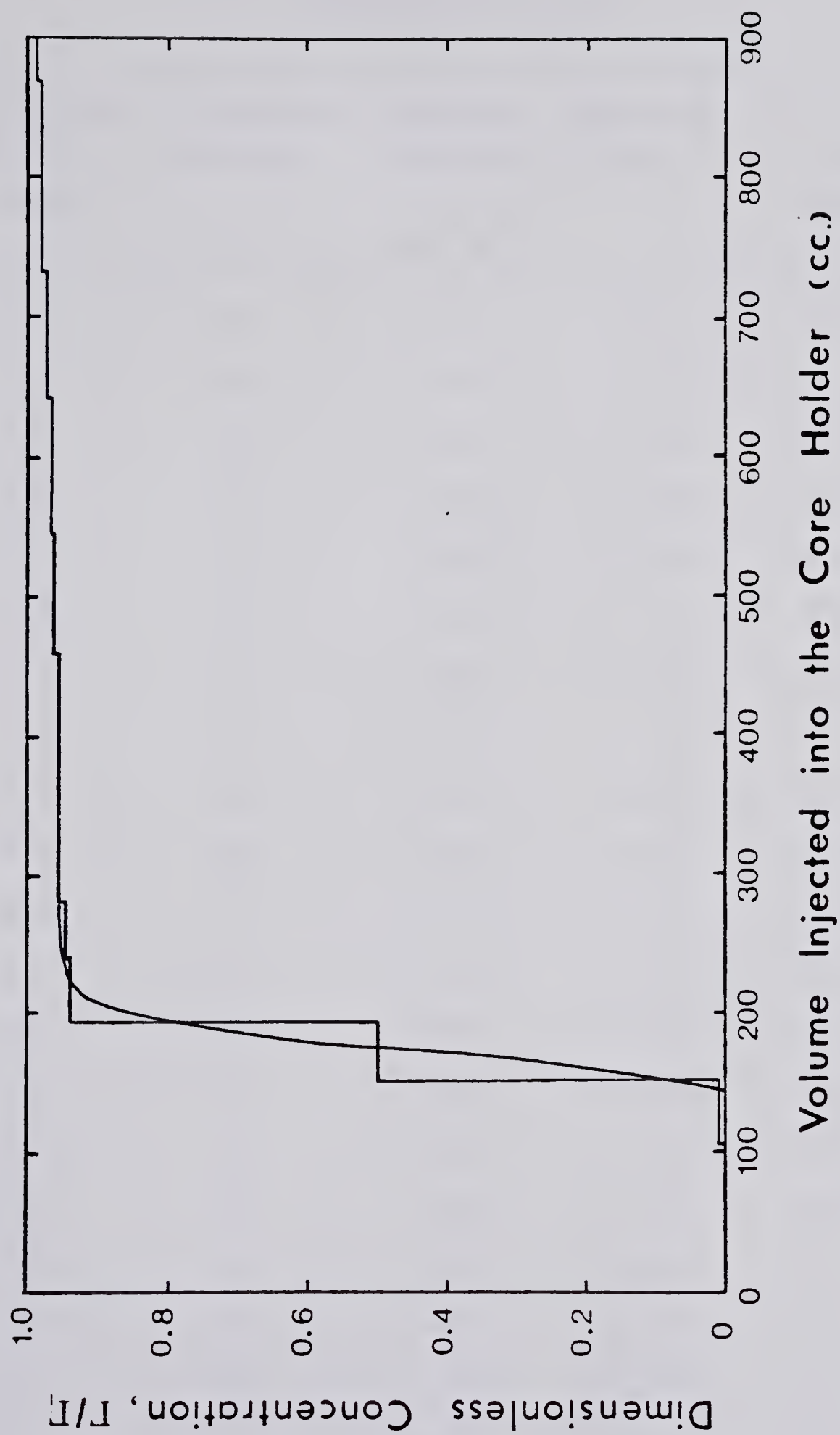


FIGURE C.1 OUTLET END CONCENTRATION : RUN 119

TABLE C1

Experimental Data

Produced Fluid Volume cc	Incremental Volume cc	Emulsion Viscosity $\text{mm}^2 \text{ s}^{-1}$	Emulsion Conc.	Oil in the Core Holder cc
104	104	1.0	0.0	15.6
152	48	1.002	0.001	22.7
194	42	1.23	0.075	25.9
238	44	1.475	0.141	26.3
280	42	1.478	0.142	26.6
322	42	1.480	0.143	26.9
372	50	1.481	0.143	27.3
416	44	1.483	0.143	27.6
458	42	1.483	0.143	27.9
500	42	1.485	0.144	28.1
546	46	1.487	0.144	28.3
586	40	1.489	0.145	28.6
642	56	1.49	0.145	28.9
688	46	1.493	0.146	29.1
732	44	1.495	0.146	29.2
780	48	1.497	0.147	29.4
824	44	1.498	0.147	29.5
868	44	1.50	0.147	29.6
906	38	1.501	0.148	29.7
950	44	1.504	0.15	29.7

TABLE C2

Produced Emulsion Concentration Profile

Pore Volumes Injected	Dimensionless Emulsion Outlet Concentration Γ/Γ_i	Predicted Emulsion Outlet End Concentration Γ/Γ_i
0.213	0.0	0.0
0.526	0.0	0.0
0.683	0.0	0.0
0.840	0.060	0.044
0.902	0.140	0.140
0.965	0.338	0.363
0.996	0.550	0.516
1.027	0.666	0.666
1.090	0.857	0.875
1.153	0.917	0.961
1.310	0.945	0.998
1.466	0.950	1.000
1.623	0.950	1.000
1.779	0.959	1.000

TABLE C3

Summary of Experimental Data and Coefficients for Model

Absolute core permeability	8.12 darcies
Core permeability to emulsion	6.71 darcies
Fractional permeability to emulsion	0.826
Maximum oil saturation	0.171
Plugged oil saturation	0.0835
Fractional porosity open to flow	0.583
Blockage coefficient	4.99
Breakthrough time (pore volumes)	0.727

Coefficients of the Mathematical Model

Rate coefficient H_o	0.812 sec^{-1}
β Factor	0.0764
t_{bt}	746 sec.
α	35.6 cm^{-1}

RUN 120

Core pore volume	157.3 cc
Inlet end block volume	6.3 cc
Outlet end block volume	7.4 cc
Outlet tube volume	2.3 cc
Total fittings volume	16.0 cc
Oil volume in the core holder	30.1 cc
Oil volume in the core	27.7 cc
Maximum oil saturation in the core	0.176

After emulsion breakthrough, the pore volumes injected into the core is given by:

$$\begin{array}{l} \text{Pore volumes injected} \\ \text{into the core} \end{array} = \frac{Q - 16.0}{157.3}$$

where Q = Cumulative emulsion injected into the core
holder (cc)

The stepwise and smoothed outlet end emulsion profile is shown in Figure C2. The experimentally recorded data for this run is shown in Table C4, with the smoothed outlet end profile shown in Table C5. The theoretically determined profile evaluated using the model is recorded in Table C5. A summary of the pertinent experimental data and the values for the coefficients of the model are shown in Table C6.

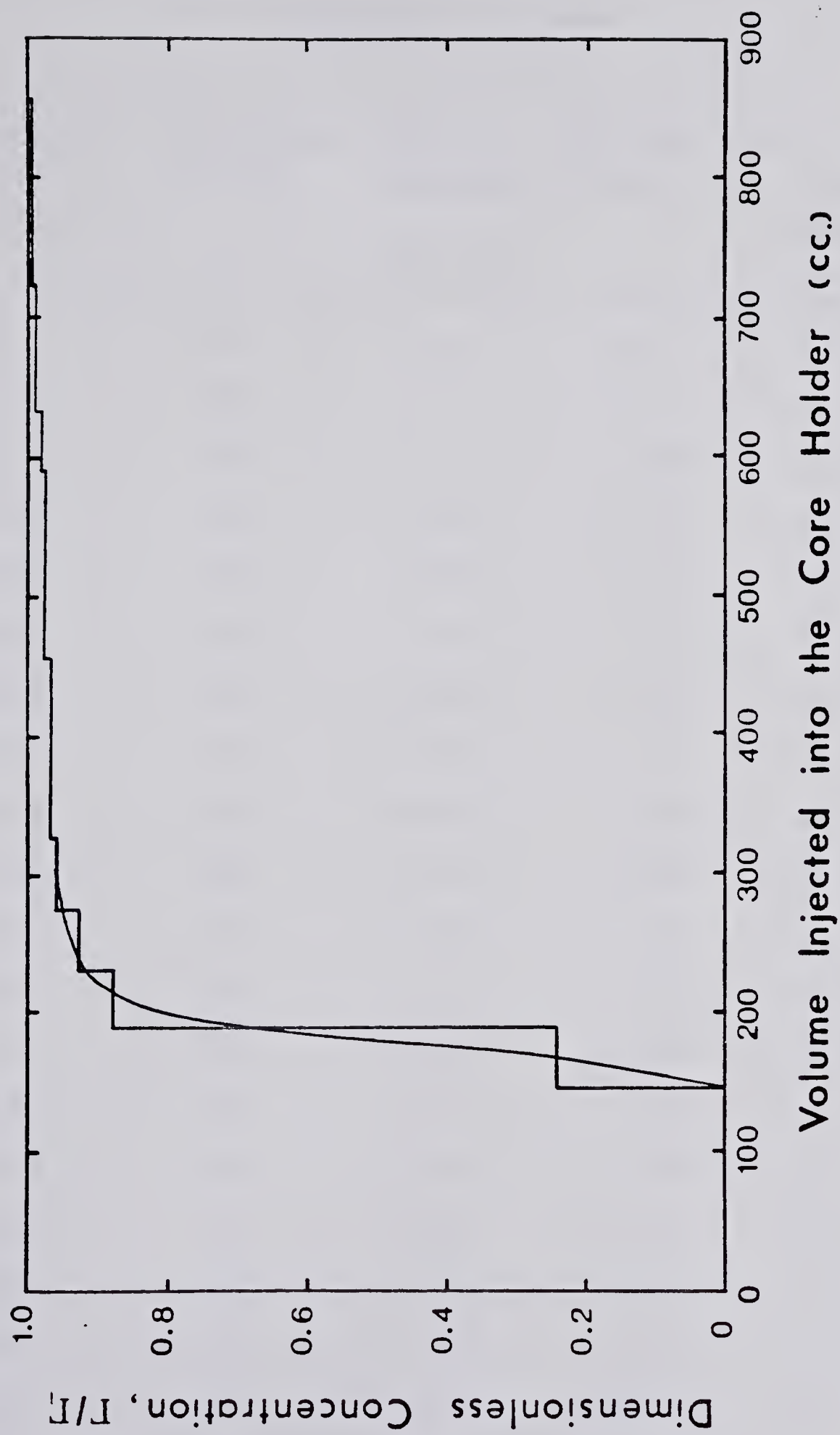


FIGURE C.2 OUTLET END CONCENTRATION : RUN 120

TABLE C4

Experimental Data

Produced Fluid Volume cc	Incremental Volume cc	Emulsion Viscosity $\text{mm}^2 \text{ s}^{-1}$	Emulsion Conc.	Oil in the Core Holder cc
110	110	1.0	0.0	16.5
146	36	1.0	0.0	21.9
190	44	1.11	0.036	26.9
232	42	1.45	0.131	27.7
274	42	1.48	0.139	28.2
326	52	1.50	0.144	28.5
366	40	1.503	0.145	28.7
410	50	1.505	0.145	28.9
454	44	1.506	0.145	29.1
502	48	1.507	0.146	29.4
544	42	1.509	0.146	29.5
590	46	1.51	0.146	29.7
634	44	1.513	0.147	29.8
682	48	1.515	0.148	29.9
724	42	1.517	0.148	30.0
764	40	1.52	0.149	30.1
808	44	1.521	0.149	30.1
856	48	1.523	0.149	30.1
900	44	1.525	0.15	30.1

TABLE C5

Produced Emulsion Concentration Profile

Pore Volumes Injected	Dimensionless Emulsion Outlet Concentration Γ/Γ_i	Predicted Emulsion Outlet End Concentration Γ/Γ_i
0.216	0.0	0.0
0.534	0.0	0.0
0.693	0.0	0.0
0.852	0.033	0.059
0.915	0.099	0.123
0.979	0.206	0.238
1.011	0.319	0.318
1.043	0.437	0.410
1.106	0.608	0.608
1.170	0.752	0.775
1.329	0.891	0.962
1.488	0.925	0.995
1.647	0.942	0.999
1.805	0.953	1.000

TABLE C6

Summary of Experimental Data and Coefficients for Model

Absolute core permeability	9.5 darcies
Core permeability to emulsion	7.27 darcies
Fractional permeability to emulsion	0.765
Maximum oil saturation	0.176
Plugged oil saturation	0.0987
Fractional porosity open to flow	0.515
Blockage coefficient	4.91
Breakthrough time (pore volumes)	0.745

Coefficients of the Mathematical Model

Rate coefficient H_o	0.422 sec^{-1}
β Factor	0.098
t_{bt}	753.2 sec
α	18.2 cm^{-1}

RUN 128

Core pore volume	168.1 cc
Inlet end block volume	6.3 cc
Outlet end block volume	7.4 cc
Outlet end tube volume	2.3 cc
Total fittings volume	16.0 cc
Oil volume in the core holder	35.7 cc
Oil volume in the core	33.3 cc
Maximum oil saturation in the core	0.198

After emulsion breakthrough, the pore volumes injected into the core is given by:

$$\begin{array}{l} \text{Pore volumes injected} \\ \text{into the core} \end{array} = \frac{Q - 16.0}{168.1}$$

where Q = Cumulative emulsion injected into the core
holder (cc)

The stepwise and smoothed outlet end emulsion profile is shown in Figure C3. The experimentally recorded data for this run is shown in Table C7, with the smoothed outlet end profile shown in Table C8. The theoretically determined profile evaluated using the model is recorded in Table C8. A summary of the pertinent experimental data and the values for the coefficients of the model are shown in Table C9.

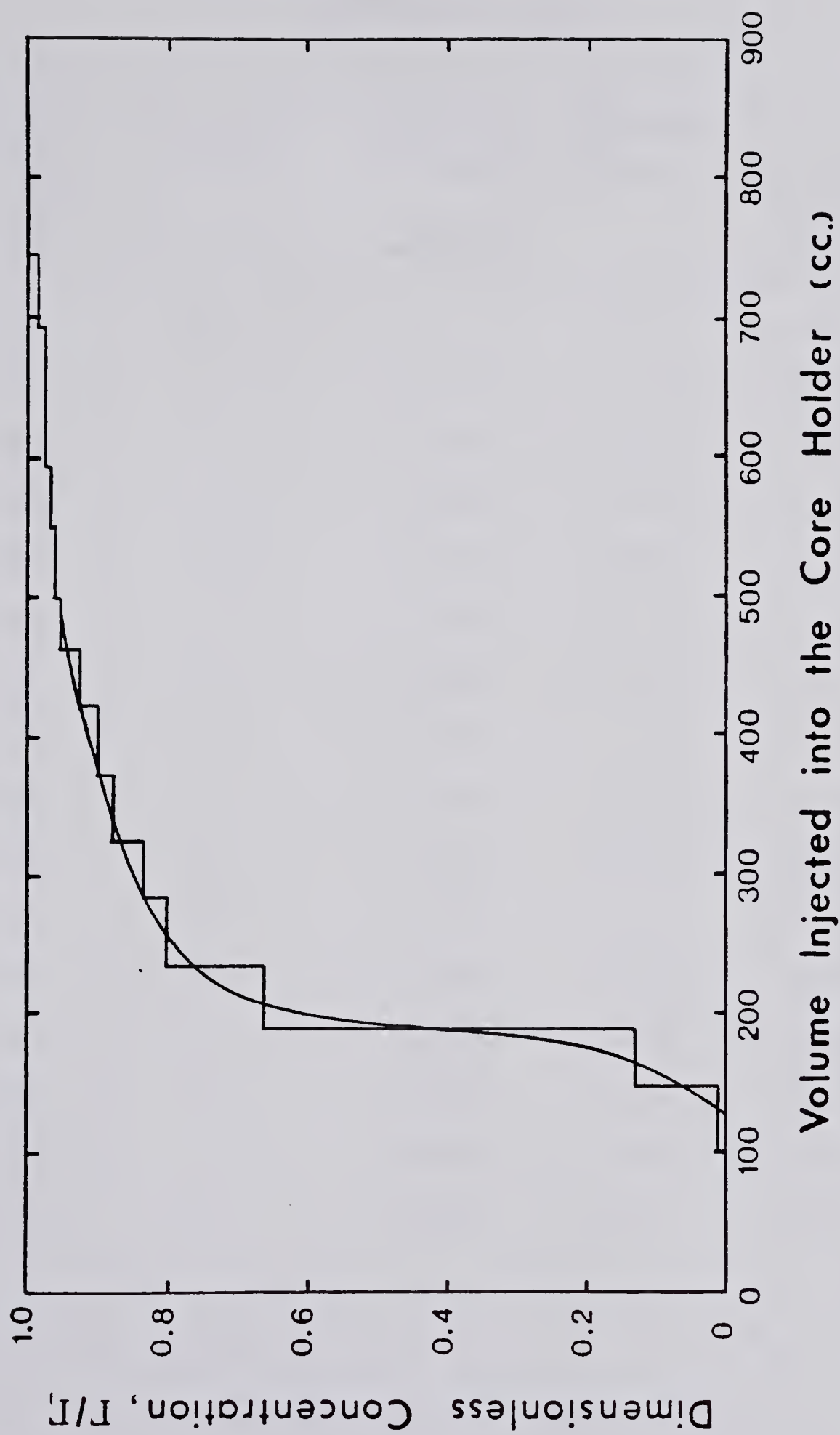


FIGURE C.3 OUTLET END CONCENTRATION : RUN 128

TABLE C7

Experimental Data

Produced Fluid Volume cc	Incremental Volume cc	Emulsion Viscosity $\text{mm}^2 \text{ s}^{-1}$	Emulsion Conc.	Oil in the Core Holder cc
100	100	1.0	0.0	15.0
147	47	1.007	0.002	22.0
190	43	1.062	0.020	27.6
236	46	1.334	0.099	29.9
282	46	1.419	0.120	31.3
323	41	1.438	0.125	32.3
368	45	1.463	0.131	33.2
419	51	1.480	0.135	33.9
460	41	1.496	0.139	34.4
500	40	1.510	0.143	34.7
547	47	1.515	0.144	35.0
592	45	1.520	0.145	35.2
632	40	1.523	0.146	35.4
692	60	1.526	0.146	35.6
742	50	1.535	0.148	35.7
782	40	1.542	0.15	35.7

TABLE C8

Produced Emulsion Concentration Profile

Pore Volumes Injected	Dimensionless Emulsion Outlet Concentration Γ/Γ_i	Predicted Emulsion Outlet End Concentration Γ/Γ_i
0.183	0.0	0.0
0.480	0.0	0.0
0.629	0.0	0.0
0.778	0.05	0.07
0.926	0.165	0.184
1.075	0.420	0.403
1.224	0.720	0.669
1.372	0.785	0.858
1.521	0.813	0.947
1.670	0.840	0.982
2.265	0.910	1.000
2.860	0.950	1.000
3.354	0.970	1.000
4.049	0.990	1.000

TABLE C9

Summary of Experimental Data and Coefficients for Model

Absolute core permeability	3.64 darcies
Core permeability to emulsion	1.90 darcies
Fractional permeability to emulsion	0.522
Maximum oil saturation	0.198
Plugged oil saturation	0.152
Fractional porosity open to flow	0.308
Blockage coefficient	4.56
Breakthrough time (pore volumes)	0.638

Coefficients of the Mathematical Model

Rate coefficient H_o	0.033 sec ⁻¹
β Factor	0.136
t_{bt}	3859 sec
α	8.54 cm ⁻¹

RUN 129

Core pore volume	160.4 cc
Inlet end block volume	8.4 cc
Outlet end block volume	8.3 cc
Outlet tube volume	2.6 cc
Total fittings volume	19.3 cc
Oil volume in the core holder	30.0 cc
Oil volume in the core	27.1 cc
Maximum oil saturation in the core	0.169

After emulsion breakthrough, the pore volumes injected into the core is given by:

$$\text{Pore volumes injected into the core} = \frac{Q - 19.3}{160.4}$$

where Q = Cumulative emulsion injected into the core holder (cc)

The stepwise and smoothed outlet end emulsion profile is shown in Figure C4. The experimentally recorded data for this run is shown in Table C10, with the smoothed outlet end profile shown in Table C11. The theoretically determined profile evaluated using the model is recorded in Table C11. A summary of the pertinent experimental data and the values for the coefficients of the model are shown in Table C12.

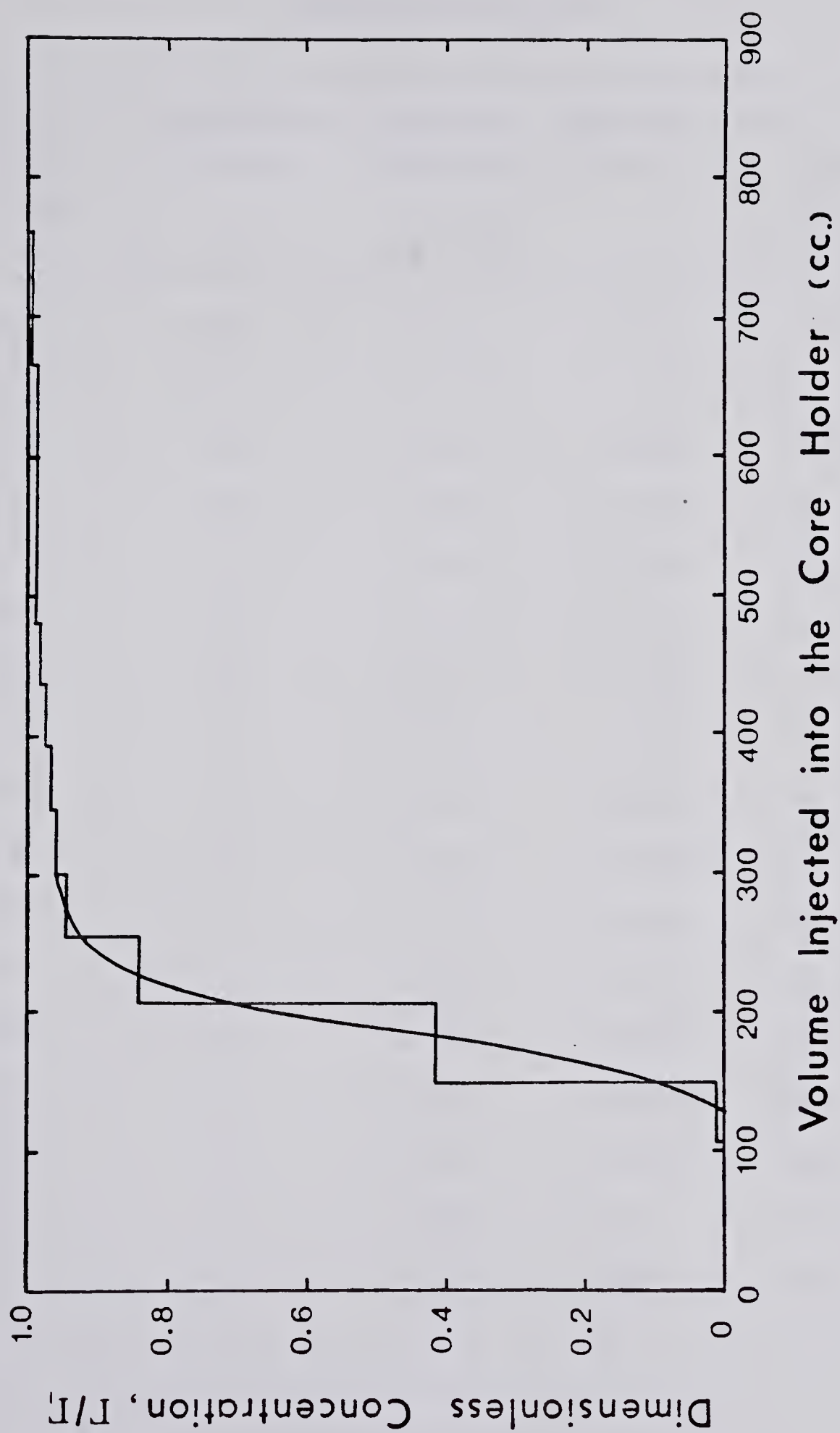


FIGURE C.4 OUTLET END CONCENTRATION : RUN 129

TABLE C10

Experimental Data

Produced Fluid Volume cc	Incremental Volume cc	Emulsion Viscosity $\text{mm}^2 \text{ s}^{-1}$	Emulsion Conc.	Oil in the Core Holder cc
104	104	1.0	0.0	15.6
149	45	1.003	0.001	22.3
204	55	1.196	0.062	27.2
253	49	1.447	0.126	28.3
300	47	1.516	0.142	28.7
346	46	1.525	0.144	29.0
391	45	1.532	0.145	29.2
436	45	1.535	0.146	29.4
481	45	1.541	0.147	29.6
531	50	1.543	0.148	29.7
576	45	1.544	0.148	29.8
622	46	1.545	0.148	29.9
668	46	1.546	0.148	29.9
713	45	1.549	0.149	30.0
759	46	1.550	0.149	30.0
805	46	1.553	0.15	30.0
849	44	1.554	0.15	30.0

TABLE C11

Produced Emulsion Concentration Profile

Pore Volumes Injected	Dimensionless Emulsion Outlet Concentration Γ/Γ_i	Predicted Emulsion Outlet End Concentration Γ/Γ_i
0.191	0.0	0.0
0.503	0.0	0.0
0.659	0.0	0.0
0.815	0.120	0.206
0.971	0.400	0.400
1.127	0.700	0.631
1.282	0.830	0.815
1.438	0.895	0.919
1.594	0.930	0.967
1.75	0.950	0.987
2.373	0.975	1.000
2.997	0.985	1.000
3.620	0.985	1.000
4.244	1.000	1.000

TABLE C12

Summary of Experimental Data and Coefficients for Model

Absolute core permeability	4.14 darcies
Core permeability to emulsion	2.26 darcies
Fractional permeability to emulsion	0.545
Maximum oil saturation	0.169
Plugged oil saturation	0.120
Fractional porosity open to flow	0.325
Blockage coefficient	5.61
Breakthrough time (pore volumes)	0.659

Coefficients of the Mathematical Model

Rate coefficient H_o	0.0296sec^{-1}
β Factor	0.116
t_{bt}	3807 sec
α	7.31cm^{-1}

APPENDIX D

EMULSION DROPLET SIZE DISTRIBUTION

RUN 129

TABLE D1

PRODUCED EMULSION DROPLET SIZE DISTRIBUTION

PERCENTAGE EACH CHANNEL

CHANNEL	TUBE															
	0	1	2	3	4	5	6	7	8	9	10	11	12	13		
	104	149	204	253	300	346	391	436	481	531	576	622	668	713		
									CUMULATIVE PRODUCED EMULSION (cc)							
3	0.0	38.3	23.0	22.1	20.5	19.2	18.6	-	19.0	18.7	18.9	18.6	18.5	18.9		
4	0.0	32.8	28.0	25.2	23.7	22.2	21.9	-	22.3	21.6	22.1	22.0	21.8	21.2		
5	0.0	18.9	26.4	27.1	24.8	24.1	24.2	-	24.2	24.0	23.2	23.2	23.6	23.7		
6	0.0	3.7	12.8	17.0	19.3	19.6	20.1	-	19.7	20.3	19.8	20.4	20.3	20.1		
7	0.0	0.7	3.3	5.6	9.2	10.8	11.0	-	10.8	11.3	10.8	10.8	10.7	10.7		
8	0.0	0.6	1.1	0.7	1.2	2.2	2.7	-	2.8	2.8	2.8	2.8	2.8	2.8		
9	0.0	1.0	1.0	0.6	0.2	0.3	0.4	-	0.5	0.6	0.6	0.6	0.6	0.6		
10	0.0	1.2	0.8	0.5	0.3	0.3	0.3	-	0.3	0.3	0.4	0.4	0.5	0.5		
11	0.0	1.2	0.9	0.3	0.4	0.2	0.2	-	0.2	0.2	0.4	0.4	0.3	0.4		
12	0.0	1.0	0.8	0.6	0.2	0.4	0.2	-	0.1	0.1	0.5	0.4	0.4	0.4		
13	0.0	0.5	0.9	0.1	0.2	0.3	0.2	-	0.2	0.1	0.4	0.3	0.4	0.3		
14	0.0	0.1	1.0	0.2	0.0	0.4	0.2	-	0.0	0.0	0.0	0.0	0.0	0.1		
15	0.0	0.0	0.0	0.0	0.0	0.0	0.0	-	0.0	0.0	0.0	0.0	0.0	0.0		
16	0.0	0.0	0.0	0.0	0.0	0.0	0.0	-	0.0	0.0	0.0	0.0	0.0	0.0		

TABLE D2

PRODUCED EMULSION DROPLET SIZE DISTRIBUTION

PERCENTAGE OF THE INLET CONCENTRATION

CHANNEL	0	1	2	3	4	5	TUBE							10	11	12	13
							CUMULATIVE PRODUCED EMULSION (cc)										
	104	149	204	253	300	346	391	436	481	531	576	622	668	713			
3	0.0	1.35	51	99	103	98	96	-	99	98	99	98	97	101			
4	0.0	1.02	54	99	104	99	99	-	102	99	102	101	101	98			
5	0.0	0.54	46	97	99	98	99	-	101	100	97	97	99	100			
6	0.0	0.12	27	73	93	96	99	-	99	102	99	103	102	102			
7	0.0	0.04	13	45	83	98	101	-	101	106	101	101	101	101			
8	0.0	0.15	17	22	43	81	100	-	105	106	106	106	106	107			
9	0.0	1.11	69	84	31	48	64	-	82	98	99	99	99	100			
10	0.0	1.6	66	84	56	57	58	-	59	59	79	79	99	99			
11	0.0	1.6	74	50	75	38	38	-	39	39	79	79	60	79			
12	0.0	0.9	47	72	27	54	27	-	14	14	70	56	56	57			
13	0.0	0.5	53	12	27	41	27	-	14	14	82	42	66	57			
14	0.0	0.1	69	28	0	64	32	-	0	0	0	0	0	16			
15	0.0	0.0	0	0	0	0	0	-	0	0	0	0	0	0			
16	0.0	0.0	0	0	0	0	0	-	0	0	0	0	0	0			

TABLE D3

Production History
4 Fractional Size Emulsion

Tube	Cumulative	Channel 3 + 4	Channel 5	Channel 6	Channel 7+	Emulsion
	Produced Emulsion cc					Conc.
-	104	0.0	0.0	0.0	0.0	0.0
1	149	1.2	0.5	0.1	0.25	0.001
2	204	52.2	45.9	27.0	24.1	0.062
3	253	99.0	97.0	73.0	43.2	0.126
4	300	104.0	99.6	93.0	66.0	0.142
5	346	99.0	98.2	96.0	85.0	0.144
6	391	97.5	99.6	99.2	88.0	0.145
7	436	-	-	-	-	0.146
8	481	101	101	98.6	86.9	0.147
9	531	99	100	102	91	0.148
10	576	100	97	99	94	0.148
11	622	100	97	103	93	0.148
12	668	99	99	102	94	0.148
13	713	99	100	102	96	0.149
14	759	Emulsion Droplet Size Not Evaluated				
15	805					

TABLE D4

Inlet Emulsion Properties

Inlet Emulsion Concentration	0.15
Channel 3 + 4 Inlet Concentration	0.0603
Channel 5 Inlet Concentration	0.03525
Channel 6 Inlet Concentration	0.0294
Channel 7+ Inlet Concentration	0.02505
Channel Size Distribution (microns)	
Channel 3 + 4	0 - 3.17
Channel 5	3.17 - 4.00
Channel 6	4.00 - 5.04
Channel 7+	5.04 - 32.0
d_g/d_d parameter, each channel	
Channel 3 + 4	∞ - 20.4
Channel 5	20.4 - 16.2
Channel 6	16.2 - 12.8
Channel 7+	12.8 - 2.02

TABLE D5

Retained Oil Saturation, Each Channel
 Used in the Mathematical Model
 Smoothed Data

Channel 3				
Produced Fluid Volume cc	Incremental Volume cc	Emulsion Conc.	Channel Conc.	Retained Oil cc
104	104	0.0	0.0	2.9
149	45	0.001	0.013	4.2
204	55	0.062	0.505	4.95
253	47	0.126	0.99	4.95
300	47	0.142	1.0	4.95
Oil Volume in the Core Holder			4.95 cc	
Oil Volume in the Core			4.4 cc	
Retained Oil Saturation in the Core			0.0275	

TABLE D5 CONTINUED

Channel 4				
Produced Fluid	Incremental	Emulsion	Channel	Retained
Volume	Volume	Conc.	Conc.	Oil
cc	cc			cc
104	104	0.0	0.0	3.3
149	45	0.001	0.01	4.8
204	55	0.062	0.537	5.6
253	47	0.126	0.99	5.6
300	47	0.142	1.0	5.6

Oil Volume in the Core Holder 5.6 cc

Oil Volume in the Core 5.0 cc

Retained Oil Saturation in the Core 0.031

TABLE D5 CONTINUED

Channel 5				
Produced Fluid Volume cc	Incremental Volume cc	Emulsion Conc.	Channel Conc.	Retained Oil cc
104	104	0.0	0.0	3.7
149	45	0.001	0.005	5.2
204	55	0.062	0.459	6.3
253	47	0.126	0.97	6.3
300	47	0.142	1.0	6.3

Volume of Oil in the Core Holder 6.3 cc

Volume of Oil in the Core 5.7 cc

Retained Oil Saturation in the Core 0.0353

TABLE D5 CONTINUED

Channel 6

Produced Fluid	Incremental	Emulsion	Channel	Retained
Volume	Volume	Conc.	Conc.	Oil
cc	cc			cc
104	104	0.0	0.0	3.1
149	45	0.001	0.001	4.4
204	55	0.062	0.27	5.6
253	47	0.126	0.73	5.9
300	47	0.142	0.93	6.0
346	46	0.144	0.96	6.1
391	45	0.145	0.99	6.1
436	45	0.146	0.99	6.1
481	45	0.147	0.99	6.1
531	50	0.148	1.0	6.1

Volume of Oil in the Core Holder 6.1 cc

Volume of Oil in the Core 5.6 cc

Retained Oil Saturation in the Core 0.0347

TABLE D5 CONTINUED

Channel 7+				
Produced Fluid	Incremental	Emulsion	Channel	Retained
Volume	Volume	Conc.	Conc.	Oil
cc	cc			cc
104	104	0.0	0.0	2.6
149	45	0.001	0.002	3.7
204	55	0.062	0.241	4.8
253	47	0.126	0.432	5.4
300	47	0.142	0.748	5.7
346	46	0.144	0.796	6.0
391	45	0.145	0.814	6.2
436	45	0.146	0.848	6.3
481	45	0.147	0.902	6.5
531	50	0.148	0.910	6.6
576	45	0.148	0.916	6.7
622	46	0.148	0.922	6.8
668	46	0.148	0.934	6.8
713	45	0.149	0.964	6.9
759	46	0.149	0.98	6.9
805	46	0.149	0.99	6.9
849	44	0.15	1.0	6.9

Volume of Oil in the Core Holder 6.9 cc

Volume of Oil in the Core 6.4 cc

Retained Oil Saturation in the Core 0.04



TABLE D6

Summary of Experimental Parameters - Each Channel

Channel	Inlet Conc. Γ_i	Retained Oil Volume cc	Retained Oil Saturation S_m	Plugged Oil Saturation σ_m
3 + 4	0.0603	9.41	0.0585	0.0394
5	0.03525	5.66	0.0353	0.0241
6	0.0294	5.56	0.0347	0.0253
7+	0.02505	6.4	0.04	0.032

TABLE D7

Summary of the Mathematical Model Parameters

Channel	Inlet Conc. Γ_i	Plugged Oil Saturation σ_m	Rate Constant H_o	β Constant	Breakthrough Time sec PV	
3 + 4	0.0603	0.0394	0.587	0.0311	3923	0.679
5	0.03525	0.0241	1.162	0.0244	3824	0.662
6	0.0294	0.0253	0.641	0.0332	3848	0.666
7+	0.02505	0.032	0.227	0.0485	3821	0.662

TABLE D8

Produced Emulsion Concentration Profile

Channel 3 + 4		
Pore Volumes Injected	Dimensionless Emulsion Outlet Concentration Γ/Γ_i	Predicted Emulsion Outlet End Concentration Γ/Γ_i
0.191	0.0	0.0
0.503	0.0	0.0
0.659	0.0	0.0
0.815	0.105	0.104
0.971	0.520	0.520
1.127	0.910	0.910
1.282	0.990	0.990
1.438	1.0	1.0
1.594	1.0	1.0
1.75	1.0	1.0
2.373	1.0	1.0
2.997	1.0	1.0
3.620	1.0	1.0
4.244	1.0	1.0

TABLE D8 CONTINUED

Channel 5		
Pore Volumes Injected	Dimensionless Emulsion Outlet Concentration Γ/Γ_i	Predicted Emulsion Outlet End Concentration Γ/Γ_i
0.191	0.0	0.0
0.503	0.0	0.0
0.659	0.0	0.0
0.815	0.105	0.105
0.971	0.410	0.410
1.127	0.820	0.805
1.282	0.960	0.961
1.438	0.990	0.993
1.594	0.997	0.999
1.75	1.0	1.0
2.373	1.0	1.0
2.997	1.0	1.0
3.62	1.0	1.0
4.244	1.0	1.0

TABLE D8 CONTINUED

Channel 6		
Pore Volumes Injected	Dimensionless Emulsion Outlet Concentration Γ/Γ_i	Predicted Emulsion Outlet End Concentration Γ/Γ_i
0.191	0.0	0.0
0.503	0.0	0.0
0.659	0.0	0.0
0.815	0.105	0.109
0.971	0.270	0.248
1.127	0.470	0.470
1.282	0.700	0.704
1.438	0.865	0.865
1.594	0.945	0.945
1.75	0.980	0.979
2.373	1.0	1.0
2.997	1.0	1.0
3.620	1.0	1.0
4.244	1.0	1.0

TABLE D8 CONTINUED

Channel 7+		
Pore Volumes Injected	Dimensionless Emulsion Outlet Concentration Γ/Γ_i	Predicted Emulsion Outlet End Concentration Γ/Γ_i
0.191	0.0	0.0
0.503	0.0	0.0
0.659	0.0	0.0
0.815	0.08	0.08
0.971	0.240	0.254
1.127	0.340	0.340
1.282	0.440	0.437
1.438	0.540	0.540
1.594	0.640	0.639
1.75	0.73	0.728
2.373	0.845	0.933
2.997	0.910	0.986
3.620	0.940	0.997
4.244	0.965	0.999

TABLE D9

Produced Emulsion Concentration Profile
4 Channel Model

Pore Volumes Injected	Dimensionless Emulsion Outlet Concentration Γ/Γ_i	Predicted Emulsion Outlet End Concentration Γ/Γ_i
0.191	0.0	0.0
0.503	0.0	0.0
0.659	0.0	0.0
0.815	0.118	0.119
0.971	0.400	0.396
1.127	0.707	0.704
1.282	0.834	0.835
1.438	0.895	0.895
1.594	0.928	0.929
1.75	0.951	0.950
2.373	0.974	0.989
2.997	0.985	0.998
3.62	0.985	0.999
4.244	0.994	1.0

APPENDIX E

EVALUATION OF THE CONSTANTS IN THE MODEL

E.1 EVALUATION OF σ_m FROM S_m

The value for the maximum retained oil concentration (σ_m) in the core had to be estimated, because it cannot be measured directly without displacing all the oil that is flowing within the core.

For emulsion flow, it can be assumed that the emulsion will plug off the small pore throats and thus the emulsion will have to flow through the large pore throats. The relationship between the porosity open to flow and the permeability was evaluated by assuming:

- 1) a simple pore model for the porous medium, which is shown in Table E.1
- 2) the permeability of the pore is proportional to the radius of the pore squared and
- 3) the tortuosity of the medium is independant of the pore plugging.

The calculated relationship between the porosity open to flow and the permeability is shown in Table E.1 and Figure E.1. This pore model is however close to the relationship

$$\left\{ \begin{array}{c} \text{Fractional Permeability} \\ \text{Plugged} \end{array} \right\} = \left\{ \text{Plugged Porosity} \right\}^2 \quad (\text{E.1})$$

and because the true pore size distribution of the model is unknown, the relationship shown in Equation E.1 was used to evaluate σ_m .

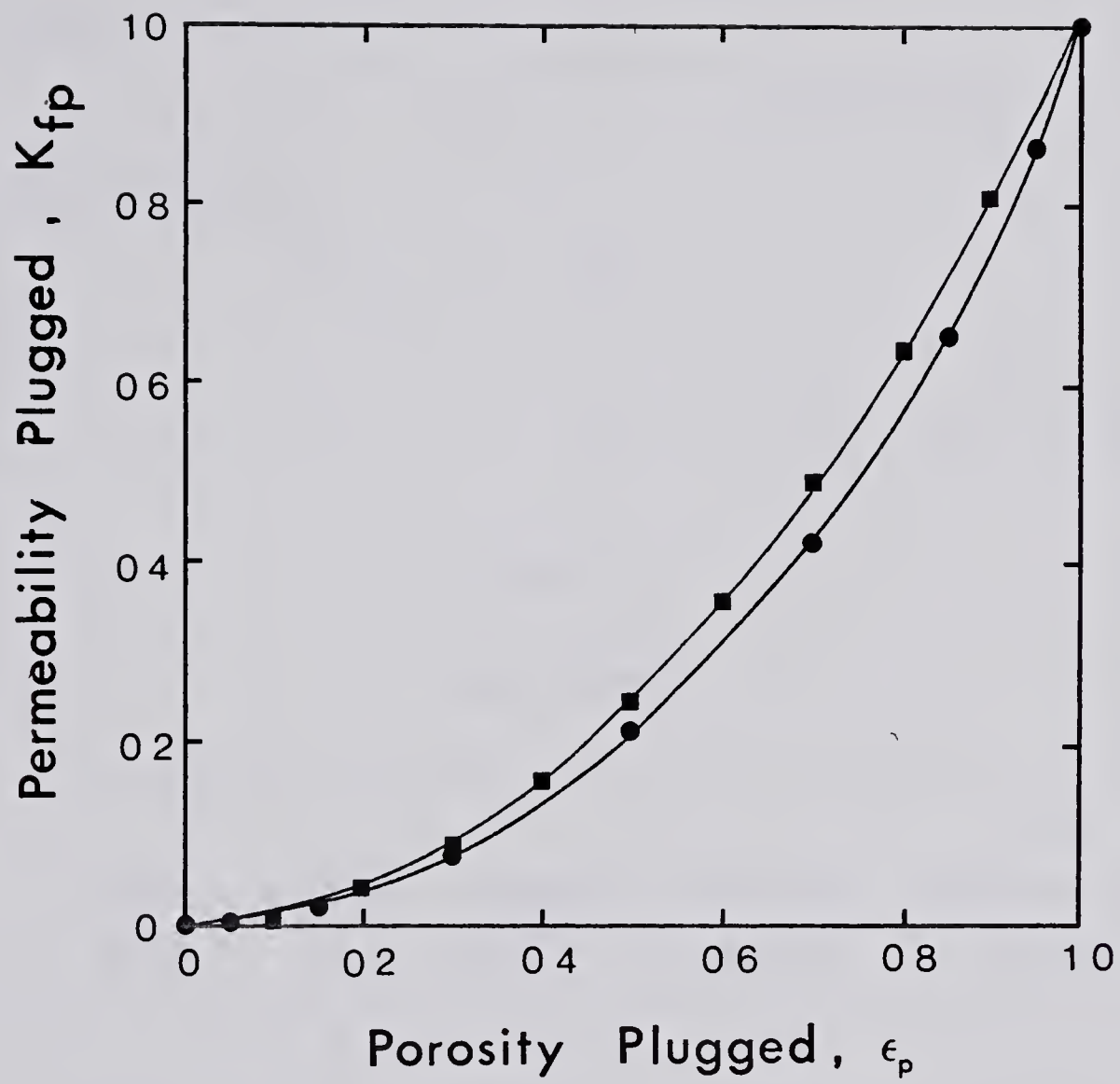


FIGURE E.1 RELATIONSHIP BETWEEN PLUGGED POROSITY AND PERMEABILITY

From Equation E.1, then

$$\left\{ \begin{array}{c} \text{Fractional Permeability} \\ \text{Open To Flow} \end{array} \right\} = 1 - \{ \text{Plugged Porosity} \}^2$$

$$K_f = 1 - (1 - \epsilon)^2$$

therefore

$$\epsilon = 1 - \sqrt{1 - K_f}$$

and remembering

$$S_m = \sigma_m + \epsilon \Gamma$$

then

$$\sigma_m = S_m - (1 - \sqrt{1 - K_f})$$

TABLE E.1

PORE MODEL

PORE SIZE	VOLUME %	NUMBER PORES	POROSITY PLUGGED	PORE PERMEABILITY PLUGGED
1	5	1000	0.05	0.002
2	10	500	0.15	0.019
3	15	333	0.30	0.076
4	20	250	0.50	0.213
5	20	160	0.70	0.426
6	15	83	0.85	0.655
7	10	41	0.95	0.864
8	5	16	1.0	1.0

E.2 USE OF THE COMPUTER PROGRAM COMPLX

In section 5.6.1, it was pointed out that there was not one unique set of constants which produced the best fit to the data. There is infact a narrow range of closely interrelated values of H_0 and β that give the same fit.

In order to find the best values for the constants and to ensure that the computer program did not converge on a false plateau of the least squares error parameter in the analysis, the program was initiated from a series of starting values forthe input variables and a true convergence was assumed if the program COMPLX converged to the same values for each variable from a number of starting locations.

BRUCE PEEL SPECIAL COLLECTIONS LIBRARY
UNIVERSITY OF ALBERTA LIBRARY

REQUEST FOR DUPLICATION

I wish a photocopy of the thesis by

_____ (author)

entitled _____

The copy is for the sole purpose of private scholarly or scientific study and research. I will not reproduce, sell or distribute the copy I request, and I will not copy any substantial part of it in my own work without permission of the copyright owner. I understand that the Library performs the service of copying at my request, and I assume all copyright responsibility for the item requested.

B30282